

2

NAVAL POSTGRADUATE SCHOOL
Monterey, California

AD-A276 377



DTIC
ELECTE
MAR 07 1994
S B D

THESIS

EXPERIMENTAL HEAT EXCHANGER
PERFORMANCE IN A THERMOACOUSTIC
PRIME MOVER

by

Nelson C. Castro

December, 1993

Thesis Advisor:
Co-Advisor:

Thomas J. Hofler
Anthony A. Atchley

Approved for public release; distribution is unlimited.

DTIC QUALITY INSPECTED 3

95px

94-07374



94 3 4 020

**Best
Available
Copy**

REPORT DOCUMENTATION PAGE

Form Approved OMB No. 0704

Public reporting burden for this collection of information is estimated to average 1 hour per response, including the time for reviewing instruction, searching existing data sources, gathering and maintaining the data needed, and completing and reviewing the collection of information. Send comments regarding this burden estimate or any other aspect of this collection of information, including suggestions for reducing this burden, to Washington Headquarters Services, Directorate for Information Operations and Reports, 1215 Jefferson Davis Highway, Suite 1204, Arlington, VA 22202-4302, and to the Office of Management and Budget, Paperwork Reduction Project (0704-0188) Washington DC 20503.

1. AGENCY USE ONLY (Leave blank)	2. REPORT DATE 19November1993.	3. REPORT TYPE AND DATES COVERED Master's Thesis	
4. TITLE AND SUBTITLE EXPERIMENTAL HEAT EXCHANGER PERFORMANCE IN A THERMOACOUSTIC PRIME MOVER		5. FUNDING NUMBERS	
6. AUTHOR(S) Nelson C. Castro			
7. PERFORMING ORGANIZATION NAME(S) AND ADDRESS(ES) Naval Postgraduate School Monterey CA 93943-5000		8. PERFORMING ORGANIZATION REPORT NUMBER	
9. SPONSORING/MONITORING AGENCY NAME(S) AND ADDRESS(ES)		10. SPONSORING/MONITORING AGENCY REPORT NUMBER	
11. SUPPLEMENTARY NOTES The views expressed in this thesis are those of the author and do not reflect the official policy or position of the Department of Defense or the U.S. Government.			
12a. DISTRIBUTION/AVAILABILITY STATEMENT Approved for public release; distribution is unlimited.		12b. DISTRIBUTION CODE A	
13. ABSTRACT (maximum 200 words) This thesis investigates the experimental heat exchanger performance in a neon filled thermoacoustic prime mover. The experimental approach is to measure the waveform and spectrum of the acoustic oscillations, as well as the relevant temperatures for heat exchangers of 0.257, 0.569, and 0.82 cm in length. A temperature gradient is established across the stack by submerging the cold heat exchanger and cold end tube in liquid nitrogen and keeping the hot heat exchanger and hot end tube at ambient temperature. Measurements are made at various mean gas pressures ranging from 1.5 to 50 kPa and for various effective positions of the stack in the standing wave. Acoustic pressure amplitudes as high as 29% of mean gas pressure are generated by the prime mover. The primary experimental controls over heat exchanger performance are the various heat exchanger lengths mentioned above, and the control of the thermal penetration depth, which decreases with increasing mean gas pressure. Results indicated that the prime mover can generate peak-to-peak displacement amplitudes that are much longer than the heat exchanger lengths.			
14. SUBJECT TERMS Acoustics; Thermoacoustic; Thermoacoustics Heat Transport; Heat Exchanger, Thermoacoustic Prime Mover		15. NUMBER OF PAGES 96	
		16. PRICE CODE	
17. SECURITY CLASSIFICATION OF REPORT Unclassified	18. SECURITY CLASSIFICATION OF THIS PAGE Unclassified	19. SECURITY CLASSIFICATION OF ABSTRACT Unclassified	20. LIMITATION OF ABSTRACT UL

NSN 7540-01-280-5500

Standard Form 298 (Rev. 2-89)

Prescribed by ANSI Std. Z39-18

Approved for public release: distribution is unlimited.

EXPERIMENTAL HEAT EXCHANGER PERFORMANCE IN A THERMOACOUSTIC PRIME MOVER

by

N. C. Castro

Lieutenant, United States Navy

B. S., University of Florida, 1987

Submitted in partial fulfillment of the
requirements for the degree of

MASTER OF SCIENCE IN PHYSICS

from the

NAVAL POSTGRADUATE SCHOOL

December 1993

Author:

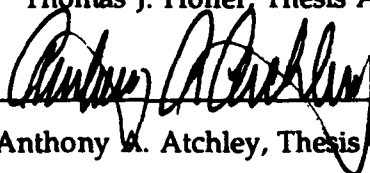


Nelson C. Castro

Approved by:



Thomas J. Hofler, Thesis Advisor



Anthony A. Atchley, Thesis Co-advisor



William B. Colson, Chairman,

Department of Physics

ABSTRACT

This thesis investigates the experimental heat exchanger performance in a neon filled thermoacoustic prime mover. The experimental approach is to measure the waveform and spectrum of the acoustic oscillations, as well as the relevant temperatures for heat exchangers 0.257, 0.569, and 0.82 *cm* in length. A temperature gradient is established across the stack by submerging the cold heat exchanger and cold end tube in liquid nitrogen and keeping the hot heat exchanger and hot end tube at ambient temperature. Measurements are made at various mean gas pressures ranging from 1.5 to 50 *kPa* and for various effective positions of the stack in the standing wave. Acoustic pressure amplitudes as high as 29% of mean gas pressure are generated by the prime mover. The primary experimental controls over heat exchanger performance are the various heat exchanger lengths mentioned above, and the control of the thermal penetration depth, which decreases with increasing mean gas pressure. Results indicated that the prime mover can generate peak-to-peak displacement amplitudes that are much longer than the heat exchanger lengths.

Accession For	
NTIS GRA&I	<input checked="" type="checkbox"/>
DTIC TAB	<input type="checkbox"/>
Unannounced	<input type="checkbox"/>
Justification	
By	
Distribution/	
Availability Codes	
Dist	Spec
A-1	

DISCLAIMER

The specific equipment described in this work in no way constitutes an endorsement of these products.

Table of Contents

I.	INTRODUCTION	1
II.	THEORY	4
III.	EXPERIMENTAL APPARATUS, INSTRUMENTATION, AND PROCEDURE	14
A.	THE PRIME MOVER	14
1.	Hot End Tube Assembly	14
2.	Hot Heat Exchanger Assembly	16
3.	Stack Assembly	17
4.	Cold Heat Exchanger Assembly	17
5.	Cold End Tube Assembly	18
B.	INSTRUMENTATION	19
1.	Temperature Measurement Equipment	19
2.	Temperature Control Equipment	19
3.	Pressure Measurement Equipment	22
C.	PROCEDURE	23
1.	Harmonic Distortion Suppression	23
2.	Heat Flow Modifications	29
3.	Prime Mover Below Onset	31
4.	Prime Mover Above Onset	33

IV.	RESULTS AND DISCUSSIONS	34
A.	THE 0.257 cm HEAT EXCHANGER	34
B.	THE 0.569 cm HEAT EXCHANGER	36
C.	THE 0.820 cm HEAT EXCHANGER	38
V.	SUMMARY, CONCLUSIONS, AND RECOMMENDATIONS	47
A.	SUMMARY	47
B.	CONCLUSIONS	49
C.	RECOMMENDATIONS	49
	APPENDIX A - PRIME MOVER SPECIFICATIONS	50
	APPENDIX B - PLOTS OF WAVEFORMS AND SPECTRA OF SOUND GENERATED BY PRIME MOVER AT 8.128 cm PLUNGER POSITION	70
	LIST OF REFERENCES	82
	DISTRIBUTION LIST	84

LIST OF SYMBOLS

c	sound speed
c_p	isobaric heat capacity per unit mass
d	distance from heat exchanger or stack to plunger
Q	heat
f	frequency
k	wavenumber
P_m	mean gas pressure
P_o	peak pressure amplitude
T	temperature
t_D	dwel time in heat exchanger
u	longitudinal component of velocity
u_o	peak longitudinal component of velocity
x	longitudinal distance
y	transverse distance
y_o	plate half-gap
β	exponent for temperature dependence of dynamic viscosity
γ	ratio of isobaric to isochoric specific heats
δ	penetration depth
Δx	plate length
κ	thermal conductivity
λ	wavelength
ξ	displacement amplitude
ξ_o	peak displacement amplitude
Π	perimeter
ρ	density

τ normalized dimensionless thermal equilibration time
 χ thermal diffusivity
 ω angular frequency

Subscripts and superscripts

c cold
 h hot
 hx heat exchanger
 s stack
 κ thermal
 v viscous

ACKNOWLEDGEMENT

The author is grateful for support of this work by the Naval Postgraduate School. The author would like to thank A. A. Atchley and T. J. Hofler for their invaluable assistance. Also, would like to thank my wife Kara for her unyielding support and my parents for teaching me that an education lasts a lifetime.

I. INTRODUCTION

There are two types of thermoacoustic engines: heat pumps and prime movers [Refs 1-4]. A thermoacoustic heat pump uses a high amplitude acoustic standing wave to transport (or pump) heat along the boundary of a plate situated in the standing wave. The acoustically generated heat flow produces a thermal gradient across the plate. Acoustic energy is converted into stored thermal energy, which in turn can be used for other practical applications.

Thermoacoustic prime movers convert stored thermal energy into useful work in the form of sound. Such a device is the subject of this thesis. An example of a prime mover is shown in Figure 1. This particular configuration is referred to as the "Hofler Tube," described elsewhere [Ref 2]. The prime mover configuration consists of a stack of plates, called the *prime mover stack* (from here on referred as "the stack"), which is in thermal contact with two heat exchangers. In this thesis, the two heat exchangers are called the hot and cold heat exchangers. One end of the stack is held at ambient (or hot) temperature, and the other end of the stack is held near liquid nitrogen (or cold) temperature. The stack and heat exchangers are part of an acoustic resonator. The assembly consisting of a stack, heat exchangers, and a resonator is called a thermoacoustic prime mover.

Thermal energy is stored in the prime mover by imposing a temperature difference across the stack. In order for the prime mover to produce net positive work (i.e., to produce sound), the amount of stored energy converted to sound must exceed

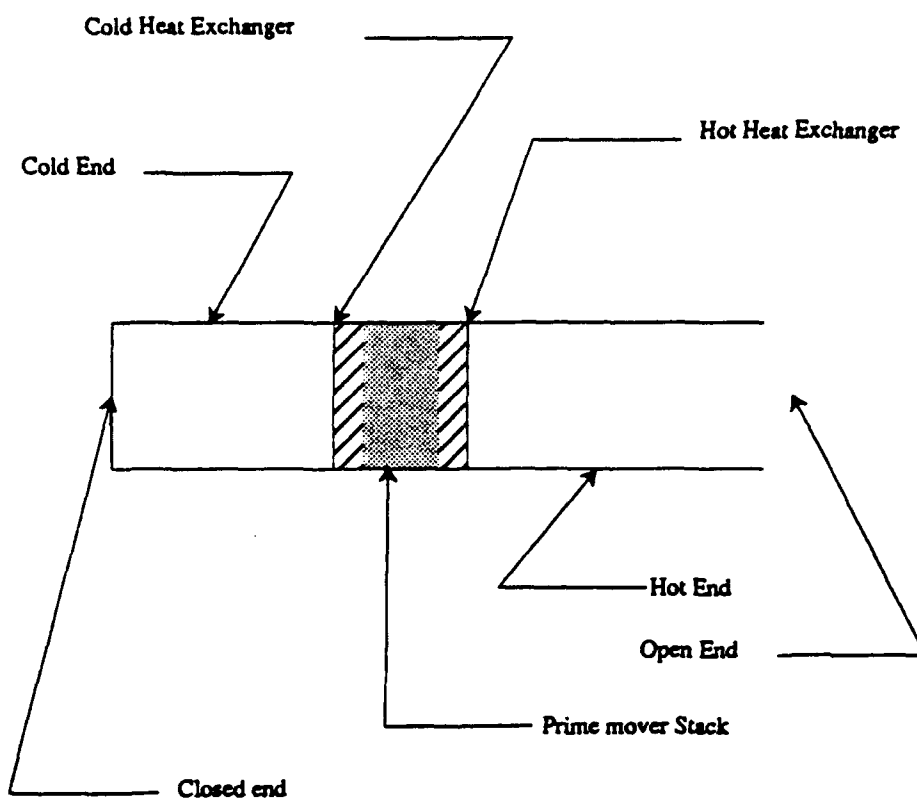


Figure 1- Hofler Tube Configuration

the amount of acoustic energy dissipated by losses within the prime mover. The dominant loss mechanisms are thermal and viscous losses at the resonator walls, stack surface, and heat exchanger surfaces. The prime mover reaches "onset" when the temperature difference across the stack is sufficient for the prime mover to generate and sustain detectable levels of sound. Typically, the steady state acoustic pressure amplitudes are 1 to 10% of the mean gas pressure.

The main purpose of this thesis is an experimental investigation of heat exchanger performance in a thermoacoustic engine. A prime mover is chosen as a vehicle for these heat exchanger experiments partially because improving the performance of the thermoacoustic prime movers is valuable in its own right, but primarily because achieving the desired high level acoustic amplitudes and gas displacement amplitudes in a thermoacoustic refrigerator is a formidable engineering challenge. Achieving large gas displacement amplitudes with prime movers is generally much simpler, if sufficient amounts of heat can be sourced and sinked at the heat exchanger. It is hoped that the lessons learned in these experiments, will also be applicable to thermoacoustic refrigerators.

The prime mover is filled with low pressure neon gas to allow for low thermal heat flux at high pressure ratios (P_o/P_m). The neon gas in the prime mover is pressurized to approximately 1.5, 8.8, 10.9, 27.6, and 50 kPa. A temperature gradient is established across the stack by keeping the cold heat exchanger submerged in liquid nitrogen and the hot heat exchanger at ambient temperature. To determine the heat exchanger performance, the spectrum of acoustic waveform at steady state, the acoustic pressure amplitude, and the temperature at strategic locations in the prime mover are measured for each heat exchanger length at the indicated mean pressures.

II. THEORY

This chapter contains a discussion of some theoretical aspects of heat exchanger performance. The first part is a summary of relevant parts of Swift's review article [Ref 1] and Figure 2 is taken from this article to briefly show Swift's arguments.

Heat exchangers are required in thermoacoustic engines to supply and extract heat to and from the ends of the stack. Figure 2.a shows one plate, cross-hatched, with heat exchangers at each end labeled T_h and T_c . Figure 2.a shows five parcels of fluid near the plate, and their extreme positions. Thus, (a) and (a') represent, respectively, the maximum expanded and maximum compressed positions of parcel (a), and similarly for (b) and (b'), (c) and (c'), (d) and (d'), and (e) and (e'). The articulated cycle for the typical "midplate" parcel (a) consists of a rapid adiabatic motion (1->2) from (a) to (a'), a wait (2->3) at (a') for thermal equilibrium with the plate, a rapid adiabatic motion (3->4) from (a') to (a), followed by a wait (4->1) again for thermal equilibrium.

One result of this cycle is a time-averaged hydrodynamic transport of heat along the direction of acoustic oscillation. For clarity in Figure 2.a, the parcels are drawn nonoverlapping, but in reality (a') and (b), or (d') and (a) occupy the same locations. It is easy to see that, at midplate locations, the time-averaged heat transfer from fluid to plate is zero; for instance, the dQ delivered to the plate by (a) is removed from the plate a half-cycle later by (d').

Now, observe what happens at the ends of the plate near the heat exchangers. For example, consider parcel (c), which makes thermal contact with the heat exchanger at point (c) of its cycle but is out of thermal contact at location (c'). After compression (1->2), the parcel is hotter at (c') than it was at (c), by the peak-to-peak

adiabatic temperature oscillation, but it has no means at (c') to thermally relax. Moreover, nothing happens to it during the waiting period (2->3), so on decompression (3->4) it comes back at (c) to the same temperature that it had at (1). Parcel (c) just idles, not contributing to any time-averaged heat flow, even though it is hotter at (c') than at (c).

Hence, there is no compensating heat flow from (c) to match the dQ removed by (b') from the heat exchanger at T_h . In this simple picture, dQ is extracted from the reservoir at T_h by (b'), passed on down the plate in successive cycles by successive parcels, and then rejected to the reservoir at T_c by (d).

It is understood from these simple arguments that the heat exchanger should have a length of about twice the displacement amplitude, ξ_{hx} , of the gas parcel at the heat exchanger. The displacement amplitude is derived by using the Mach number relation,

$$Ma = \frac{u_o}{c} = \frac{1}{\gamma} \frac{P_o}{P_m}.$$

The relation between displacement and velocity amplitude for sinusoidal waves,

$$\xi_o = \frac{u_o}{\omega}.$$

The local peak displacement amplitude is given by,

$$\xi_{hx} = \xi_o \sin (k x_{hx}).$$

For this experiment, it is assumed that $kx_{hx} \ll 1$ which allows for the approximation that $\xi_{hx} = \xi_o kx_{hx}$. Now, using the Mach number relation and the peak displacement amplitude relation, the local displacement amplitude equation is given by,

$$\xi_{hx} = \frac{1}{\gamma} \frac{P_o}{P_m} x_{hx}. \quad [1]$$

Figure 2.b shows a heat exchanger that is longer than $2\xi_{hx}$. In that case, there are some parcels of fluid that contact only the heat exchanger, at both extremes of their positions, so that they perform no useful function. Their presence is purely dissipative, by virtue of both viscous and thermal processes.

On the other hand, Figure 2.c shows a heat exchanger that is shorter than $2\xi_{hx}$, so that there are parcels that "jump" from the plate to well past the heat exchanger, and contact the heat exchanger only for a very short time. Such parcels are, in Swift's estimation, ineffective in carrying heat to and from the heat exchangers.

This is because Swift assumes that a thermal boundary layer of gas exits between the parcel and the plate, and that this boundary layer represents too large of a thermal impedance for a significant amount of heat to diffuse through the boundary layer in such a short time. However, Hofler has proposed a simple heuristic model [Ref 5] that suggests that a heat exchanger can be both thermally effective and short in the longitudinal direction $\Delta x_{hx} \ll 2\xi_{hx}$, if the plate separation, in the transverse direction, is comparable to a thermal penetration depth $2y_o \approx \delta_K$.

The model begins with a number of simplifying assumptions. Gas viscosity and compressibility are ignored as are the details of the thermal contact between the stack and the gas parcels. The latter issue is complicated by the fact that the stack has a longitudinal temperature distribution $T(x)$. The thickness of the plates is assumed to be negligibly small. Referring to Figure 3, we will also assume that there is a discontinuity in the temperature $T(x)$, between the end of the stack and the beginning of the heat exchanger plates.

Furthermore, the attention focuses on the second gas parcel from the top of Figure 3, which is the parcel with the shortest dwell time, t_D , in the heat exchanger. This is the shortest dwell time because the parcel has its peak velocity at the center of its excursion, or approximately $t_D = \Delta x_{hx} / \omega \xi_{hx}$. This particular parcel is important because it has the poorest thermal contact with the heat exchanger.

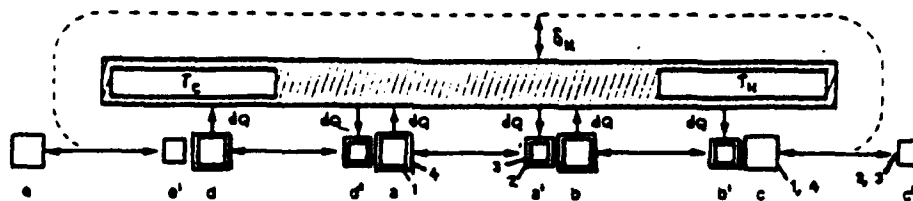


Figure 2.a- A set of oscillating fluid parcels about a thermal penetration depth from one plate of a thermoacoustic engine, with exchangers as its ends.

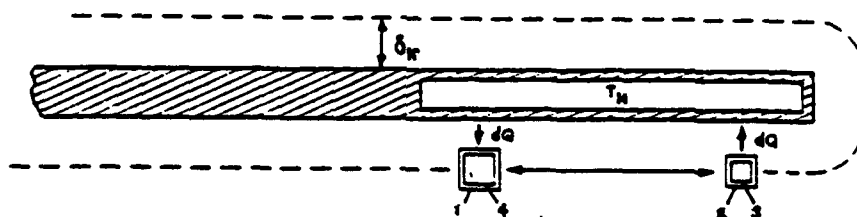


Figure 2.b- If the heat exchanger is too long, the parcel of fluid shown merely shuttles heat from one part of the heat exchanger to another, absorbing work.

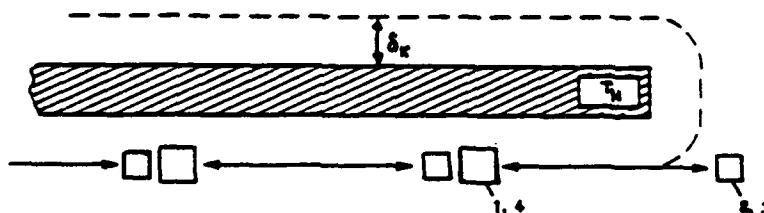


Figure 2.c- If the heat exchanger is too short, the chain of parcels shown has no source of heat.

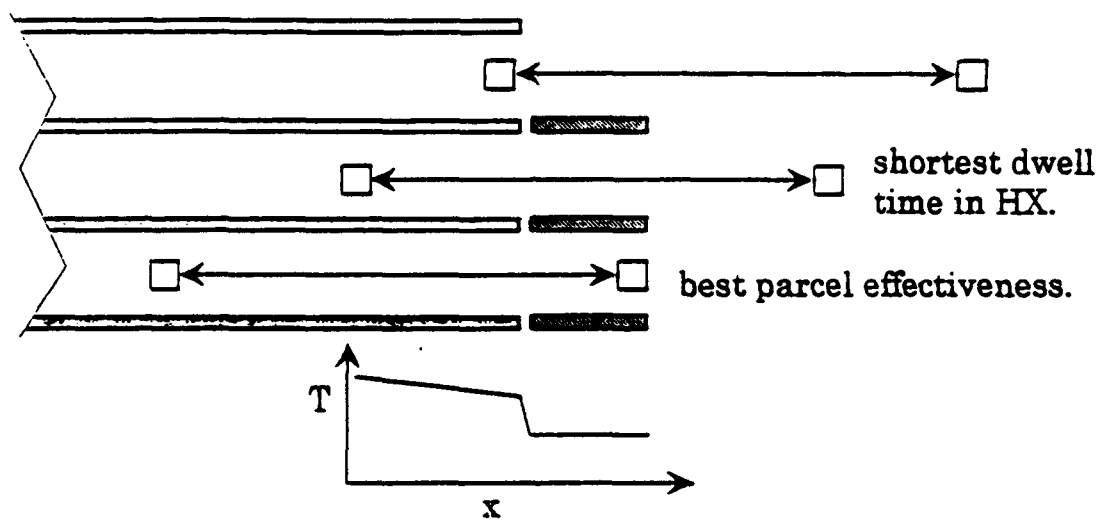


Figure 3- Parcel movement in short and narrow heat exchangers.

The question of thermal effectiveness can be stated thus: How long does the parcel have to remain in the heat exchanger to thermally equilibrate with the exchanger plates? It is important to note that perfect thermal equilibration is probably not a sensible goal, because this will require long heat exchangers, such as those in Swift's analysis.

Long heat exchangers are not desirable because high acoustic dissipation is incurred. A more sensible goal might be 90% thermal equilibration. That is, the final temperature of the gas parcel after passing through the exchanger is different from that of the exchanger by an amount that is only 10% of the temperature discontinuity in $T(x)$.

The problem can be recasted from one of a static temperature distribution in the plates and moving gas parcels, to one of a stationary slab of gas having a time dependent temperature at its boundaries. In Figure 4, it is assumed that the temperature of the slab boundaries has a step discontinuity in the temperature at time $t=0$ and lets the gas thermally equilibrate for a time equal to the dwell time, t_D .

The solution to the ratio of the gas temperature to the boundary temperature, averaged over the slab, can be found in a standard text [Ref 6]. This solution is indicated by the solid curve in Figure 5, where a y-axis value of one represents perfect equilibration, and the x-axis values are normalized time, $\tau = \chi t_D / y_o^2$. If the approximate value for the dwell time is substituted into the expression for τ , and the definition for the thermal penetration depth, $\delta_\kappa = \sqrt{2\chi/\omega}$, is used to obtain,

$$\tau \approx [2(\frac{\xi_{hx}}{\Delta x_{hx}})(\frac{y_o}{\delta_\kappa})^2]^{-1}.$$

The solid curve represents the amount of equilibration after one pass through the exchanger and the long dash curve represents the amount of equilibration after two

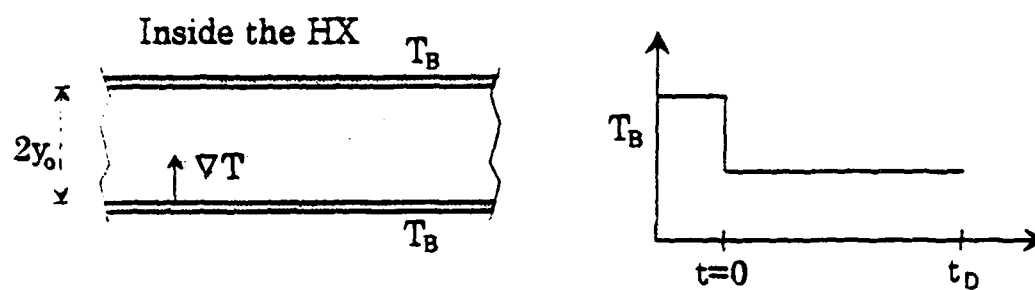


Figure 4- Temperature distribution in stationary plate.

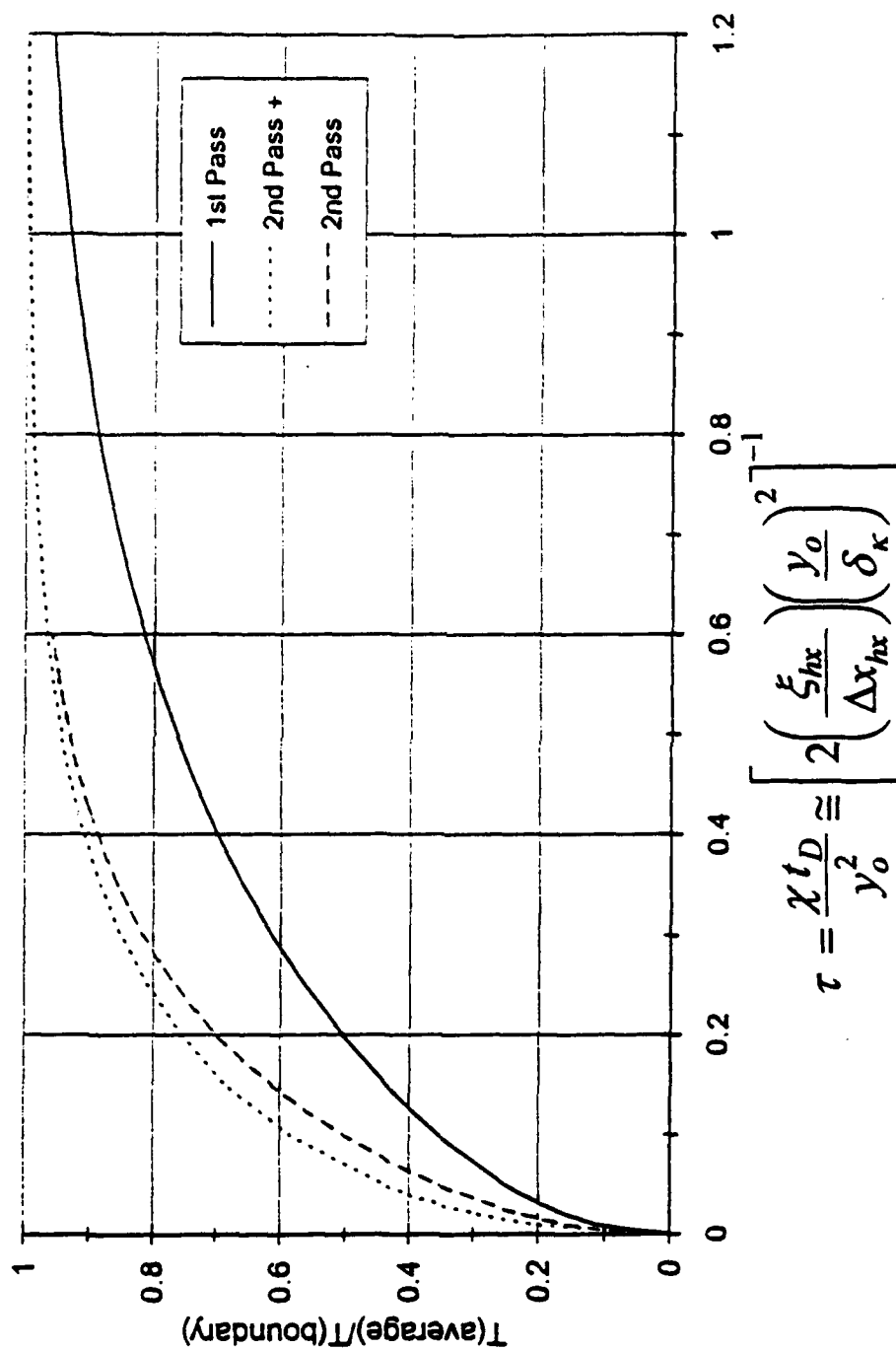


Figure 5- Averaged thermal equilibration.

passes, in one acoustic cycle. This assumes that the gas parcels are doing nothing when they are not in contact with either the stack or the heat exchanger. That is, they are thermally static.

In fact, the temperature of the gas parcels may be stratified in the transverse direction after one pass through the exchanger and they will be thermally equilibrating with their nearest neighbors. The short dash curve assumes perfect equilibration of the gas with itself, in between the first and second passes. The true solution will lie somewhere between the two dashed curves.

Note some values of equilibration versus τ . For $\tau = 0.25$, the equilibration is about 77%; for $\tau = 0.5$, the equilibration is about 93%; and for $\tau = 0.75$, the equilibration is about 98%. In Figure 6, the hatched area indicates the range of parameters y_o/δ_K and $\xi_{hx}/\Delta x_{hx}$, for which the worst case of thermal effectiveness is between 77 and 93%. Short heat exchangers with $\xi_{hx}/\Delta x_{hx}$ in the range of 4 to 8 can be thermally effective if y_o/δ_K is in the range of 0.75 to 0.5.

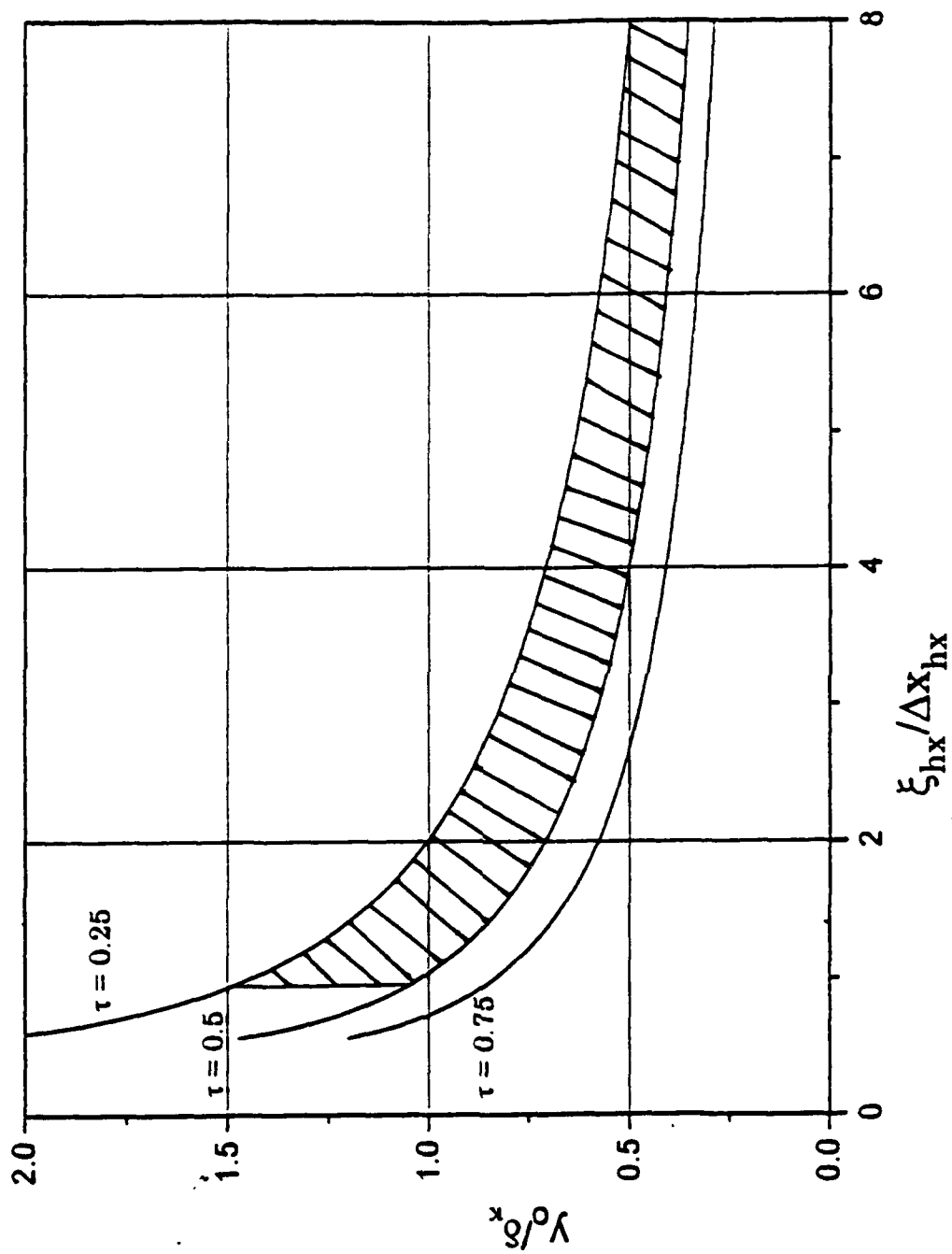


Figure 6- Curves of thermal effectiveness.

III. EXPERIMENTAL APPARATUS, INSTRUMENTATION, AND PROCEDURE

The primary goal of this thesis is to measure the pressure ratio, the steady state spectrum waveform, and temperatures at various locations in the prime mover. Figure 7 shows an overview of the main components of the prime mover. The prime mover is specifically designed to generate very high pressure ratios. Notice that the lower part of the drawing is not to scale. Detailed engineering drawings are found in Appendix A.

A. THE THERMOACOUSTIC PRIME MOVER

1. Hot End Tube Assembly

The hot end assembly consists of the tube, attachment plate, and an assembly consisting of an end-cap, end-cap clamp, and movable plunger. The upper copper tube (see A-1) is 3.81 *cm* I.D. and 22.018 *cm* long. The lower end of the tube is fitted with a 7.366 *cm* O.D., 3.81 *cm* I.D. and 0.9525 *cm* long copper attachment plate (see A-2) that has eight radial holes to be used as thermocouple feed-throughs to the inside of the prime mover. The attachment plate has a groove for an O-ring and eight holes used to bolt the assembly to the hot heat exchanger and stack holder.

The upper end of the tube is fitted with an assembly consisting of an end-cap, end-cap clamp, and movable plunger. The copper end-cap (see A-3) fits into the copper tube and is held in place by a control rod threaded in a 6061-T6 Aluminum clamp (see A-4). The end-cap has three holes that allows free passage for the control rod, a transducer cable, and a 0.3175 *cm* copper gas line that attach to the movable plunger.

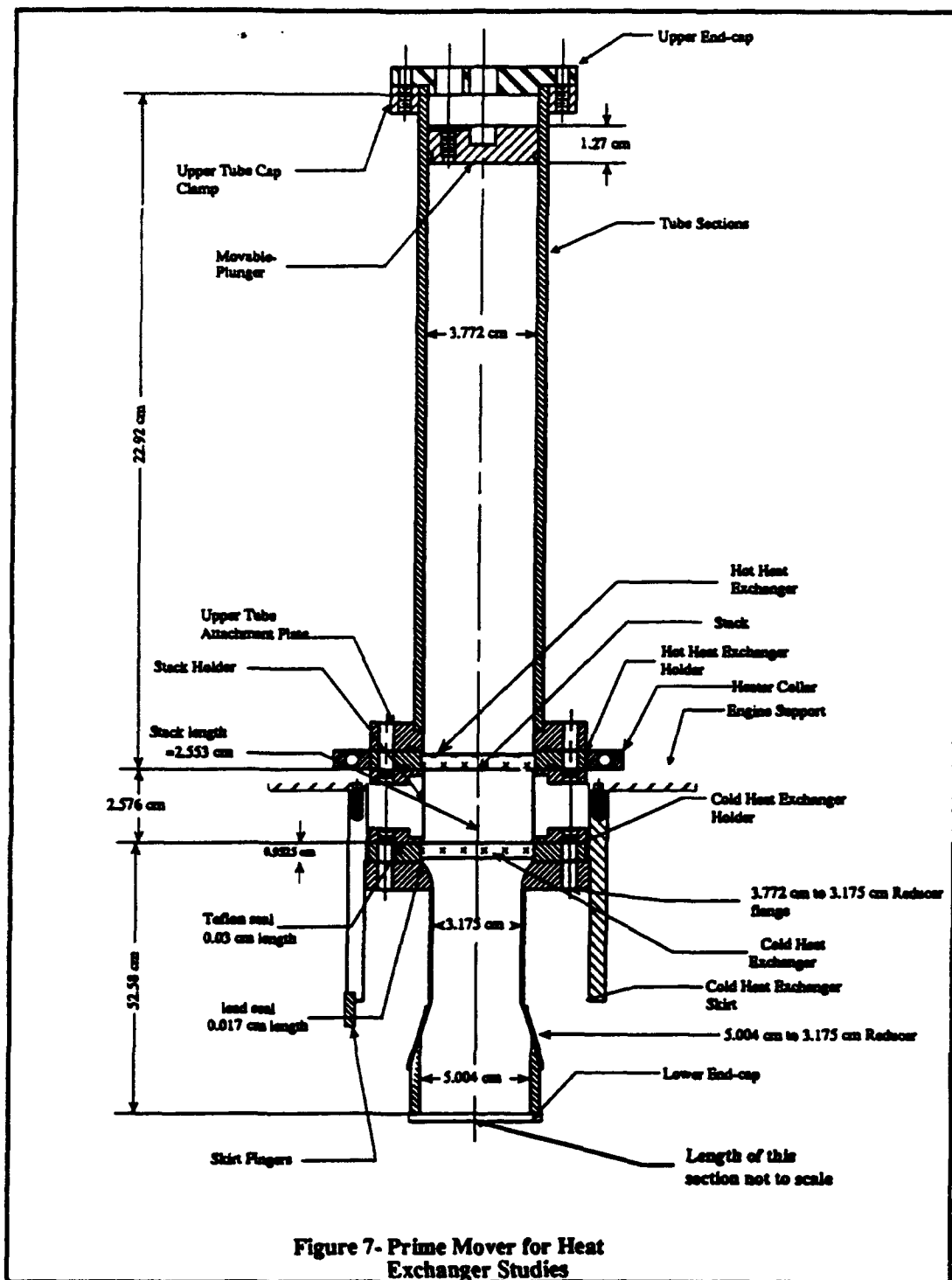


Figure 7- Prime Mover for Heat Exchanger Studies

The copper movable plunger (see A-5) is 3.81 *cm* in diameter and 1.27 *cm* long. The holes for the transducer and the copper line are bored through the plunger to provide access to the interior of the prime mover. The plunger has a groove for an O-ring. The copper gas line is soldered into the hole. A copper-nickel capillary tube of 0.025 *mm* O.D. is inserted and soldered inside the 0.3175 *cm* copper gas line. The capillary provides a high impedance to the acoustic pressure oscillations.

The total internal length of the hot end tube assembly from the top most position of the plunger face to attachment plate bottom is 21.64 *cm*.

2. Hot Heat Exchanger Assembly

The assembly consists of hot heat exchanger, hot heat exchanger holder, hot heat exchanger heater collar, and spacers (if necessary). The purpose of the hot heat exchanger is to supply heat to the stack.

The copper heat exchangers (see A-6) are 3.924 *cm* in diameter and have lengths of 0.257, 0.569, and 0.82 *cm*. Each plate within the heat exchanger is 0.0292 *cm* thick. The plate gap is 0.0584 *cm*. The heat exchangers are soldered into the heat exchanger holder.

The heat exchanger holders (see A-7) are 7.366 *cm* O.D., 3.924 *cm* I.D., and 0.953 *cm* long. There is an O-ring groove in the side facing the stack. For the 0.257 and 0.569 *cm* heat exchangers, bronze spacers (see A-8) are used to support the heat exchangers flush with the side of the heat exchanger holder facing the stack.

The hot heat exchanger heater collar (see A-9) is made of copper and bolted onto the hot heat exchanger holder. It has a 7.37 *cm* I.D. and is 0.953 *cm* long. There are two 0.625 *cm* diameter holes fitted to hold two heater cartridges [Ref 7], used to maintain a constant hot heat exchanger temperature.

3. Stack Assembly

The prime mover stack assembly consists of the stack and the stack holder. The stack (see A-10) is made of polyester film of gauge 0.01 mm and 114.2 cm long. The film is rolled spirally around a phenolic core 0.635 cm in diameter and 2.529 cm long. The polyester film is separated by 0.851 mm diameter fishing line. The total spiral stack is 2.553 cm long, 3.772 cm O.D. and has a total surface area of $\pi \Delta x = 583 \text{ cm}^2$.

The 304 stainless steel stack holder (see A-11) is 2.576 cm long and 3.772 cm I.D. The stack holder is 0.22 mm longer than the stack creating a 0.11 mm gap on each side of the stack inside the holder. The stack holder has eight 8-32 machine screw holes in each flange to attach the assembly consisting of the hot end tube and hot heat exchanger on one side and the assembly consisting of the cold end heat exchanger and cold end tube on the other.

4. Cold Heat Exchanger Assembly

In order to impose a temperature gradient across the stack, the cold heat exchanger is employed to remove heat from the stack and maintain one end of the stack close to liquid nitrogen temperature. The cold heat exchanger assembly is similar to the hot heat exchanger assembly, except that the cold heat exchanger (see A-12) holder has no O-ring groove. The cold heat exchanger is sealed by using a 0.03 cm thick teflon gasket in the stack side of the cold heat exchanger holder and a 0.17 cm lead wire diameter gasket in the cold end tube side of the cold heat exchanger holder.

5. Cold End Tube Assembly

The purpose of the cold end tube assembly is to provide a cold heat sink to the cold heat exchanger, determine the acoustic length, and to eliminate harmonics in the acoustic pressure waveform. It consists of a cold heat exchanger skirt, lower reducer flange, a 3.175 *cm* I.D. lower tube section, a cold end reducer, a 5.08 *cm* I.D. lower tube section, a lower tube end-cap, and an prime mover dewar support.

The purpose of the cold heat exchanger copper skirt (see A-13) is to provide a cold heat sink and to support the prime mover on the dewar. The skirt is 7.19 *cm* long. It has a 7.62 *cm* I.D. and 8.89 *cm* O.D. One end is bored to 8.64 *cm* I.D. and 4.763 *cm* deep to provide a lip to solder on to the lower reducer plate. The skirt has six 2.54 *cm* by 2.54 *cm* equally separated flat faces with 0.188 *cm* diameter holes to attach copper skirt fingers (see A-14) to increase the cold heat sink area. A 304 stainless steel dewar support plate (see A-15) is attached to the cold heat exchanger end of the skirt.

The purpose of the lower reducer copper flange (see A-16) is to provide the first change in diameter to eliminate the harmonics in the waveform and to conduct the liquid nitrogen temperature to the cold heat exchanger. The flange is 2.563 *cm* long and has a 7.72 *cm* O.D. The inside diameter starts at 3.797 *cm* on the face towards the cold heat exchanger and reduces to 3.23 *cm*. The plate is bored to 3.49 *cm* I.D. and 0.508 *cm* in depth to provide a lip to solder on to the 3.175 *cm* I.D. lower tube.

The 3.175 *cm* I.D. lower end copper tube (see A-17) is 26.99 *cm* long and has a 3.49 *cm* O.D. One end of the tube is soldered to the lower reducer flange and the other end to the cold end reducer. The purpose of the cold end copper reducer (see A-18) is to join the 3.175 *cm* I.D. lower tube to the 5.08 *cm* I.D. lower tube and provide the second diameter change to eliminate the harmonics. The cold end reducer is 2.95 *cm* long.

The 5.08 *cm* I.D. lower end copper tube (see A-19) is 19.3 *cm* long and has a 5.595 *cm* O.D. The lower tube copper end-cap (see A-20) is soldered to the 5.08 *cm* I.D. lower tube. It is 1.016 *cm* long. It has a 5.395 *cm* I.D. and 5.76 *cm* O.D.

B. INSTRUMENTATION

Figure 8 shows the overall measurement set-up utilized in this experiment.

1. Temperature Measurement Equipment

Figure 9 shows the placement of the ten type E thermocouples (T/C) in the prime mover. These T/C are connected to the temperature scanner [Ref 8] which is connected to a printer [Ref 9] that provides printouts of all thermocouple readings. Each heat exchanger assembly has a T/C soldered at the center of the longest heat exchanger plate, the inside heat exchanger wall, and the outside heat exchanger holder wall. These points are chosen to provide a temperature map of the heat exchanger behavior in the radial direction. The T/C at the ends of the stack are placed there for two reasons: to provide an axial temperature measurement across the stack, and to provide an axial temperature measurement between the stack and center of the heat exchangers. The rest of the T/C are used to monitor resonator temperatures.

2. Temperature Control Equipment

Control of the hot heat exchanger is achieved by a digital temperature controller [Ref 10], heater cartridges, and a power supply amplifier [Ref 11]. The reference temperature for the temperature controller is taken from a type J T/C placed between the hot heat exchanger holder and the heater clamp. The signal is processed and is sent via the temperature controller's 10 volt DC analog output to the mono input in the power supply amplifier.

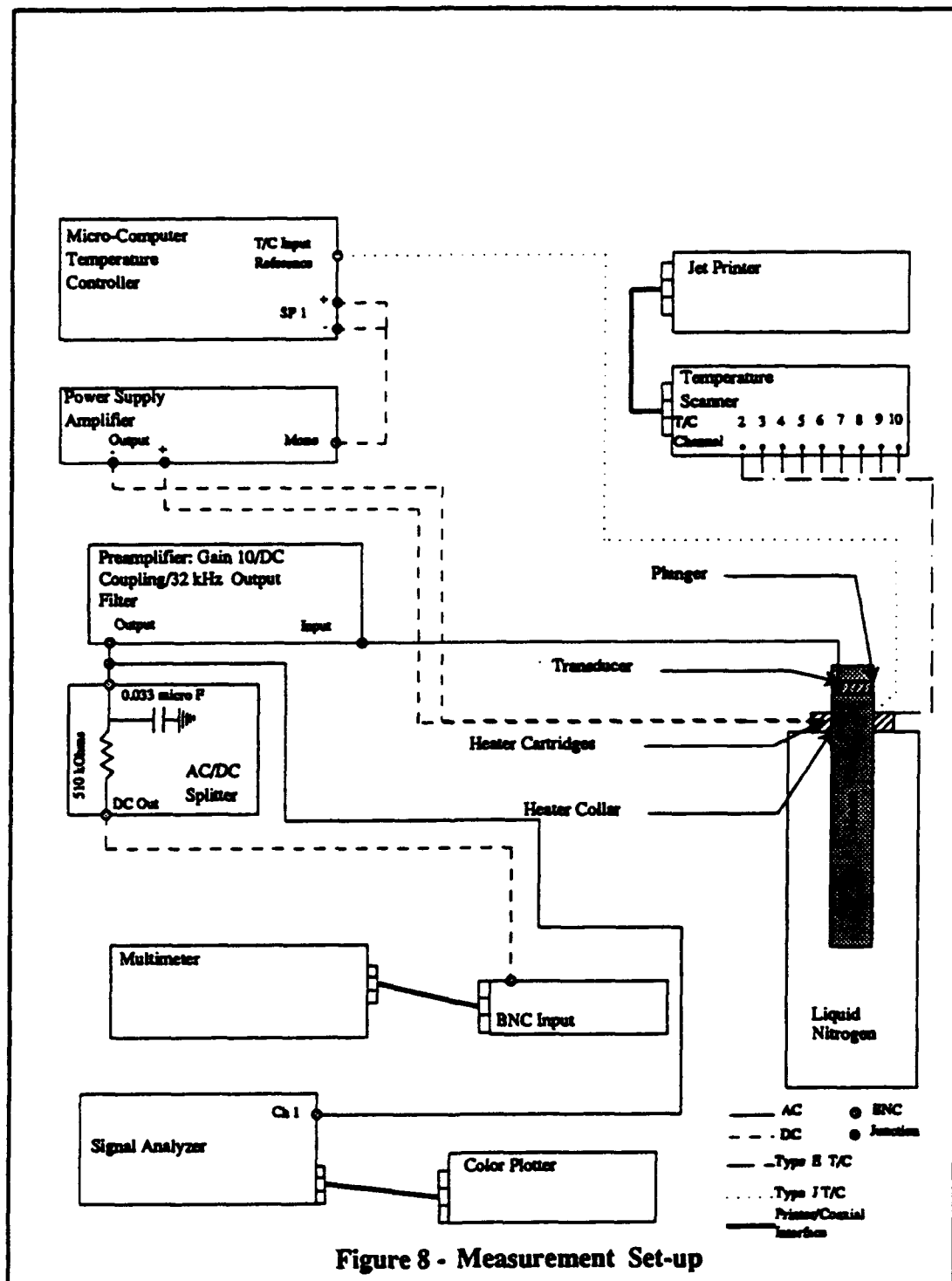
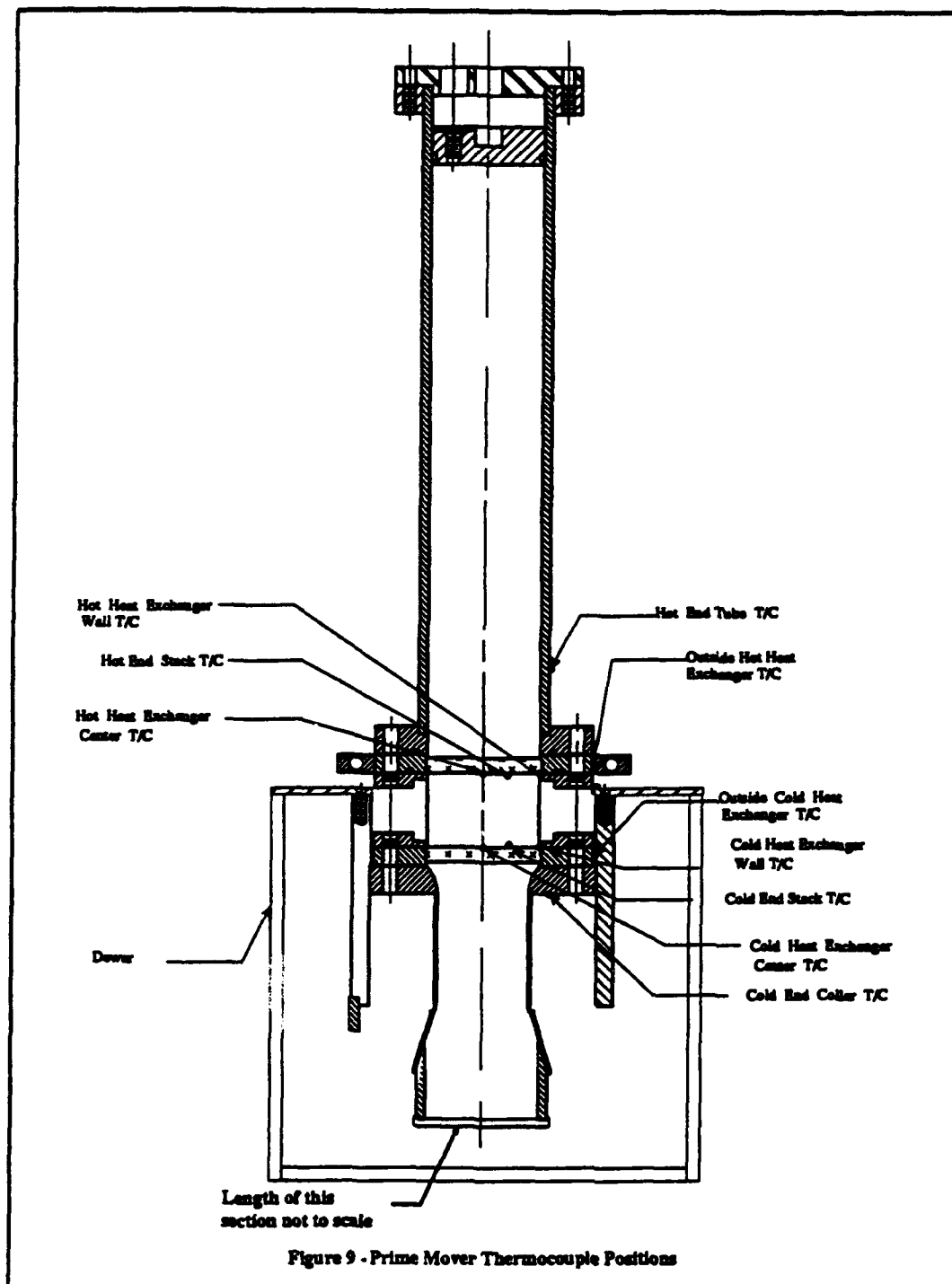


Figure 8 - Measurement Set-up



Power to the heater cartridges is provided by the output of the power supply amplifier. The heater cartridges are inserted into the copper heater collar. Once steady state thermal conditions are achieved in the experiment, the current and voltage delivered is approximately constant in time and can be measured in order to determine the heater power. We do not have a complete set of heater power measurements, because the heater controller circuitry was modified during the course of the experiment.

3. Pressure Measurement Equipment

The pressure amplitudes inside the prime mover are measured with a piezoresistive transducer [Ref 12] with a sensitivity of 16.38 mV/psi . The transducer is located on the prime mover plunger. The transducer senses absolute pressure and its zero offset was calibrated on a turbomolecular pump high vacuum system.

The transducer measures the mean pressure as a DC signal and the acoustic pressure amplitude as an AC signal, simultaneously. The transducer output is sent to a DC coupled preamplifier with a gain of 10 and a 32 kHz low-pass output filter. This output signal is split. One output is connected to channel 1 of the signal analyzer [Ref 13]. The signal analyzer displays the waveform and frequency spectrum of the AC component of the signal. These results are plotted on the color plotter [Ref 14]. The second output from the preamplifier is filtered to obtain a DC signal component by passing through a low-pass filter with a $0.033 \mu\text{F}$ capacitor and $510 \text{ k}\Omega$ resistor. This DC voltage signal is then measured with the multimeter [Ref 15]. This allows the pressure ratio, P_o/P_m , to be accurately measured with which gas displacement amplitudes, ξ , can be calculated.

C. PROCEDURE

Two main modifications were made to the original straight bore prime mover design to achieve the desired experimental characteristics. The first modification was to reduce the harmonic distortion in the resonator. The second modification was to improve the heat flow within the prime mover parts.

As discussed at the beginning of this chapter, the primary goal is to measure the pressure ratio, temperatures, and steady state spectrum for three heat exchanger lengths. The measurement technique employed is to drive the prime mover by placing as big of a temperature gradient as possible across the stack at specific mean pressures. The design goal is to have the temperature gradient be nearly equal for all measurements. The three different heat exchanger lengths serve to vary $\xi/\Delta x$, and the differing mean pressures, change δ_x and thus vary y_o/δ_x . The measurements consisted of two phases: prime mover below onset and above onset.

1. Harmonic Distortion Suppression

The experiment was started using a straight bore resonator of 3.81 cm in diameter. However, the harmonic distortion was unacceptable as shown in Figure 10. There was a severe discontinuity in the waveform that produces the multiple harmonics observed in the frequency spectrum.

Large amounts of harmonic distortion of driven plane standing waves in constant bore tubes is common at higher amplitudes. This readily occurs when driving at the fundamental frequency because the higher modes of the tube have frequencies that are nearly integer multiples of the fundamental. Any distortion component contained in the drive waveform or arising from nonlinear propagation of the wave in the tube can coincide with one of the higher mode resonant frequencies and be "amplified" by the quality factor of that mode.

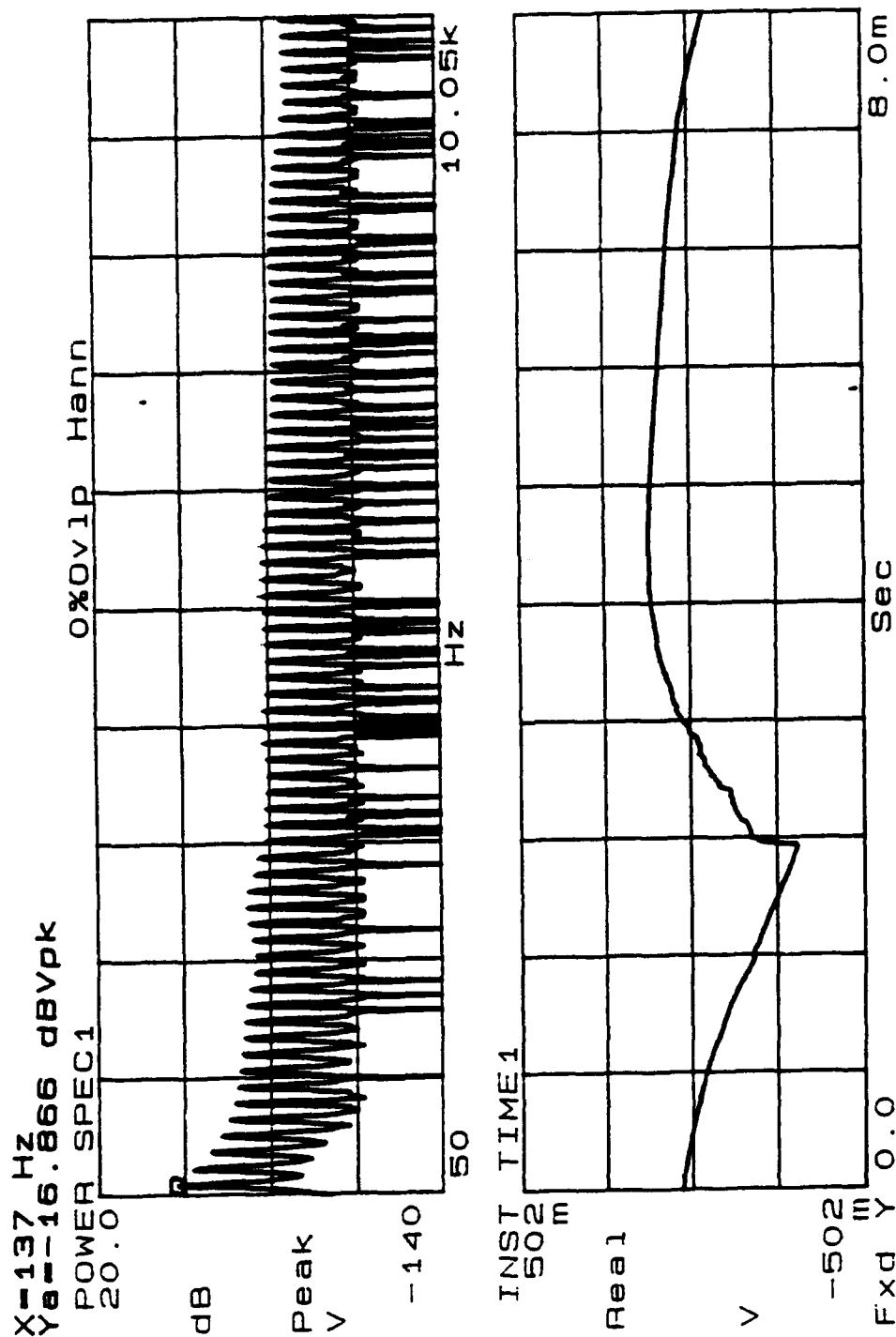


Figure 10 - Spectrum and waveform of the sound generated by the prime mover using a straight bore 3.81 cm diameter tube.

More advanced theories for this type of waveform distortion suggest that there is an interaction between the first and second harmonics that generates the third harmonic, and so on; the acoustic energy cascades up to the higher frequencies. If this is true, then by modifying the interaction between the first and second harmonics, all of the higher harmonics may be suppressed.

This can be accomplished by shifting the frequency of the second mode relative to the first so that it is not exactly a factor of two higher. Changes in the cross section of the tube can produce this type of frequency shift, and can be very effective in suppressing harmonic distortion. This type of approach has been used for conventional piston driven tubes and thermoacoustically driven prime movers [Ref 16]. However, the thermoacoustic prime mover is unique in that it may spontaneously oscillate at a higher mode as well as at the fundamental. Whether or not this can occur, is an issue that is distinct from the issue of acoustic energy cascading to higher modes and suppression by frequency shifting.

A computer model for the thermoacoustic heat engines has been developed by Hofler based on the linear ordinary differentials equations of Rott [Ref 3]. This model has recently been improved to handle tubes with arbitrary cross-section correctly. This was used to propagate acoustic wave solutions from a starting point at the plunger, through the resonator having both a temperature distribution and a cross-section profile, and stopping at the cold termination. An arbitrary frequency is assumed at the beginning. While the acoustic boundary conditions are properly matched at the rigid plunger initially, the final boundary conditions at the cold termination are not generally satisfied because linear equations are being used to model a nonlinear system.

At the rigid cold termination, the calculated acoustic work flow is generally not zero (as it must be in a real system) and this quantity can be interpreted as a thermoacoustic drive result. If it is positive, then the system will spontaneously oscillate at that modal frequency and if it is negative, then the mode will be damped. The frequencies of the modes can be determined by a peak in the magnitude of the acoustic impedance or by the imaginary part (i.e., the reactive part) of the impedance going to zero.

A frequency sweep of this type of computation is shown in Figure 11 for the prime mover with 3.81 *cm* and 3.17 *cm* bores. The first three modes can be seen from the solid curve representing the impedance magnitude. Note that the frequency of the second mode is somewhat higher than twice the first, although the frequency of the third mode is about three times the first. The height of the peaks is not important. The dashed curve shows that the work flow is positive for both the first and second modes, but negative for the third. This means that there will be substantial second harmonic distortion regardless of the frequency of the second mode.

To speed up the computational investigation, only the results at the peaks of the first three modes was generated. The frequencies of the first three peaks and work flows at those frequencies were generated for various resonator geometries having the original 3.81 *cm* and 3.17 *cm* diameters, but with a new larger third diameter at the cold end. The diameters investigated were 3.81, 4.45, and 5.08 *cm*. The length of the new tube section was a second variable.

These results are shown in Figure 12. The x-axis is the frequency normalized with respect to the fundamental. The two 4.45 *cm* diameter data points represent different lengths. Note that while both the 4.45 and 5.08 *cm* diameter tube segments shift the frequencies of the second and third modes substantially, only the 5.08 *cm* diameter tube segment causes the work flow to be negative at the second mode. If the second mode is damped and its frequency is substantially shifted from twice the fundamental, the harmonic distortion should be substantially suppressed.

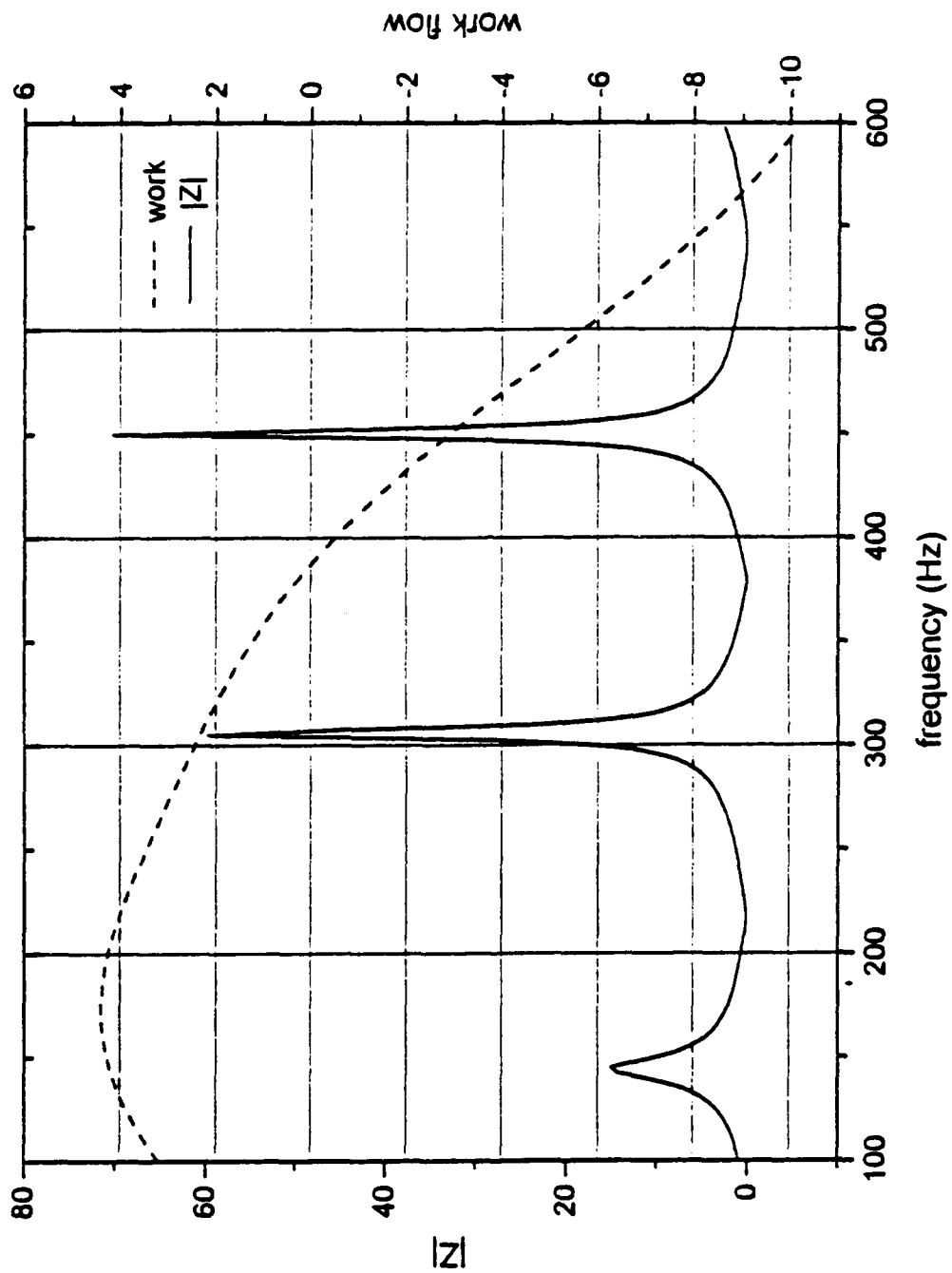


Figure 11 - Impedance and work flow at cold termination.

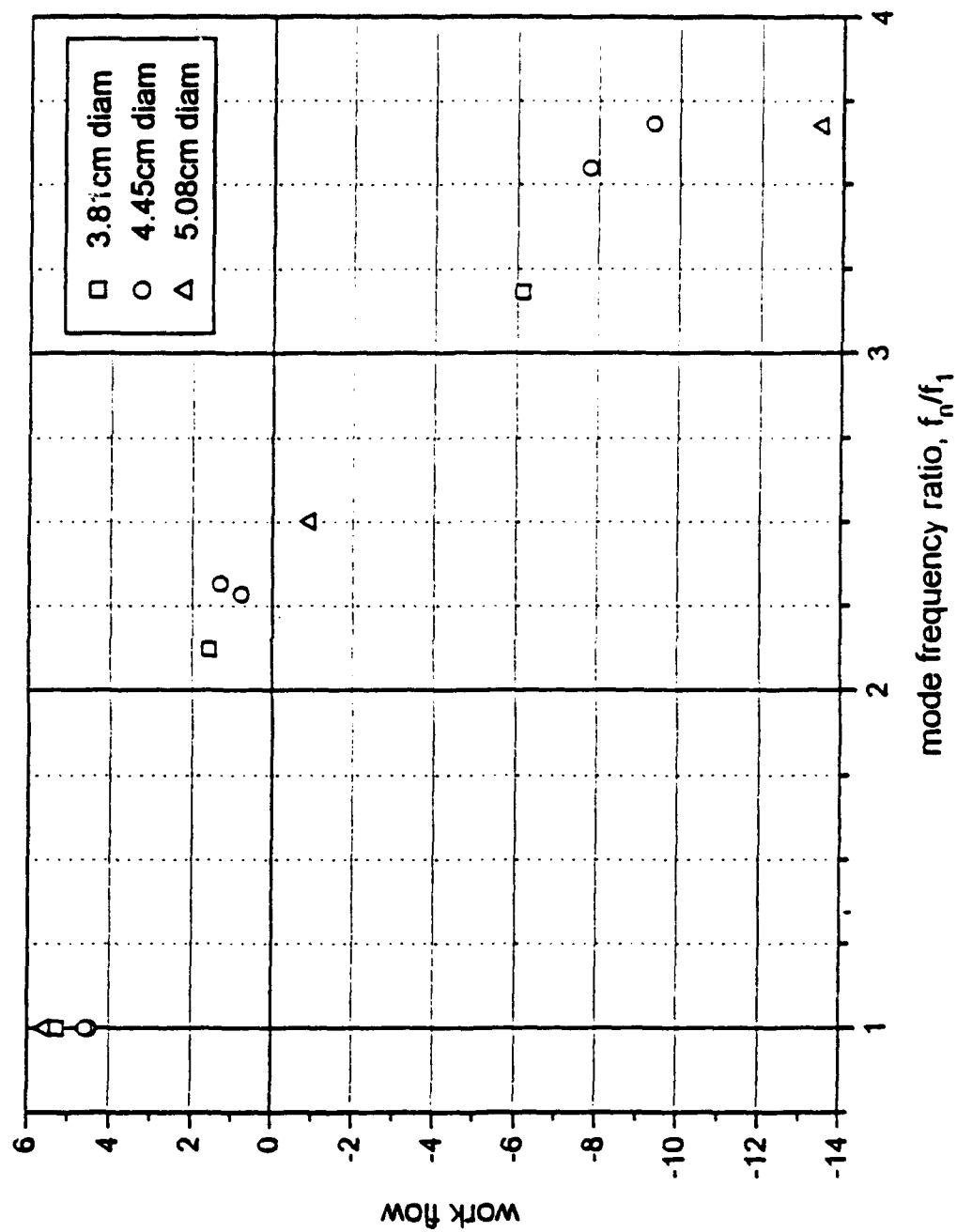


Figure 12 - Modes with three cold end diameters.

From the computer simulation results, geometric changes were done in the prime mover to reduce the harmonic distortion. First, the cold end resonator diameter was reduced from 3.81 *cm* to 3.17 *cm*. The waveform and frequency spectrum remained basically unchanged from the straight bore configuration.

The next step was to have two changes in the diameter of the cold end from 3.81 *cm* to 3.17 *cm* and back to 3.81 *cm*. This new geometry generated the sound waveform and spectrum shown in Figure 13. The discontinuity in the waveform was less dramatic in this prime mover configuration.

The final configuration used for this experiment is the one shown in Figure 3 of Chapter III, where the diameter of the resonator was decreased from 3.81 *cm* to 3.17 *cm* and then increased to 5.08 *cm*. Appendix B shows the smooth sinusoidal waveforms and the spectra of the sound generated by the prime mover above onset at a 8.128 *cm* plunger position.

2. Heat Flow Modifications

The goal was to have the cold and hot heat exchanger temperatures to remain constant through this experiment. However, after the first experimental trial, it was observed that the heat exchanger temperatures were not constant. As a result, several modifications were performed. Again, drawings and specifications for the prime mover parts are provided in Appendix A.

Originally, heat was supplied by a nozzle heater clamped around the hot end tube just above the attachment plate. This heater was replaced with a heater collar clamped around the hot heat exchanger holder. This provides a constant supply of heat source going into the prime mover. The conductance of heat is improved by applying a silicone heat sink compound [Ref 17] at the side of the hot heat exchanger holder that faces the upper attachment plate. This modification worked fairly well in keeping the hot end of the prime mover at close to ambient temperature.

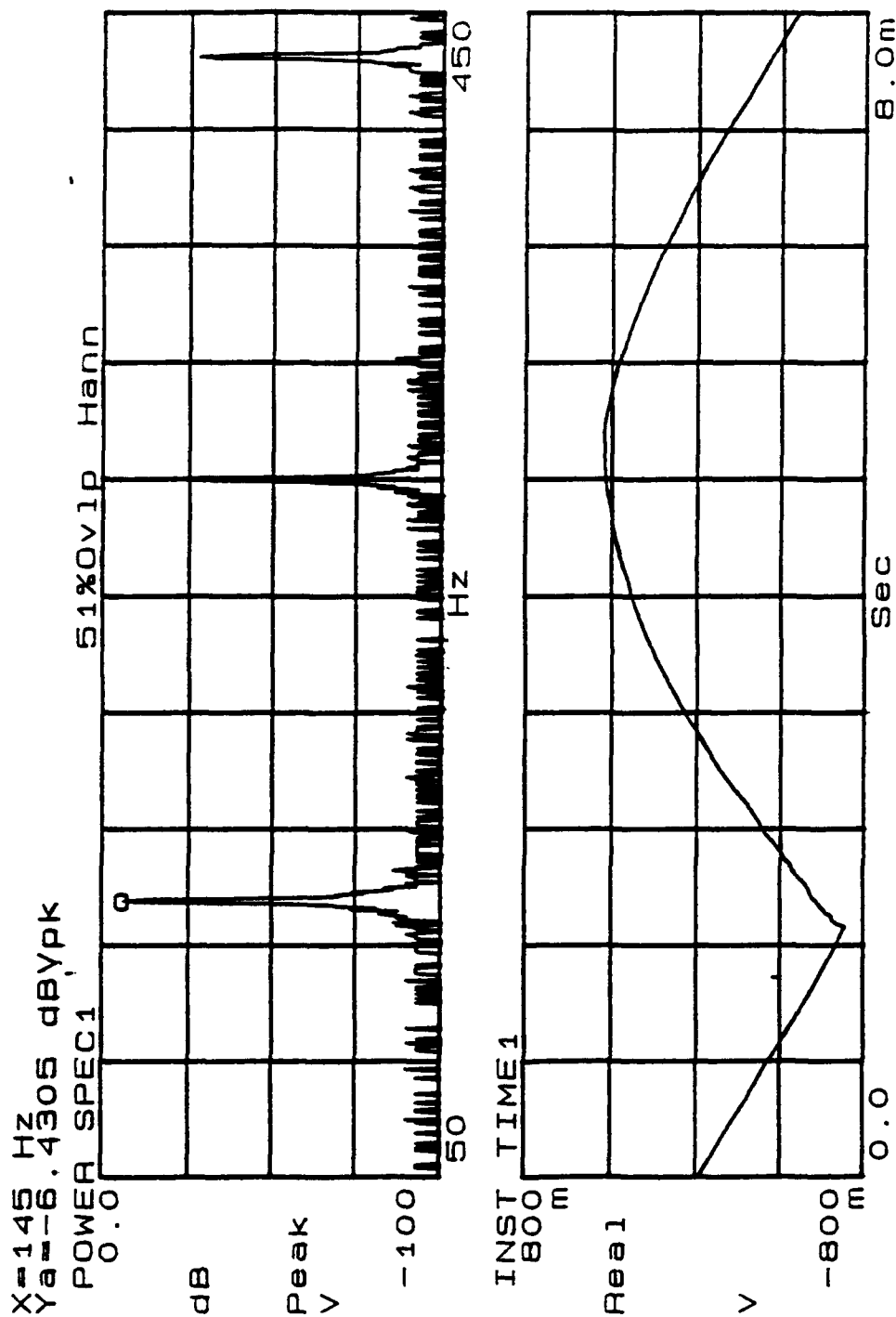


Figure 13 - Spectrum and waveform of the sound generated by
 the prime mover using a 3.81 to 3.17 cm
 diameter tube configuration.

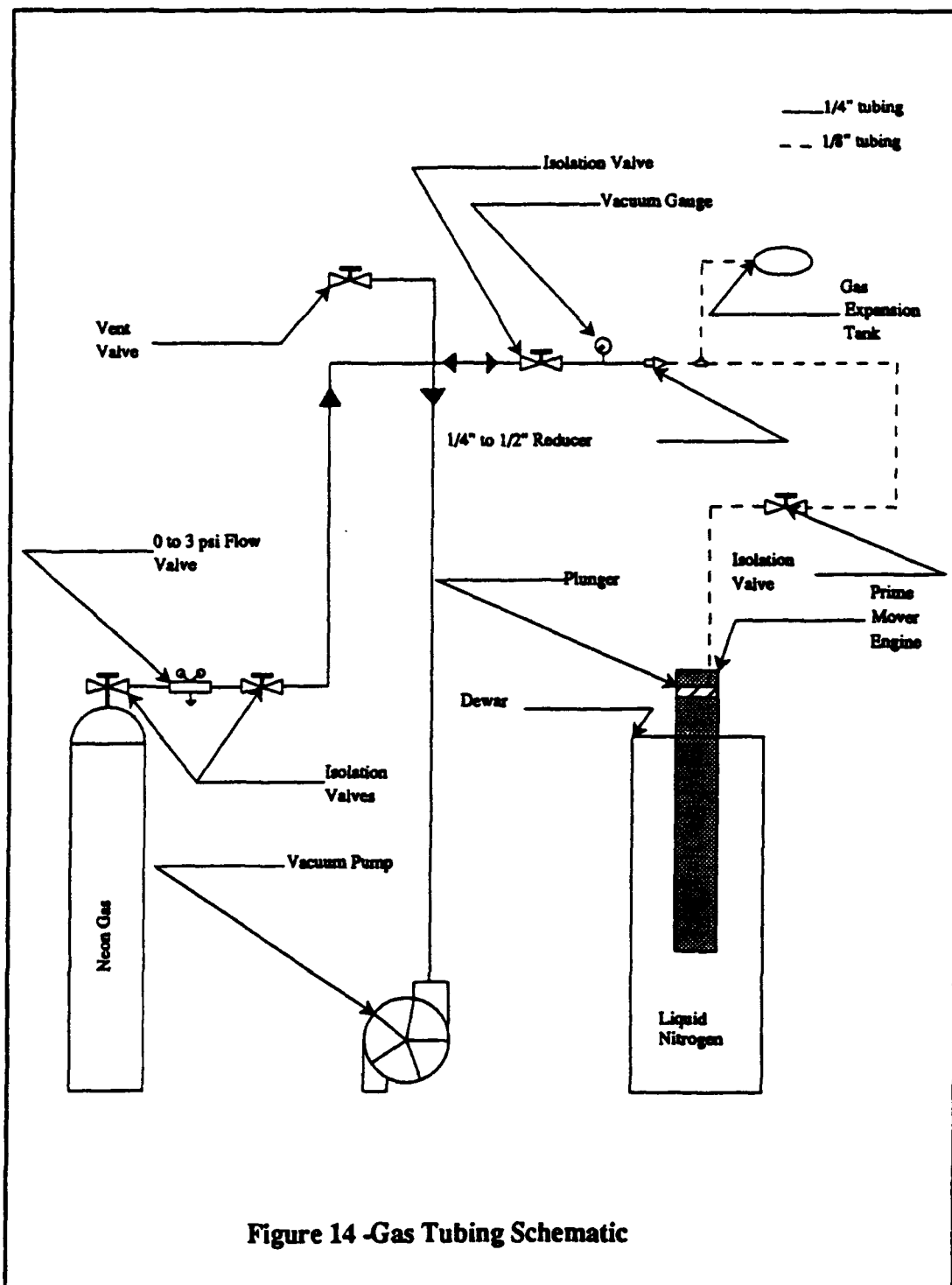
The heat flow into the cold heat exchanger was improved by increasing the surface area in contact with the liquid nitrogen. The cold heat exchanger copper skirt was modified to fit four copper skirt fingers. The conduction between the fingers and the skirt is improved by applying silicone heat sink compound between them. The thermal conductance between the cold heat exchanger holder and the lower reducer flange is improved by replacing the original teflon gasket with a conducting lead wire that is crushed between the two flanges.

Lastly, the stack holder is insulated from the ambient air and the hot end of the prime mover. The hot end tube and hot heat exchanger assemblies are insulated from the stack holder by wrapping them with fiberglass cloth. This increases the heat flux going into the hot heat exchanger, instead of the environment. Also, the cold end of the prime mover is insulated from the stack and the hot end of the prime mover by covering the dewar support and cold end skirt exposed to the environment with fiberglass cloth.

3. The Prime Mover Below Onset

The first phase of this experiment consists of measuring the thermal load of the prime mover below onset. Figure 14 shows the gas tubing schematic. The prime mover is pumped down using the vacuum pump to approximately 7 kPa and filled back with neon to approximately 110 kPa. This procedure is performed three times to ensure the gas inside the prime mover is substantially pure neon.

The prime mover is then pumped down to approximately 1.5 kPa. The prime mover is below onset at this pressure. The hot heat exchanger electric heater temperature is set at 25 °C and the dewar is filled with liquid nitrogen. The hot end tube assembly and the hot heat exchanger collar are insulated from the room environment by covering it with fiberglass cloth. After thermal equilibrium is reached,



the prime mover temperatures are obtained from the temperature scanner. This procedure is repeated for each heat exchanger length. Also, the electric power delivered to the heater can be measured with zero thermoacoustic heat transport. This power represents a nuisance heat leak to the colder parts below.

4. The Prime Mover Above Onset

The second phase consists of measuring the temperatures, the pressure ratio, and steady state waveform for two plunger positions at four mean pressures above onset. The hot heat exchanger electric heater temperature is set to 35°C , so at higher mean pressures the temperature in the wall of the hot heat exchanger does not drop below freezing. The plunger positions are measured from lower face of the plunger to the hot end of the stack. The two plunger positions used are 8.13 *cm* and 10.66 *cm*. The pressure is increased by using the low pressure flow valve to gradually fill the prime mover with neon to the selected pressures. The measurements are taken at mean pressures of approximately 8.8, 10.9, 27.6, and 50 *kPa*.

After the prime mover reaches steady state, the prime mover temperatures are obtained from the temperature scanner. The acoustic pressure amplitude and steady state frequency response are obtained from the signal analyzer. The mean pressure is obtained from the multimeter. This procedure is repeated for each heat exchanger length.

IV. RESULTS AND DISCUSSIONS

The results of the experiment are presented and discussed in this chapter. The results for the pressure ratios, the temperatures, the penetration depths, and the displacement amplitudes generated in the prime mover are presented for each heat exchanger length.

Figure 15 shows the ratio of the acoustic pressure amplitude of the fundamental component to the mean gas pressure in percent versus mean gas pressure for each heat exchanger length at two plunger positions. Table 1 shows the temperatures in the prime mover for each heat exchanger length at the selected experimental mean gas pressures for two plunger positions. Figure 16 shows the ratio of the center hot heat exchanger temperature to the center cold heat exchanger temperature versus mean gas pressure for each heat exchanger length. Figures 17 and 18 show the ratio of the heat exchanger and stack half plate separation to the thermal penetration depth versus mean gas pressure for each heat exchanger length. Figure 19 shows the ratio of the peak displacement amplitude at the midpoint of the element to the stack and heat exchanger length versus mean gas pressure for each heat exchanger length.

A. THE 0.257 cm HEAT EXCHANGER

The first mode acoustic pressure amplitudes are 1.082, 1.791, 5.366, and 8.84 kPa at mean gas pressures of 8.794, 10.92, 27.62, and 50.12 kPa, respectively. As shown in Figure 15, these amplitudes correspond to 12.3, 16.5, 19.4, and 17.6% of mean gas pressure. The first mode acoustic pressure amplitudes for a 10.688 cm plunger position are 0.749, 1.532, 5.021, and 8.05 kPa at mean gas pressures of 8.69, 10.81, 27.44, and 49.7 kPa, respectively. As shown in Figure 15, these amplitudes correspond to 8.62, 14.2, 18.3, and 16.2% of mean gas pressure.

From Table 1, the temperature differences across the stack vary from 172.7 to 77.8 °C, from the lowest to the highest mean gas pressure. These temperatures correspond to temperature differences from the wall to the center of the cold heat exchanger of 2.4 to 9.2 °C and temperature differences from the wall to the center of the hot heat exchanger of 3.9 to 32.5 °C.

As shown by Figure 16, the T_h / T_c ratios change from 3.51 to 2.02 for a 8.128 cm plunger position. This represents a T_h / T_c ratio decrease of 42% from the lowest to the highest mean gas pressure. The T_h / T_c ratios change from 3.53 to 1.97 for a 10.688 cm plunger position. This represents a T_h / T_c ratio decrease of 44% from the lowest to the highest mean gas pressure.

For purposes of reducing the experimental data, the thermal penetration depth is obtained for each pressure and frequency by using Equation [2],

$$\delta_x = \sqrt{\frac{\kappa}{\pi f \rho c_p}}. \quad [2]$$

Now, the relation $\rho c_p = \gamma P_m / T_m (\gamma - 1)$ and $T_m = 296$ K are substituted into Equation [2] to obtain,

$$\delta_x(T_m) = \sqrt{\frac{\kappa (\gamma - 1) T_m}{\pi f \gamma P_m}}. \quad [3]$$

For neon at 296 K, $\kappa = 0.0493$ W/m K. Then the thermal penetration depth is obtained for each temperature, for its respective pressure and frequency, by using Equation [4],

$$\delta_x(T_m) = \delta_x(296 \text{ K}) \left(T_m / 296 \right)^{\frac{(1 + \beta)}{2}}. \quad [4]$$

For neon, $\beta = 0.66$.

From Figure 17, the y_o / δ_x ratios for the cold heat exchanger change from 0.638 to 1.066. The thermal penetration depth change is caused by the decreasing T_h / T_c ratio and the increasing temperature in the cold heat exchanger with increasing mean pressure. This represents a y_o / δ_x ratio increase of 67% from the lowest to the highest

mean gas pressure. The y_o/δ_x ratios for the hot heat exchanger change from 0.224 to 0.594. This represents a y_o/δ_x ratio increase of 165% from the lowest to the highest mean gas pressure. From Figure 18, the y_o/δ_x ratios for the stack change from 0.56 to 1.234. This represents a y_o/δ_x ratio increase of 120% from the lowest to the highest mean gas pressure.

The displacement amplitude is calculated using Equation [2]. From Figure 19, the $\xi_{hx}/\Delta x_{hx}$ ratios for the cold heat exchanger change from 3.11 to 4.45, from the lowest to the highest mean gas pressure. The peak displacement amplitudes are as much as five times the heat exchanger length! For the hot heat exchanger, the $\xi_{hx}/\Delta x_{hx}$ ratios change from 2.25 to 3.21, from the lowest to the highest mean gas pressure. Note: the peak displacement amplitudes are as much as three and one-half times the heat exchanger length! For the stack, the $\xi_s/\Delta x_s$ ratios change from 0.27 to 0.39, from the lowest to the highest mean gas pressure. The peak-to-peak displacement amplitudes, except for the lowest pressure, are nearly as long as the stack length!

B. THE 0.569 cm HEAT EXCHANGER

The first mode acoustic pressure amplitudes are 0.398, 1.21, 4.65, and 9.0 kPa at mean gas pressures of 8.82, 10.91, 27.81, and 50.16 kPa, respectively. As shown in Figure 15, these amplitudes correspond to 4.5, 11.1, 16.7, and 17.9% of mean gas pressure. The first mode acoustic pressure amplitudes at a 10.688 cm plunger position are 0.885, 3.32, and 7.46 kPa at mean gas pressures of 10.77, 27.42, and 49.53 kPa, respectively. As shown in Figure 15, these amplitudes correspond to 8.2, 12.1, and 15.1% of mean gas pressure.

From Table 1, the temperature differences across the stack are from 186.3 to 65.4 °C, from the lowest to the highest mean gas pressure. These temperatures correspond to temperature differences from the wall to the center of the cold heat exchanger of 0.6 to 28.5 °C and temperature differences from the wall to the center of the hot heat exchanger of 0 to 12.4 °C.

As shown by Figure 16, the T_h / T_c ratios change from 3.59 to 1.67 for a 8.128 cm plunger position. This represents a T_h / T_c ratio decrease of 53% from the lowest to the highest mean gas pressure. The T_h / T_c ratios change from 3.70 to 1.62 for a 10.688 cm plunger position. This represents a T_h / T_c ratio decrease of 56% from the lowest to the highest mean gas pressure.

From Figure 17, the y_o / δ_x ratios for the cold heat exchanger change from 0.645 to 0.872. This represents a y_o / δ_x ratio increase of 35% from the lowest to the highest mean gas pressure. The y_o / δ_x ratios for the hot heat exchanger change from 0.223 to 0.574. This represents a y_o / δ_x ratio increase of 157% from the lowest to the highest mean gas pressure. From Figure 18, the y_o / δ_x ratios for the stack change from 0.559 to 1.154. This represents a y_o / δ_x ratio increase of 106% from the lowest to the highest mean gas pressure.

From Figure 19, the $\xi_{hx} / \Delta x_{hx}$ ratios for the cold heat exchanger change from 0.523 to 2.08, from the lowest to the highest mean gas pressure. The peak displacement amplitudes are as much as two times the heat exchanger length. For the hot heat exchanger, the $\xi_{hx} / \Delta x_{hx}$ ratios change from 0.373 to 1.484, from the lowest to the highest mean gas pressure. The peak displacement amplitudes are as much as one and one-half times the heat exchanger length. For the stack, the $\xi_s / \Delta x_s$ ratios change from 0.099 to 0.396, from the lowest to the highest mean gas pressure. The peak-to-peak displacement amplitudes, except for the lowest pressure, are as long as the stack length.

C. THE 0.820 cm HEAT EXCHANGER

The first mode acoustic pressure amplitudes are 0.74, 1.944, 7.07, and 13.68 kPa at mean gas pressures of 8.814, 10.898, 27.62, and 49.95 kPa, respectively. As shown in Figure 15, these amplitudes correspond to 8.39, 17.8, 25.5, and 27.3% of mean gas pressure. The first mode acoustic pressure amplitudes at a 10.688 cm plunger position are 1.385, 6.355, and 11.36 kPa at mean gas pressures of 10.668, 27.287, and 48.966 kPa, respectively. As shown in Figure 15, these amplitudes correspond to 12.98, 23.3, and 23.2% of mean gas pressure.

From Table 1, the temperature differences across the stack are from 176 to 73.2 °C, from the lowest to the highest mean gas pressure. These temperatures correspond to temperature differences from the wall to the center of the cold heat exchanger of 0.9 to 13.7 °C and temperature differences from the wall to the center of the hot heat exchanger of 0 to 24.9 °C.

As shown by Figure 16, the T_h / T_c ratios change from 3.71 to 2.22 for a 8.128 cm plunger position. This represents a T_h / T_c ratio decrease of 40% from the lowest to the highest mean gas pressure. The T_h / T_c ratios change from 3.76 to 2.164 for a 10.688 cm plunger position. This represents a T_h / T_c ratio decrease of 42% from the lowest to the highest mean gas pressure.

From Figure 17, the y_o / δ_x ratios for the cold heat exchanger change from 0.661 to 1.124. This represents a y_o / δ_x ratio increase of 88% from the lowest to the highest mean gas pressure. The y_o / δ_x ratios for the hot heat exchanger change from 0.222 to 0.579. This represents a y_o / δ_x ratio increase of 161% from the lowest to the highest mean gas pressure. From Figure 18, the y_o / δ_x ratios for the stack change from 0.563 to 1.252. This represents a y_o / δ_x ratio increase of 122% from the lowest to the highest mean gas pressure.

From Figure 19, the $\xi_{hx} / \Delta x_{hx}$ ratios for the cold heat exchanger change from 0.684 to 2.224, from the lowest to the highest mean gas pressure. The peak displacement amplitudes are as much as two times the heat exchanger length. Also, the peak-to-peak displacement amplitude at the lowest pressure is as long as the heat exchanger length. For the hot heat exchanger, the $\xi_{hx} / \Delta x_{hx}$ ratios change from 0.473 to 1.541, from the lowest to the highest mean gas pressure. The peak displacement amplitudes are as much as one and one-half times the heat exchanger length. Again, the peak-to-peak displacement amplitude at the lowest pressure is as long as the heat exchanger length. For the stack, the $\xi_s / \Delta x_s$ ratios change from 0.186 to 0.604, from the lowest to the highest mean gas pressure. The peak-to-peak displacement amplitudes, except for the lowest pressure, are as long as the stack length.

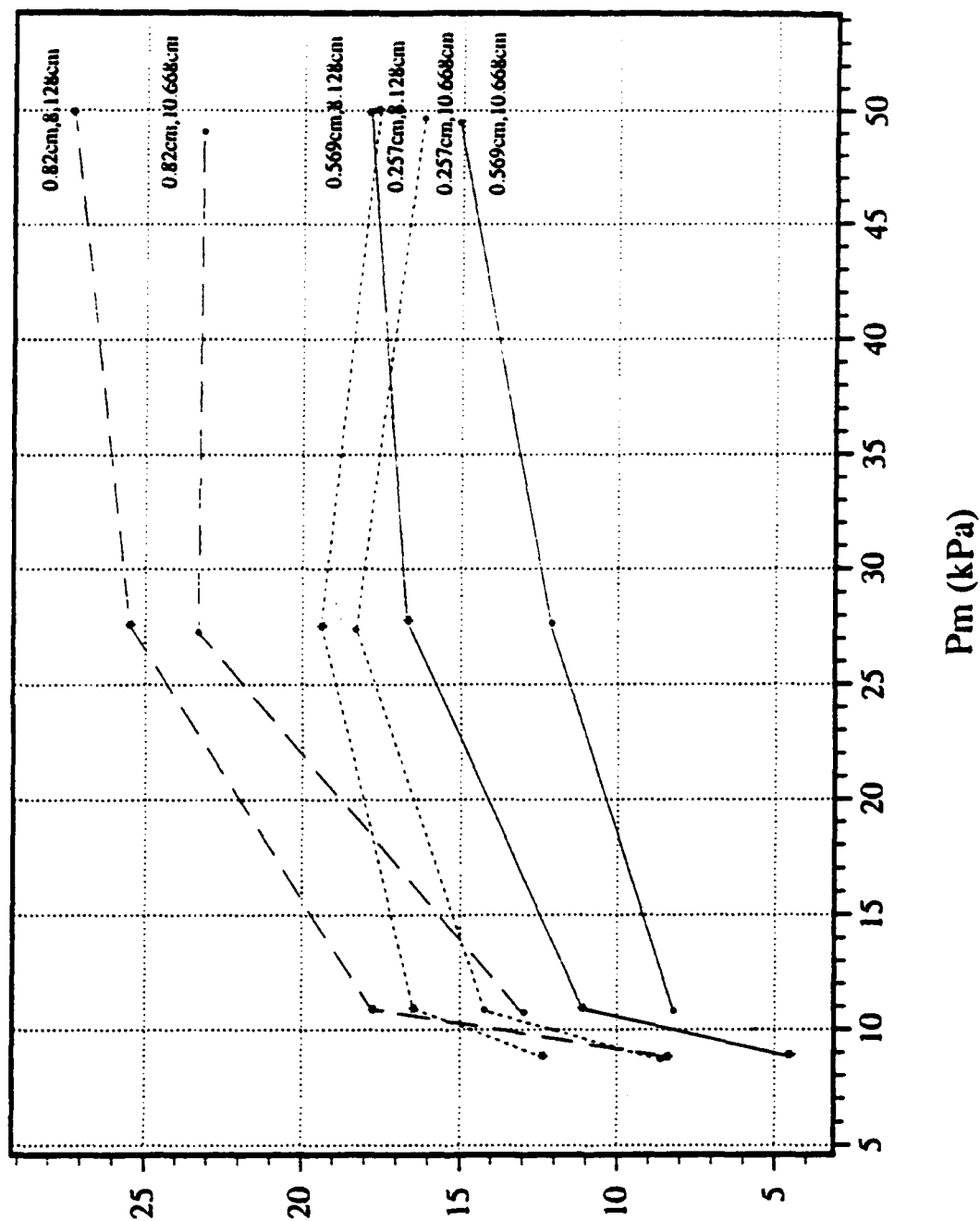


Figure 15 - Ratio of acoustic pressure amplitude to mean gas pressure versus mean gas pressure.

TABLE 1 - PRIME MOVER THERMAL LOAD FOR EACH HEAT EXCHANGER LENGTH AT DESIGNATED MEAN PRESSURES AND PLUNGER POSITIONS.

Mean Pressure	Set At	1.5 MPa	0.0 MPa	10.0 MPa					
Plunger	Distance--	0.128 cm							
Cold Hs Length (cm)		0.257	0.599	0.82					
Hot Hs Length (cm)		0.253	0.599	0.82					
Mean pressure (MPa)		1.428	1.42	1.793					
Acoustic Pressure (MPa)		0	0	0					
Frequency (Hz)		0	0	0					
Prime Mover	Temperatures (Centigrade)								
Cold End		-191.7	-191.6	-191.5					
Cold Hs	Outside	-191.7	-191.7	-191.2					
Cold Hs	Wall	-191.5	-191.4	-191.4					
Cold Hs	Center	-190.8	-188.2	-190.8					
Cold End	Stack	-188.7	-188.1	-188.8					
Hot End	Stack	1.6	2.3	-1.3					
Hot Hs	Center	20.4	20.1	21.3					
Hot Hs	Wall	21.1	20.1	21.7					
Hot Hs	Outside	21.3	20	21.4					
Hot End	Tube	21.2	20.7	21.7					
Plunger	Distance--	10.000 cm							
Cold Hs Length (cm)		0.257	0.599	0.82					
Hot Hs Length (cm)		0.253	0.599	0.82					
Mean pressure (MPa)		0.899	0.784	0.7					
Acoustic Pressure (MPa)		0.749	0	0					
Frequency (Hz)		166.16	0	0					
Prime Mover	Temperatures (Centigrade)								
Cold End		-191.4	-191.7	-191.6					
Cold Hs	Outside	-191.1	-191.0	-191.4					
Cold Hs	Wall	-189.1	-190.6	-191.6					
Cold Hs	Center	-188.9	-190	-191					
Cold End	Stack	-170.7	-176.7	-164.6					
Hot End	Stack	3.6	6.6	12.1					
Hot Hs	Center	31.3	34.3	35.4					
Hot Hs	Wall	34.9	34.3	35.9					
Hot Hs	Outside	36.7	35	35.9					
Hot End	Tube	36.4	34	34.6					

TABLE 1 - PRIME MOVER THERMAL LOAD FOR EACH HEAT EXCHANGER LENGTH AT DESIGNATED MEAN PRESSURES AND PLUNGER POSITIONS. (CONTINUED)

Mean Pressure	Sat. At	8.128 cm	27.6 kPa	50 kPa	
Plunger Distance--					
Cold Hs Length (cm)	0.257	0.569	0.82	0.257	0.569
Hot Hs Length (cm)	0.253	0.569	0.82	0.253	0.569
Mean pressure (kPa)	27.42	27.61	27.62	50.12	50.16
Acoustic Pressure (kPa)	5.368	4.85	7.07	8.84	8
Frequency (Hz)	184.45	163.87	188.41	161.72	163.87
Prime Mover Temperatures (Centigrade)					
Cold End Cooler	-190.5	-190.5	-189.7	-190.2	-190.3
Cold Hs Outside	-188.2	-189.8	-184.4	-188.8	-188.1
Cold Hs Wall	-183.8	-180.2	-178.6	-184.8	-180.1
Cold Hs Center	-188.1	-129.3	-187.1	-148.3	-110.6
Cold End Stack	-124.8	-109.4	-126.7	-112.6	-91.9
Hot End Stack	-24.1	-12.7	-29.7	-34.8	-22.3
Hot Hs Center	0.3	10.1	8.7	-14.8	-3.9
Hot Hs Wall	24.1	18.4	26.3	17.7	6
Hot Hs Outside	38	35.1	36.8	37.6	35.4
Hot End Tube	34.3	33.8	35.3	33.4	32.7
Plunger Distance--					
Cold Hs Length (cm)	0.257	0.569	0.82	0.257	0.569
Hot Hs Length (cm)	0.253	0.569	0.82	0.253	0.569
Mean pressure (kPa)	27.44	27.42	27.287	49.7	49.53
Acoustic Pressure (kPa)	5.021	3.32	6.355	8.05	7.48
Frequency (Hz)	188.78	188.78	181.82	165.47	165.47
Prime Mover Temperatures (Centigrade)					
Cold End Cooler	-190.5	-190.5	-189.7	-190.2	-190.2
Cold Hs Outside	-187.8	-189.7	-186	-186.6	-188.8
Cold Hs Wall	-182.8	-149.1	-178	-162.8	-135.8
Cold Hs Center	-186.7	-126.8	-166.9	-143.3	-107.3
Cold End Stack	-121.6	-107.5	-124.6	-108	-88.4
Hot End Stack	-24.8	-12.5	-30.6	-38.3	-23
Hot Hs Center	-1	9.7	8.1	-17.4	-6.2
Hot Hs Wall	23.3	18.1	24.8	16.7	7.2
Hot Hs Outside	38	34.7	34.2	37.6	34.7
Hot End Tube	34.2	33.7	35	33.2	32.7

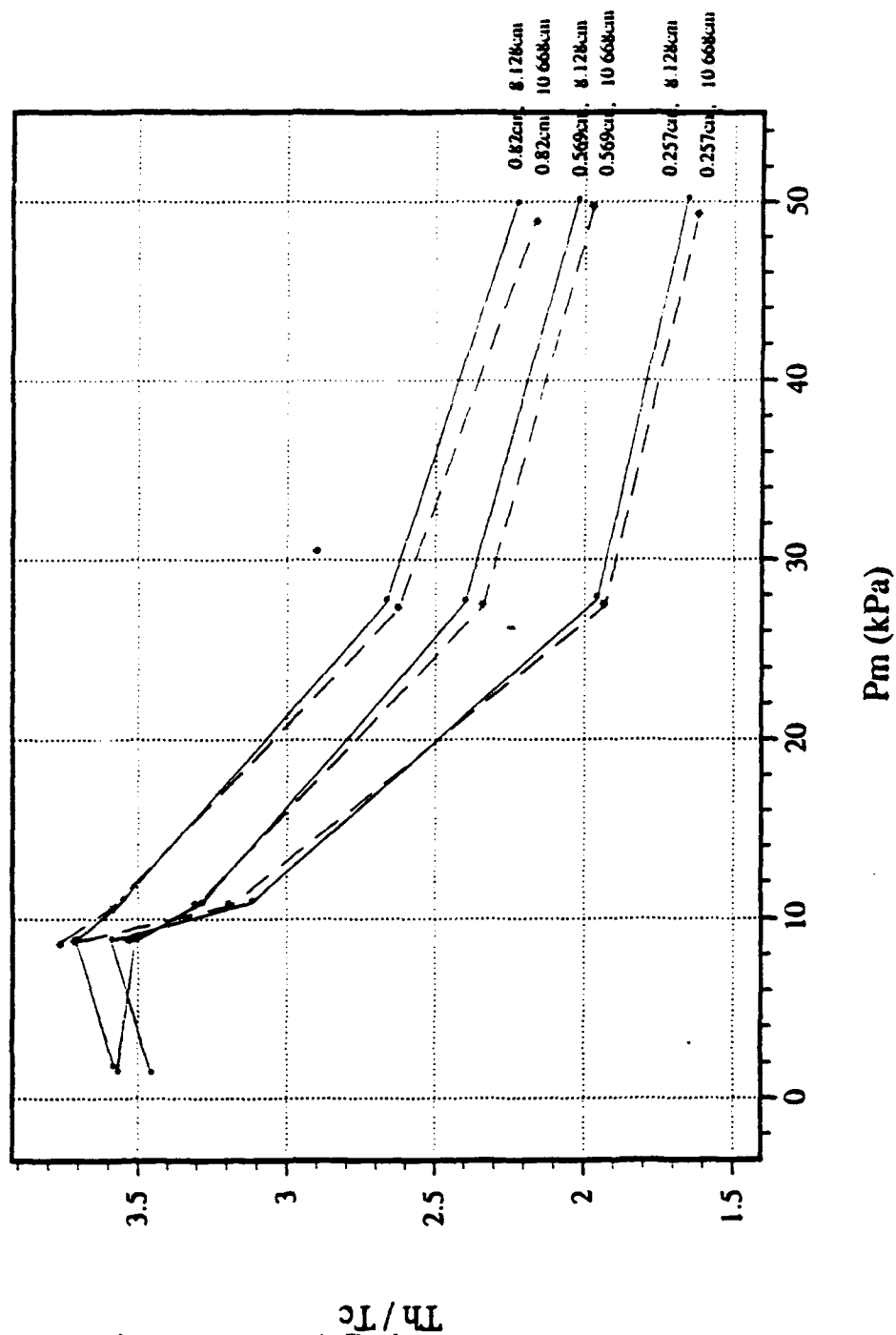


Figure 16 - Ratio of center of hot heat exchanger temperature to center center cold heat exchanger temperature versus mean gas pressure.

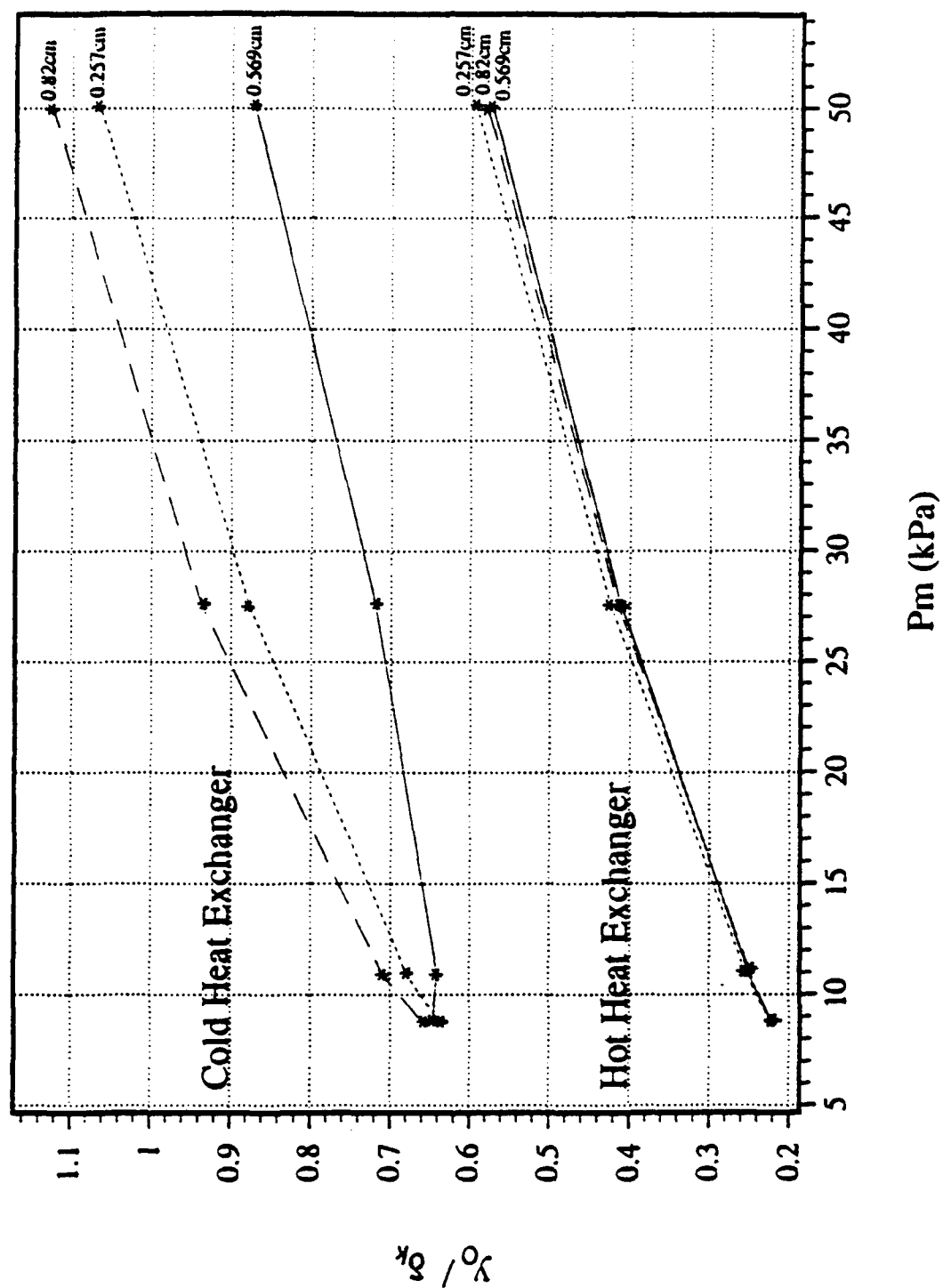


Figure 17- Ratio of heat exchanger plate half separation to thermal penetration depth versus mean gas pressure.

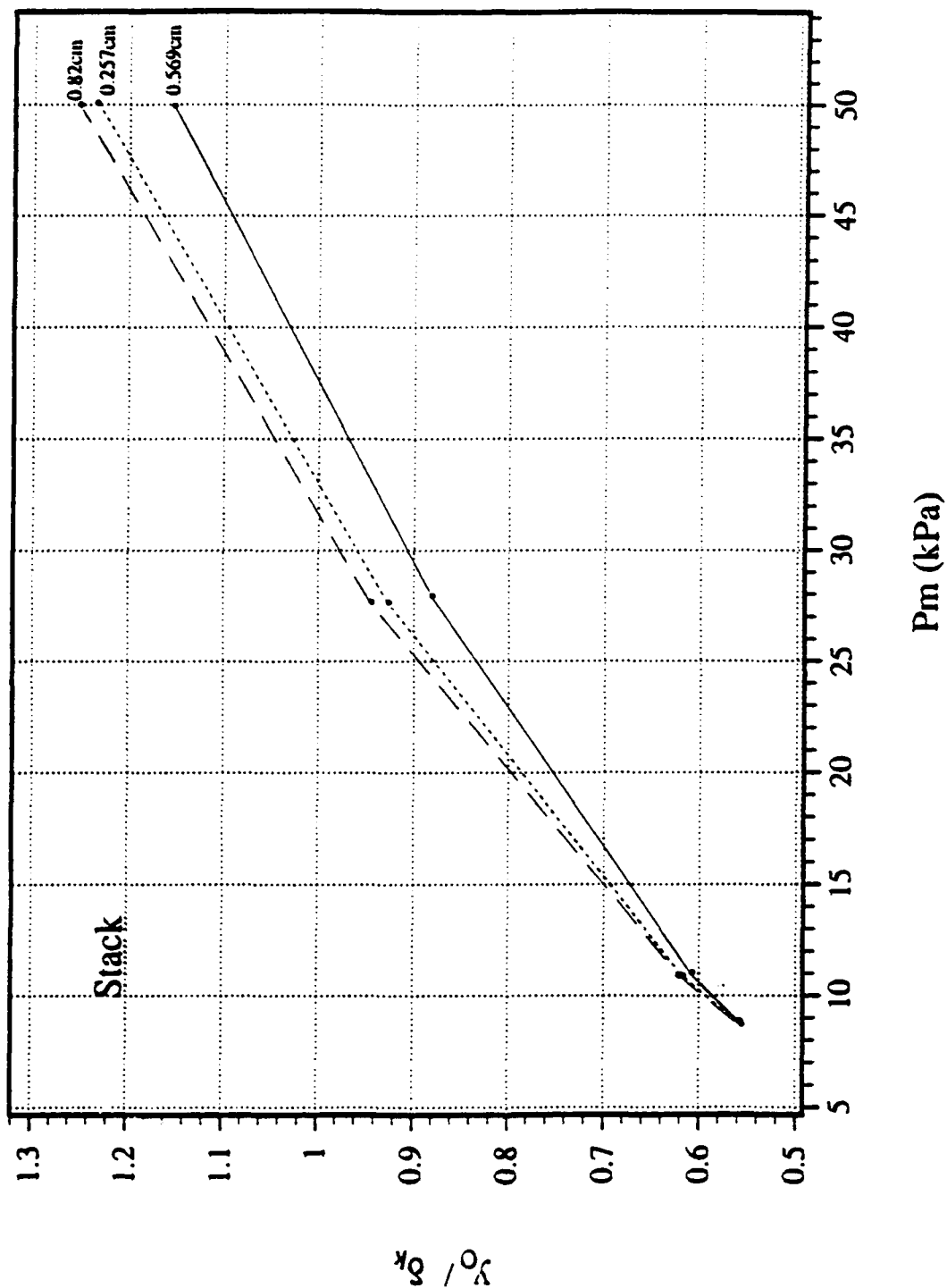


Figure 18 - Ratio of heat exchanger plate half separation to thermal penetration depth versus mean gas pressure.

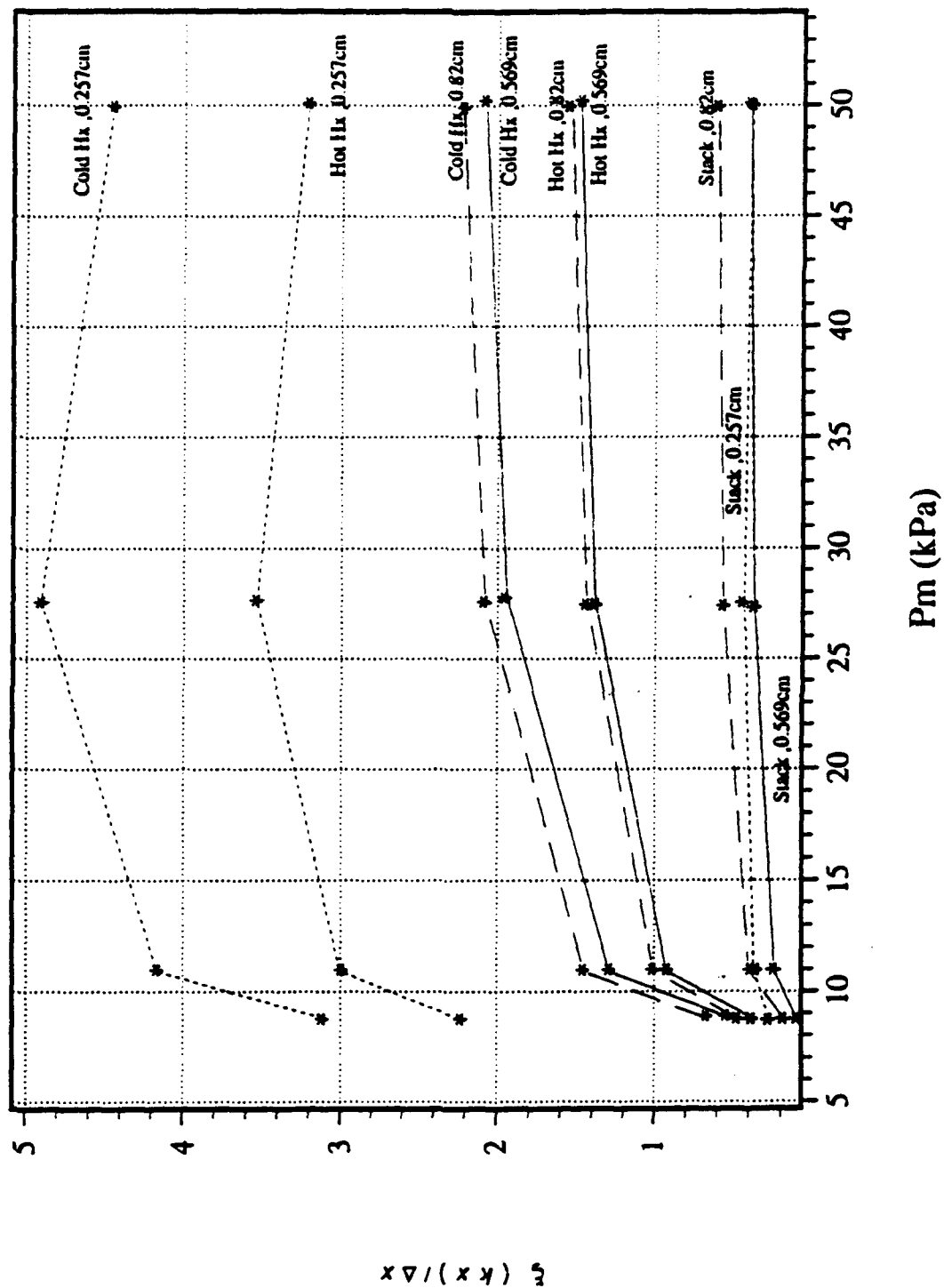


Figure 19 - Ratio of peak displacement amplitude to stack or heat exchanger length versus mean gas pressure.

V. SUMMARY, CONCLUSIONS, AND RECOMMENDATIONS

A. SUMMARY

The goal of this thesis is to investigate the experimental heat exchanger performance in a thermoacoustic prime mover filled with neon gas. The experimental approach is to measure the pressure ratio, the steady state waveforms, and the temperatures for heat exchangers lengths of 0.257, 0.569, and 0.82 *cm* for a variety of mean gas pressures. A temperature gradient is established across the stack by keeping the cold heat exchanger submerged in liquid nitrogen and the hot heat exchanger near ambient temperature. The prime mover is designed to achieve very high acoustic displacement amplitudes with modest heat flows. Measurements are made at mean gas pressures of approximately 1.5, 8.8, 10.9, 27.6, and 50 *kPa* and plunger positions of 8.128 and 10.688 *cm*. The signal waveforms and spectra generated by the prime mover are also reported.

The overall results can be summarized as follows. Acoustic pressure amplitudes as high as 29% of mean gas pressure are generated by the prime mover. As the mean gas pressure increases, the pressure ratio increases for all heat exchanger lengths as the penetration depth approaches optimum value for this prime mover design. The shorter 0.257 *cm* long heat exchanger has higher acoustic pressure amplitudes at low mean gas pressures when compared to the longer heat exchangers.

There are three possible effects that may explain this behavior. First, the heat flows are small at low gas pressures, \dot{P}_m , and so the limited thermal conductance of the shorter 0.257 *cm* heat exchanger is not a problem as it is at higher gas pressures and heat flows. Secondly, the acoustic losses for the 0.257 *cm* heat exchanger are the lowest of the three heat exchangers, which should increase the amplitude. Lastly, the

larger value of δ_x at low gas pressures decreases the y_o/δ_x , and thus the effective thermal diffusion distance from gas parcel to heat exchanger plate. This tends to corroborate Hofler's hypothesis that the short heat exchangers with $(\Delta x_{hx} / \xi_{hx}) < 1$, may be thermally effective if $(y_o / \delta_x) < 1$.

In theory, heat exchangers are assumed to be isothermal. However, a pronounced radial temperature difference of as much as 9.2, 27.6, and 13.7 °C in the cold heat exchanger and 32.5, 11.9 and 24.9 °C in the hot heat exchanger for lengths of 0.257, 0.569, and 0.82 cm, respectively, are generated at a mean gas pressure of 50 kPa. This difference results in radially varied thermal penetration depths.

The T_h / T_c ratio ideally is constant. However, experimentally, it is not. This ratio decreases by as much as 56%. This decrease is primarily due to the cold heat exchanger. Its temperature is not constant. On the other hand, the hot heat exchanger temperature is nearly constant.

The y_o/δ_x ratios are similar in slope for the hot heat exchangers, for all the heat exchangers lengths, and increases approximately by 160% from the lowest to the highest mean gas pressure. However, the y_o/δ_x ratio for different cold heat exchanger lengths increases between 35 to 88% and has different slopes with increasing mean gas pressure. Similarly, the y_o/δ_x ratio for the stack increases by as much as 122%. The δ_x is decreasing with increasing mean gas pressure which decreases the effective distance over which heat can diffuse transversely between a gas parcel and the heat exchanger plate.

The peak displacement amplitudes for the 0.257 cm long heat exchanger are as much as two times the heat exchanger length at the lowest mean gas pressure to as much as five times the heat exchanger length at the highest mean gas pressure.

Overall, the peak-to-peak displacement amplitudes are bigger than any of the heat exchanger lengths even at the lowest mean gas pressure. For the stack, the peak-to-peak displacement amplitudes are as long as the stack length, except at the lowest mean gas pressure. The displacement amplitudes increase with increasing mean gas pressure for all heat exchanger lengths.

B. CONCLUSIONS

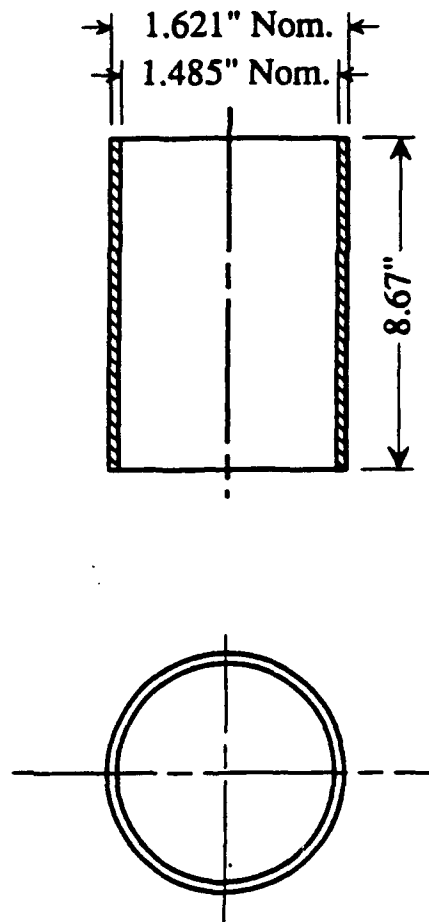
Several conclusions can be drawn from these results. The first conclusion is that the longest heat exchanger generated the largest pressure amplitudes. Secondly, the theoretical equations need to take into account the radial temperature gradient in the heat exchangers. The final conclusion is that the heat exchangers generate large pressure amplitudes even though the peak-to-peak displacement amplitudes are much larger than the heat exchanger lengths.

C. RECOMMENDATIONS

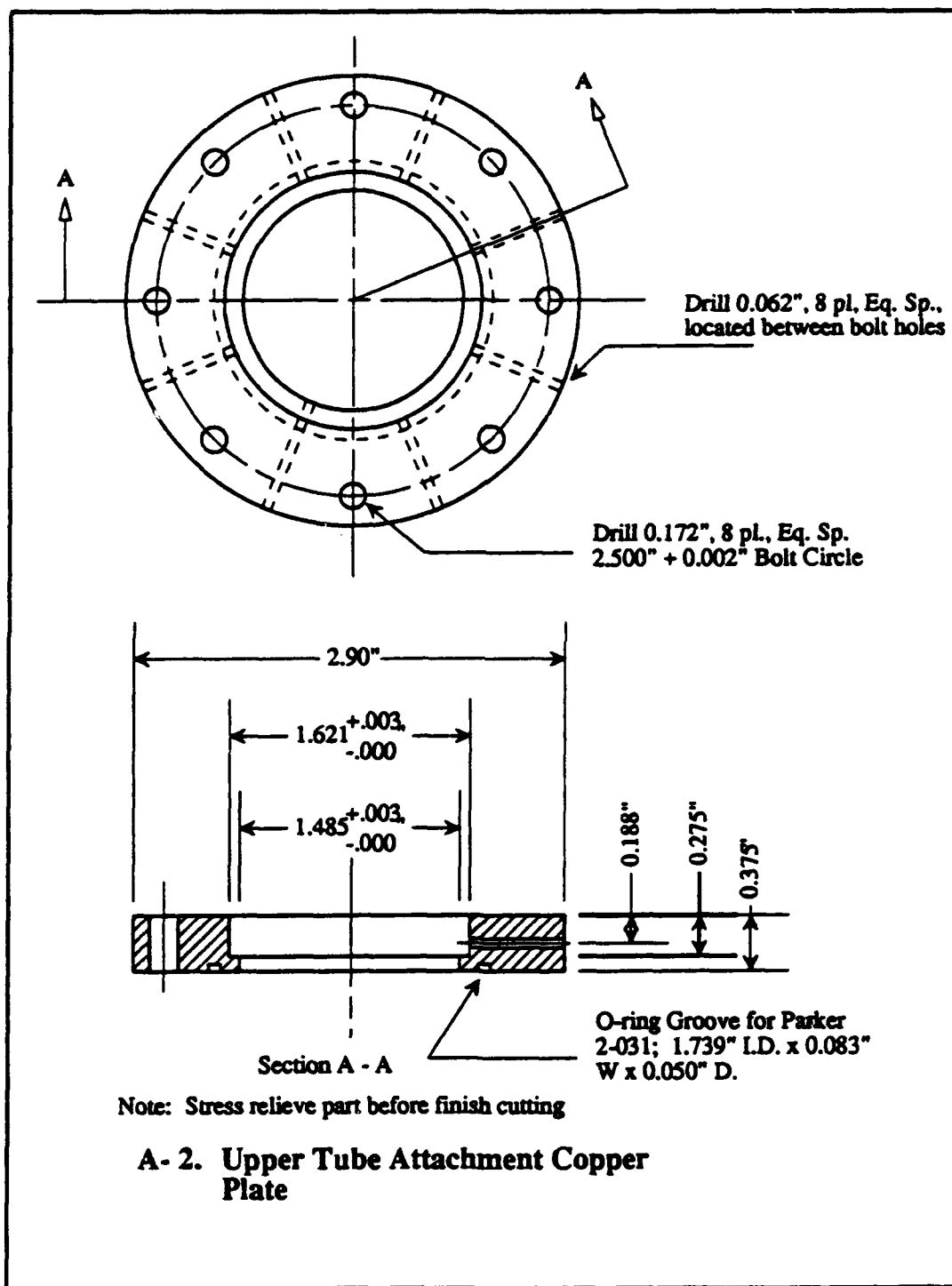
In order to better understand the thermoacoustic process, there is a need for more theoretical work to be performed to understand these experimental results. It is uncertain at this point what is the optimum heat exchanger length. However, several recommendations are proposed as follows:

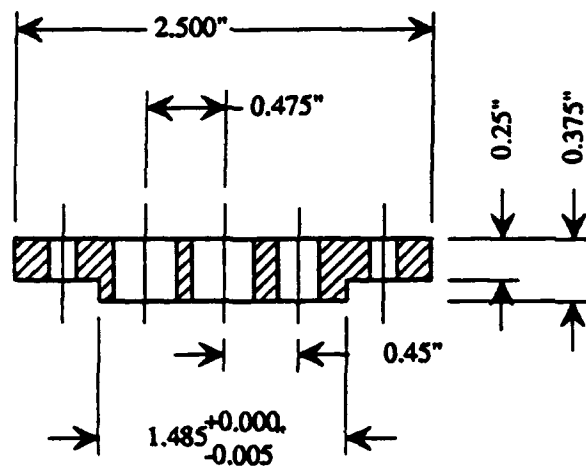
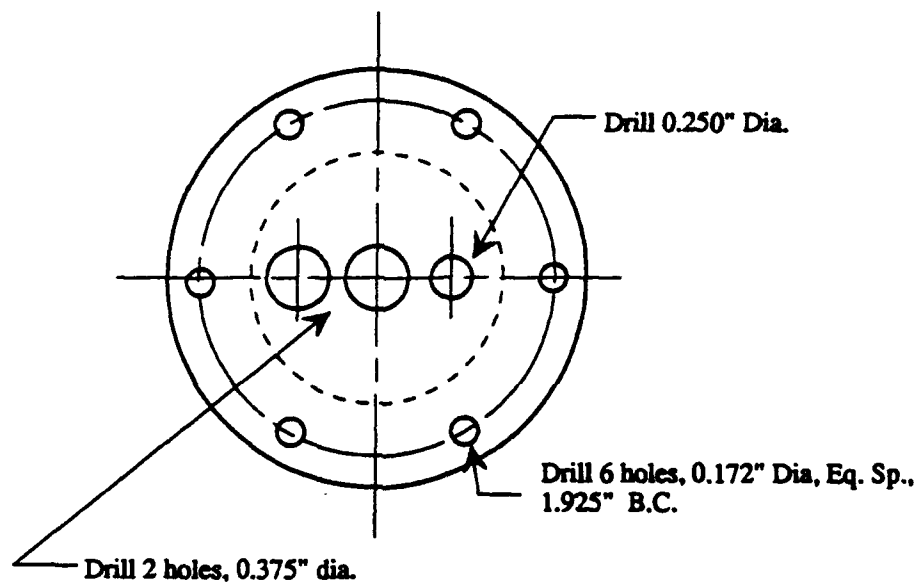
- Keep the T_c also constant and as low as possible.
- Measure heater powers carefully for all data points.
- Use cold heat exchangers of smaller y_o so that y_o/δ_x is similar for both hot and cold heat exchangers.

APPENDIX A - PRIME MOVER SPECIFICATIONS

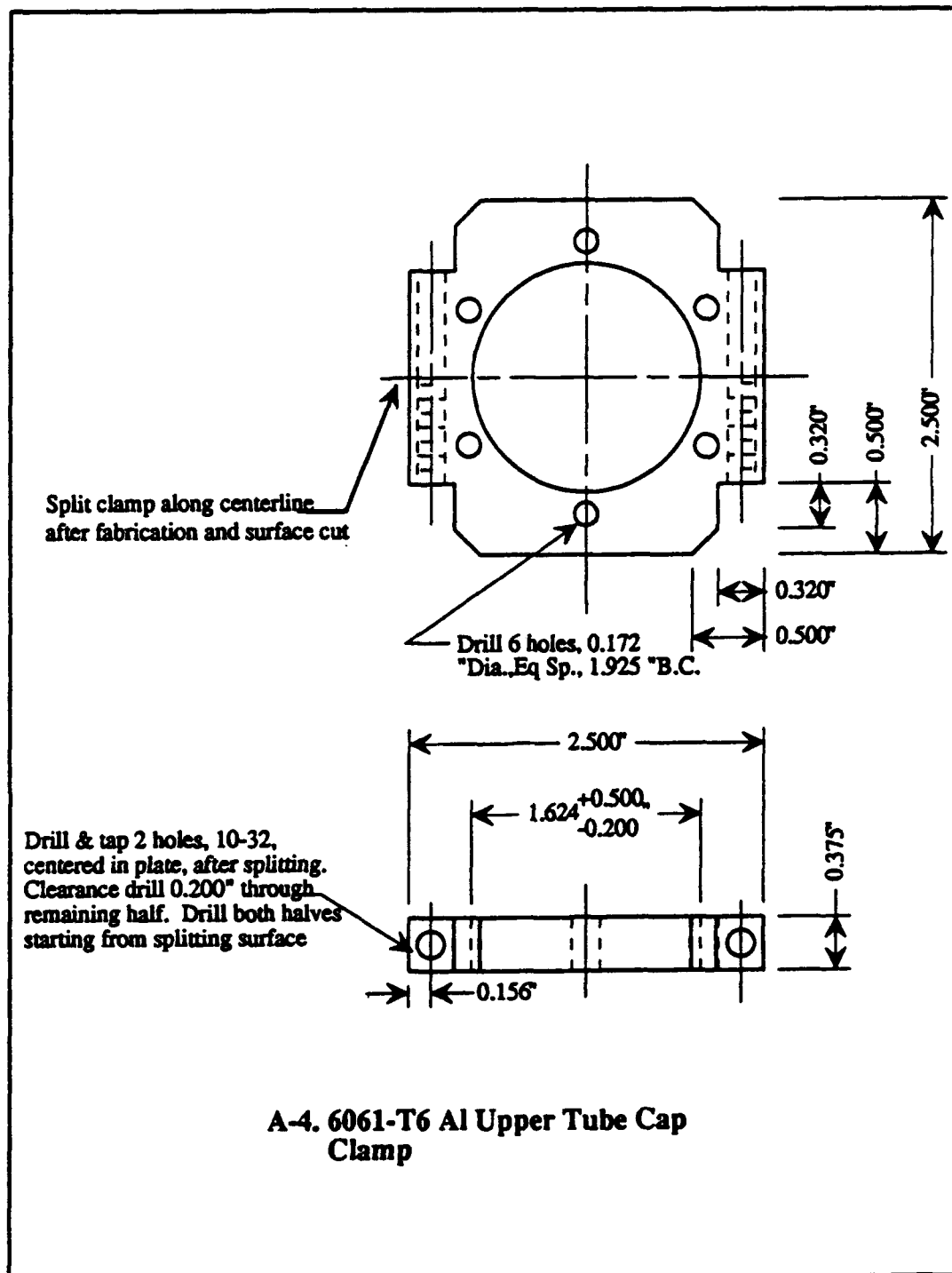


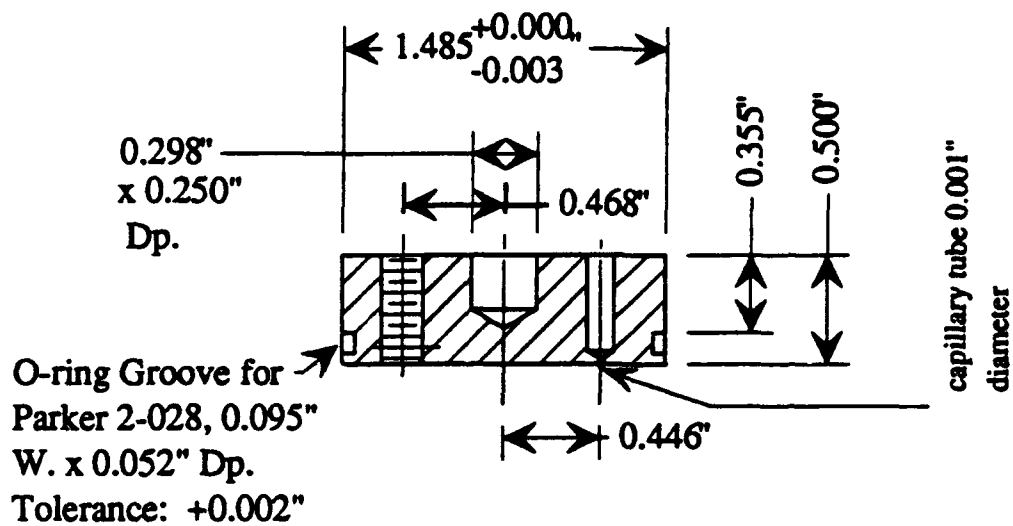
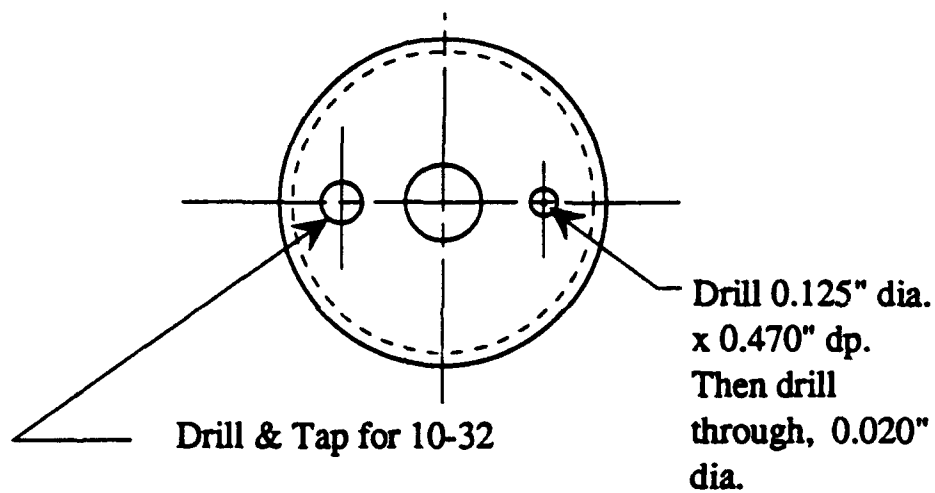
A-1. Upper Tube Copper Section





A-3. Upper Tube Copper End-cap

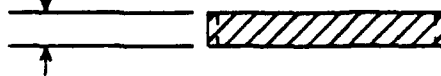




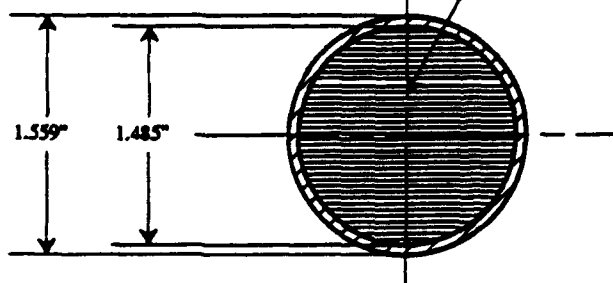
Note: Stress relieve part before finish cutting

A-5. Movable Plunger

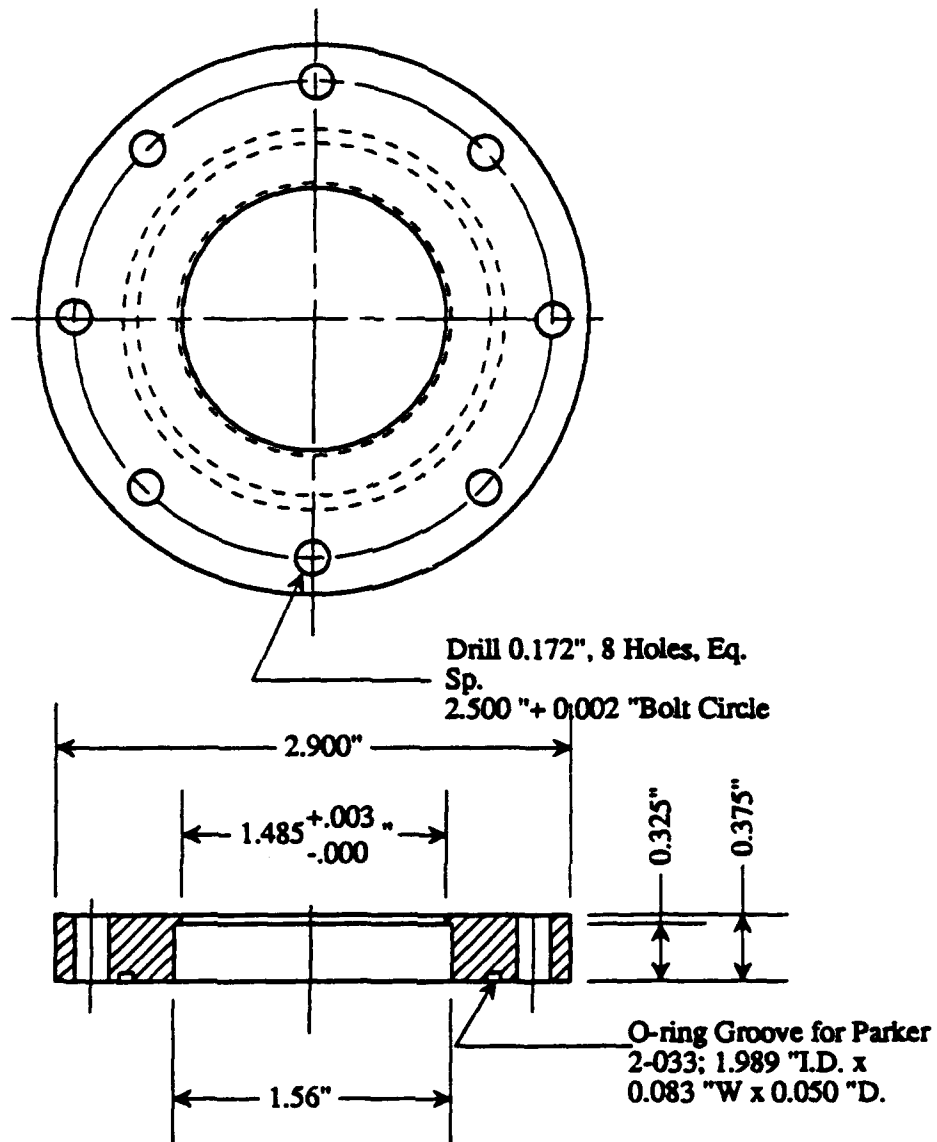
6 Heat Exchangers Total:
Two 0.1035" in length,
Two 0.224" in length,
and Two 0.325"
in length.



Each plate is 0.01" in width,
and plate separation is 0.02"



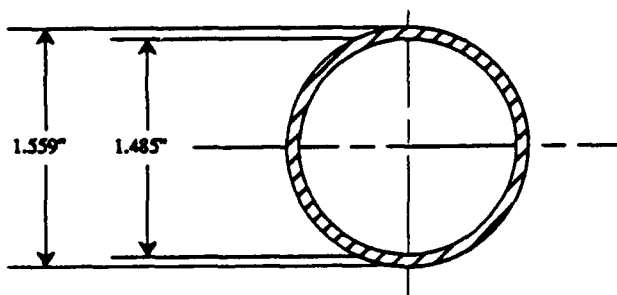
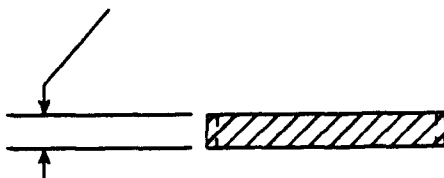
A-6 . Copper Heat Exchangers



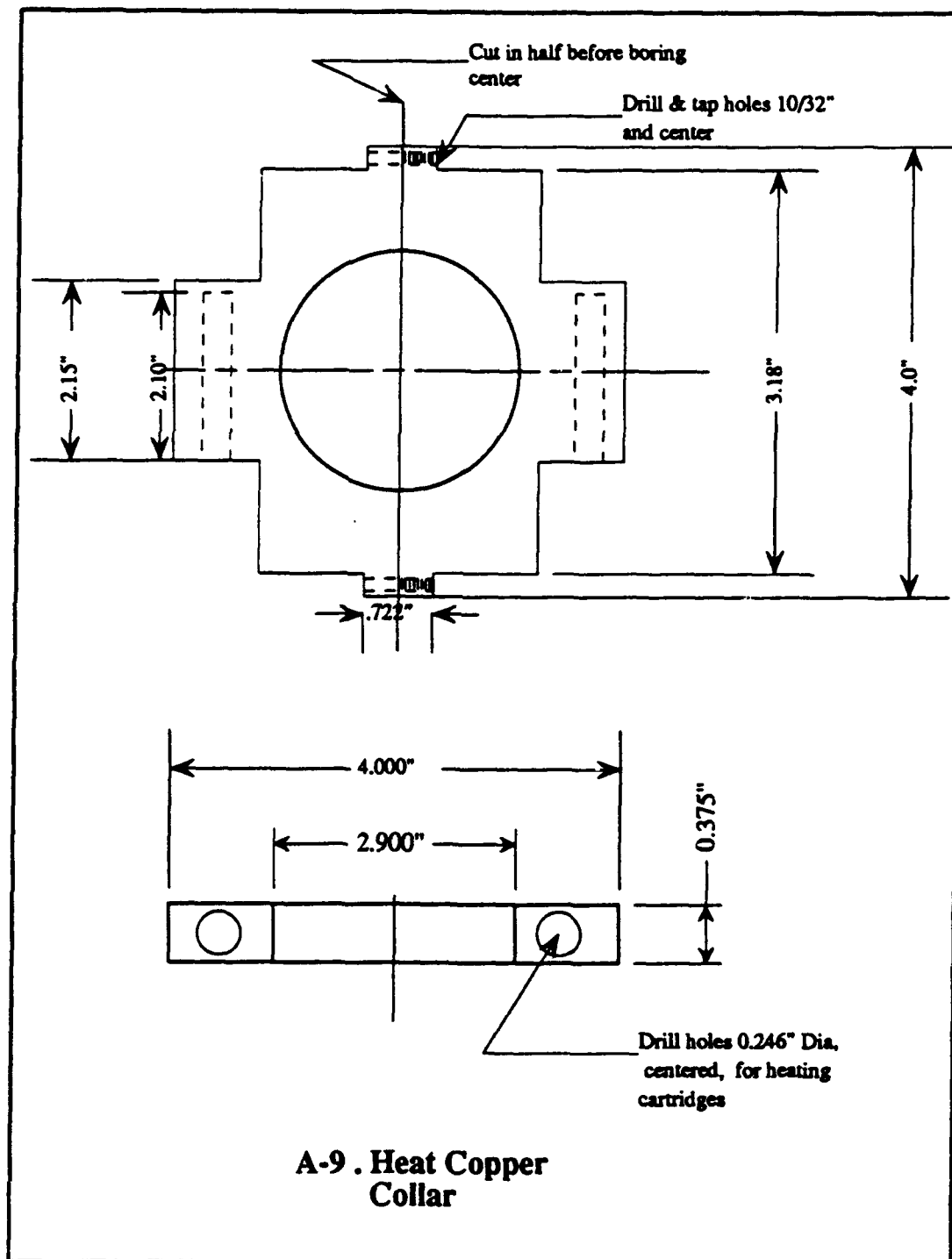
Note: Stress relieve part before finish cutting

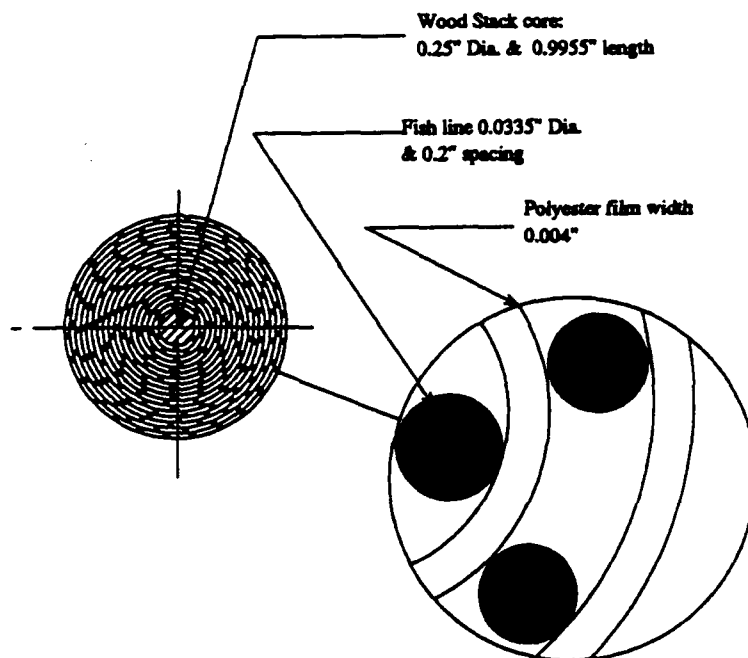
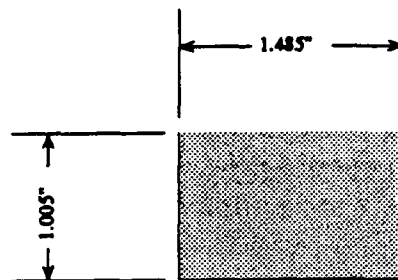
A-7. Hot Heat Exchanger Copper Holder

Four spacers total:
two 0.1035" in length,
and two 0.2235" in length.

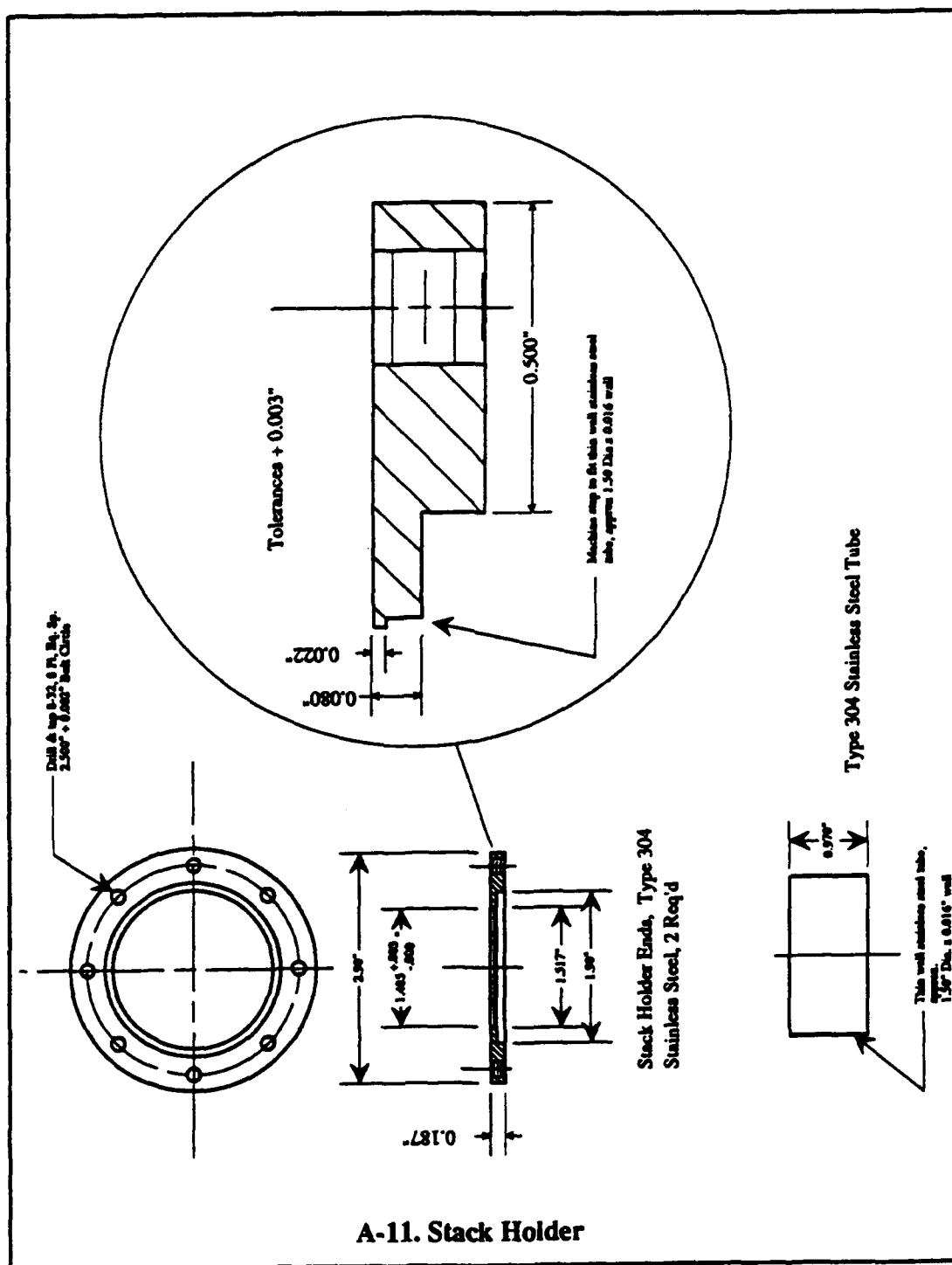


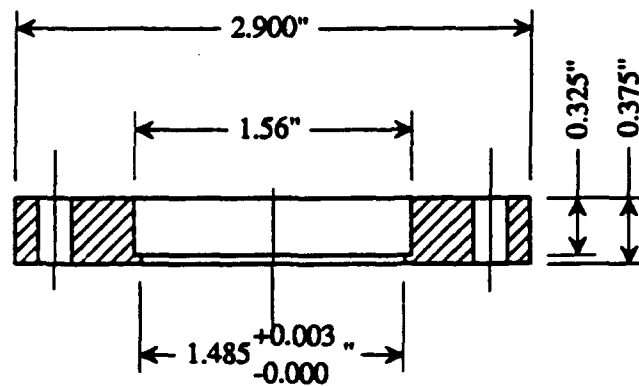
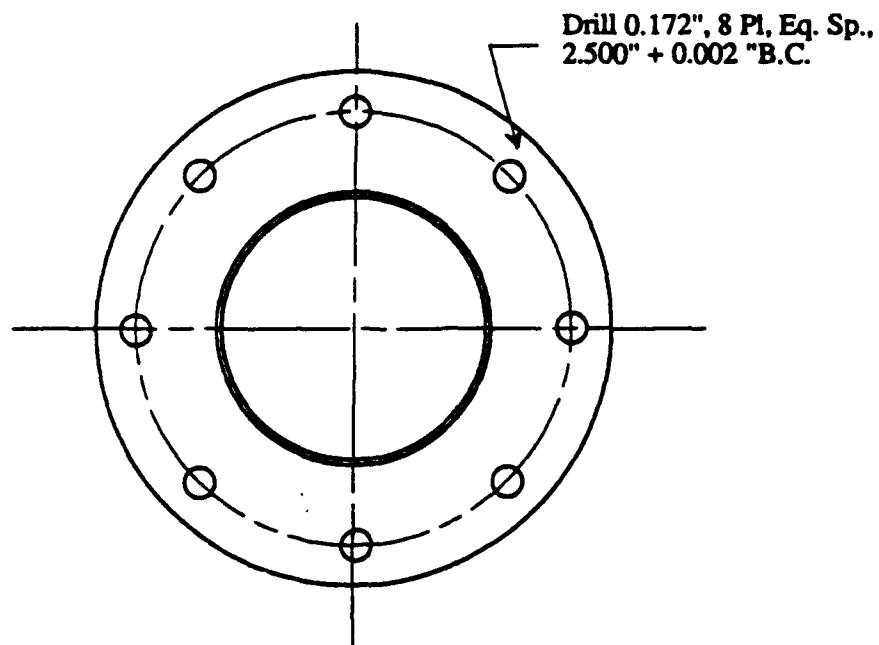
**A-8 . Bronze heat exchanger
spacers**





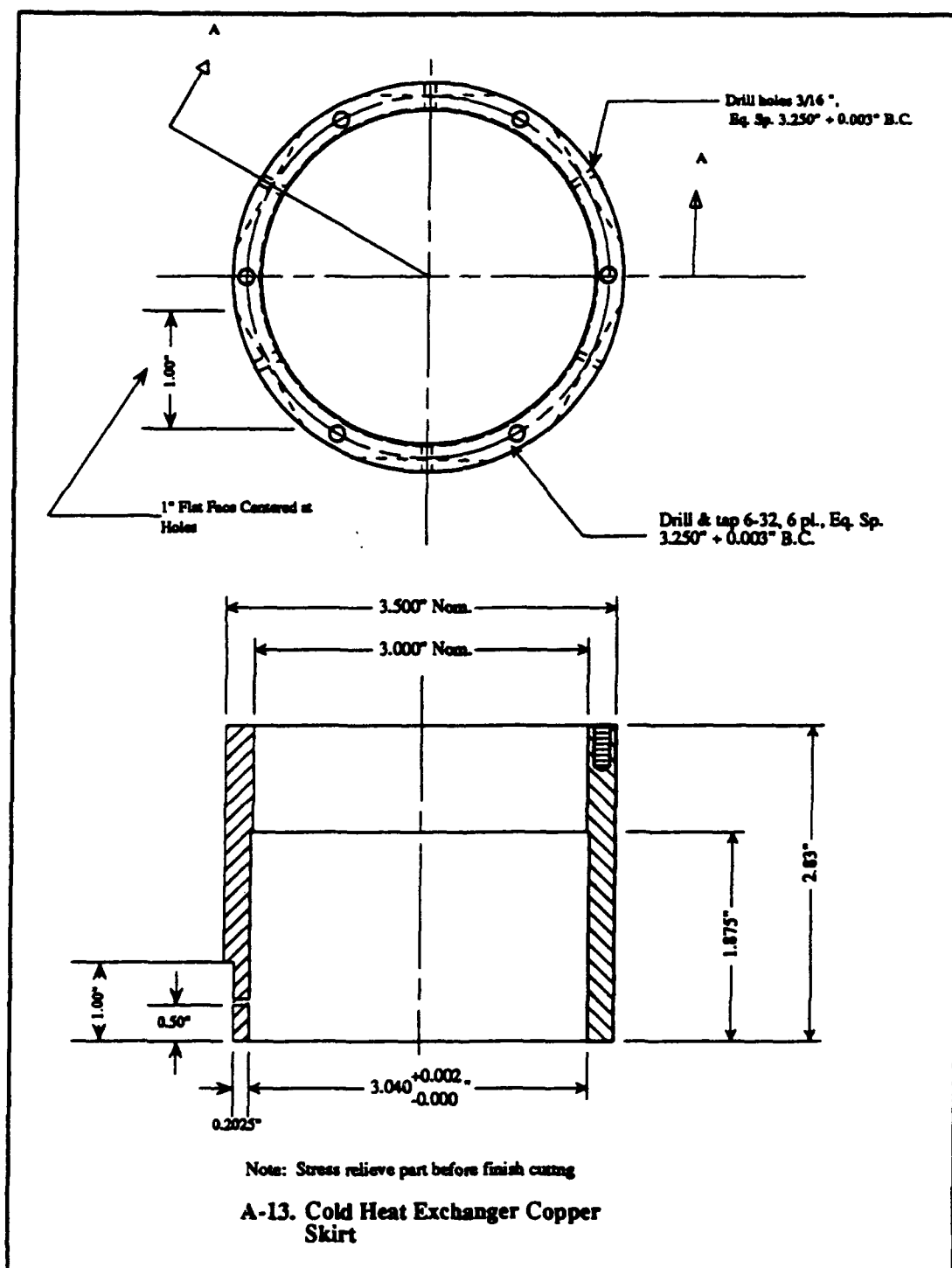
**A-10. Prime Mover
Stack**

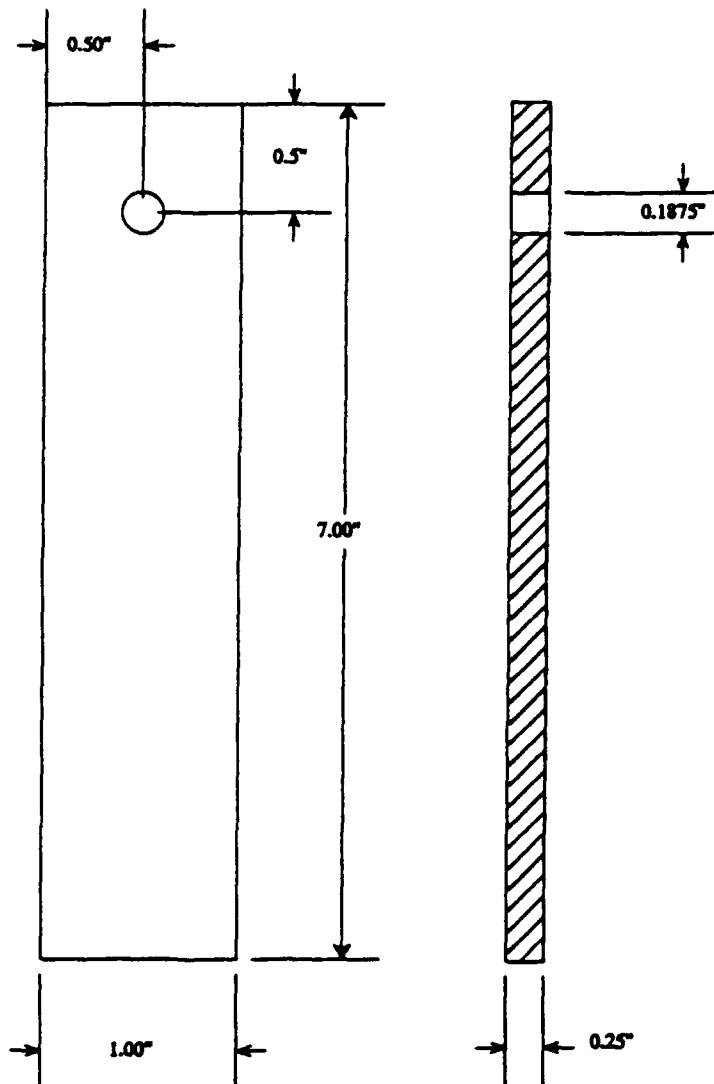




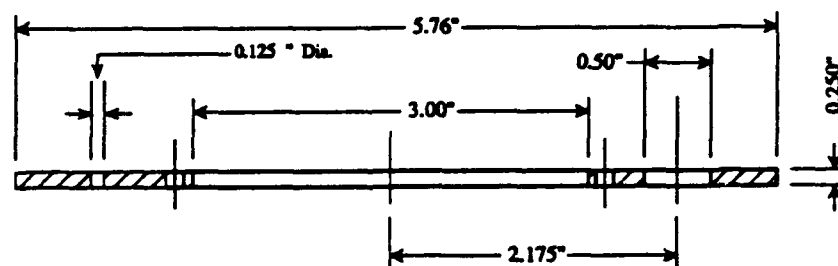
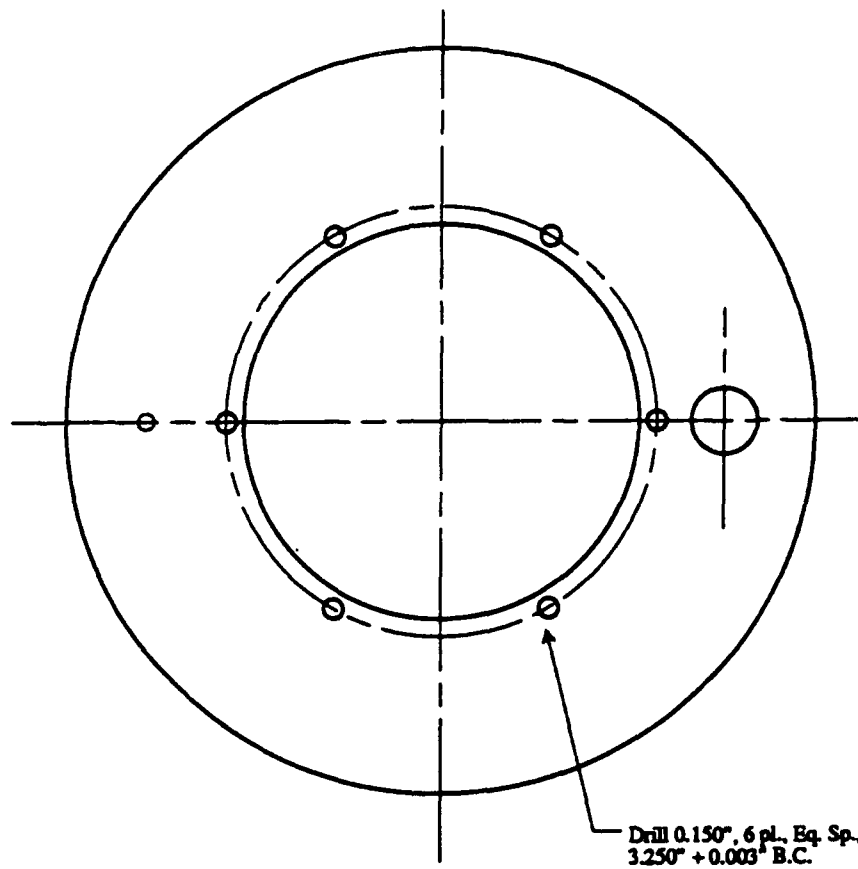
Note: Stress relieve part before finish cutting

A-12. Cold Heat Exchanger Copper Holder

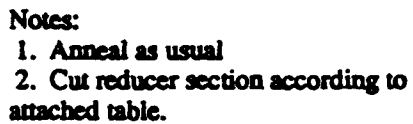


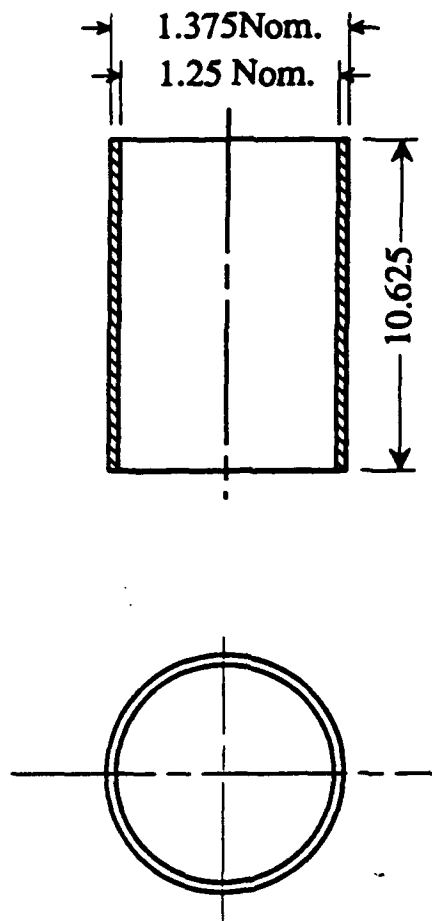


A-14. Skirt Copper Fingers

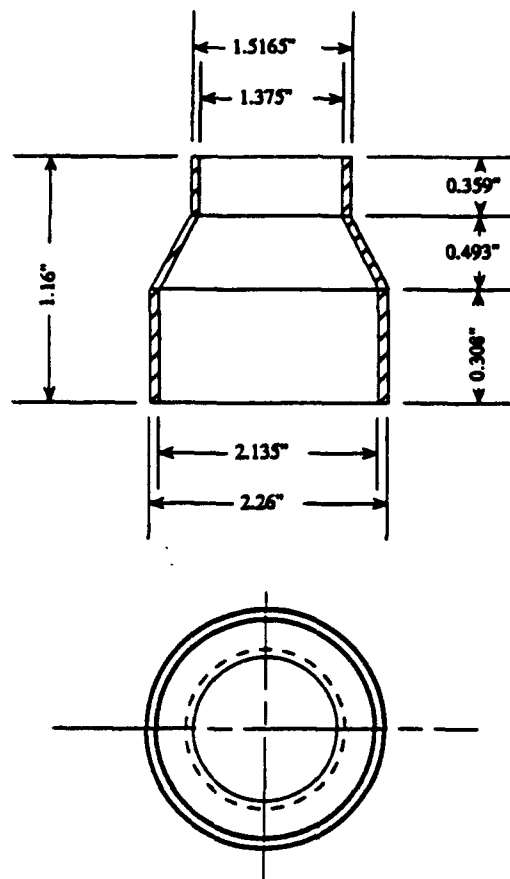


A-15. 304 SS Engine Support On Dewar

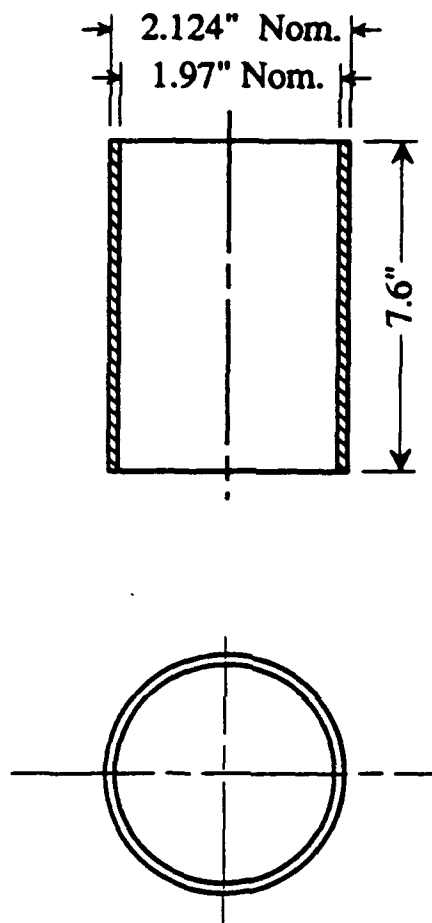




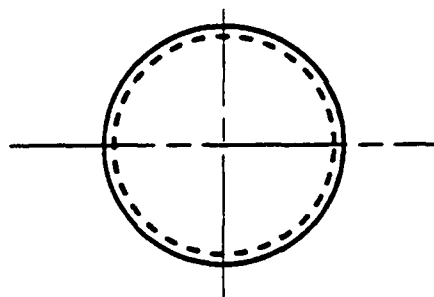
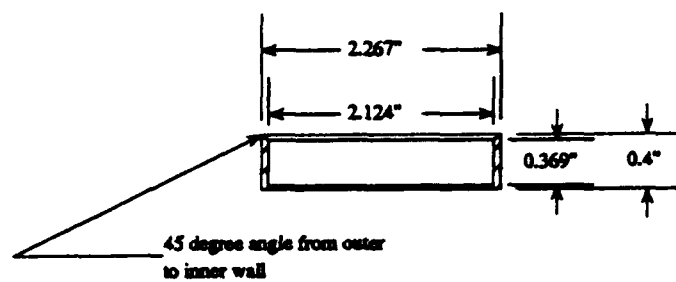
**A-17. Lower Small Copper Tube
Section**



A-18. Cold End Copper Reducer



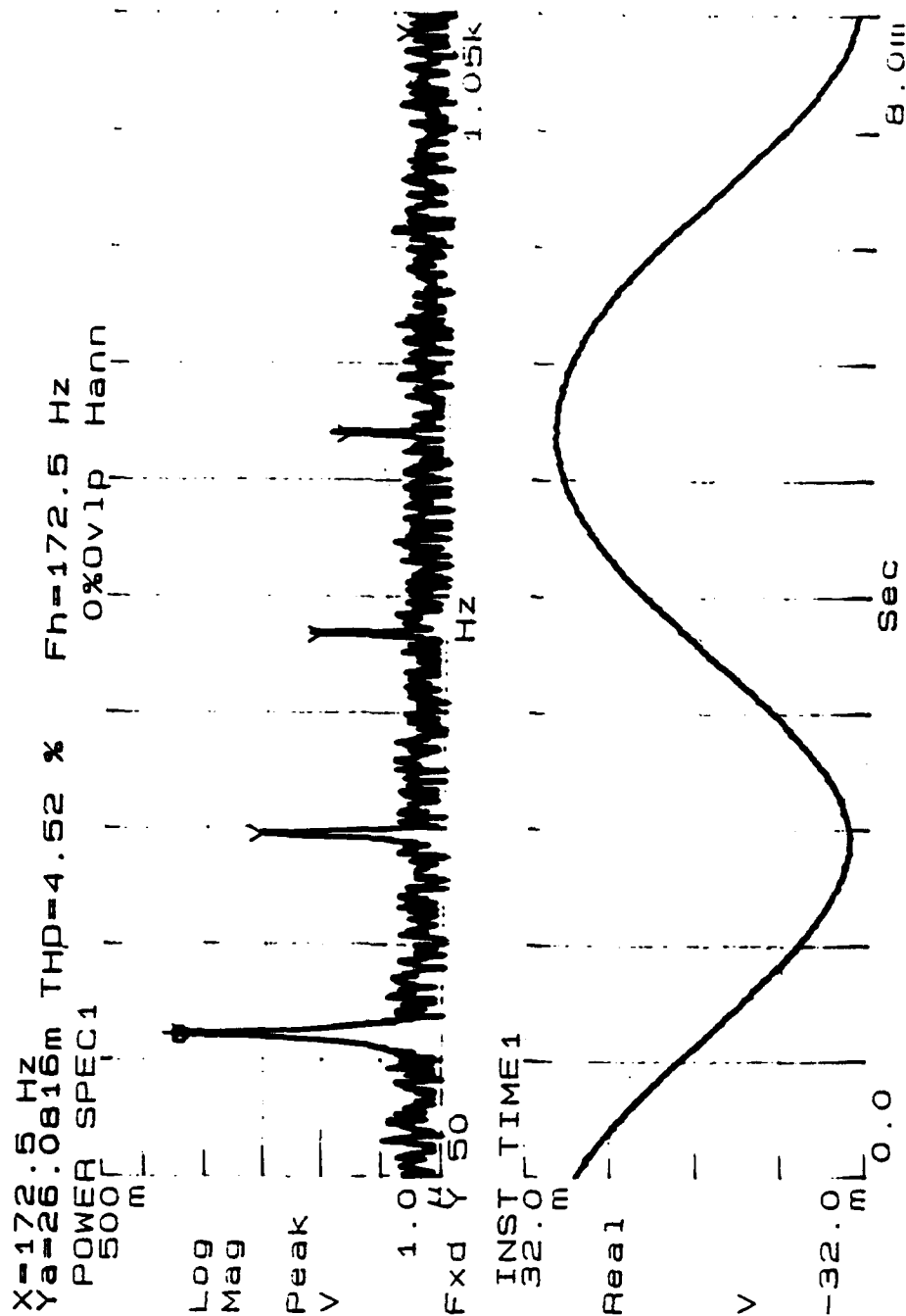
A-19. Lower Big Copper Tube Section



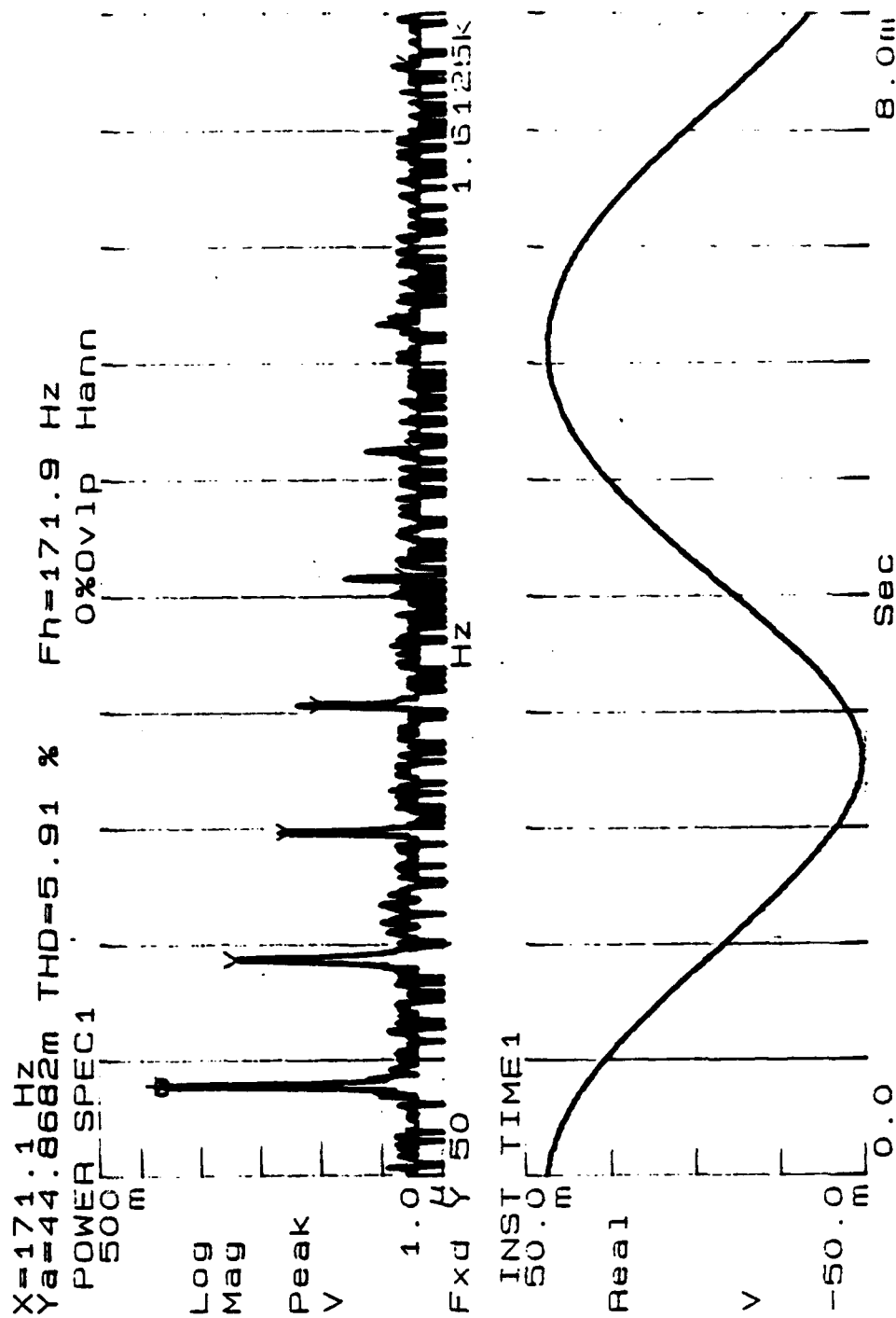
**A-20. Lower Tube Copper
End-cap**

APPENDIX B - PLOTS OF WAVEFORMS AND SPECTRA OF SOUND GENERATED BY PRIME MOVER

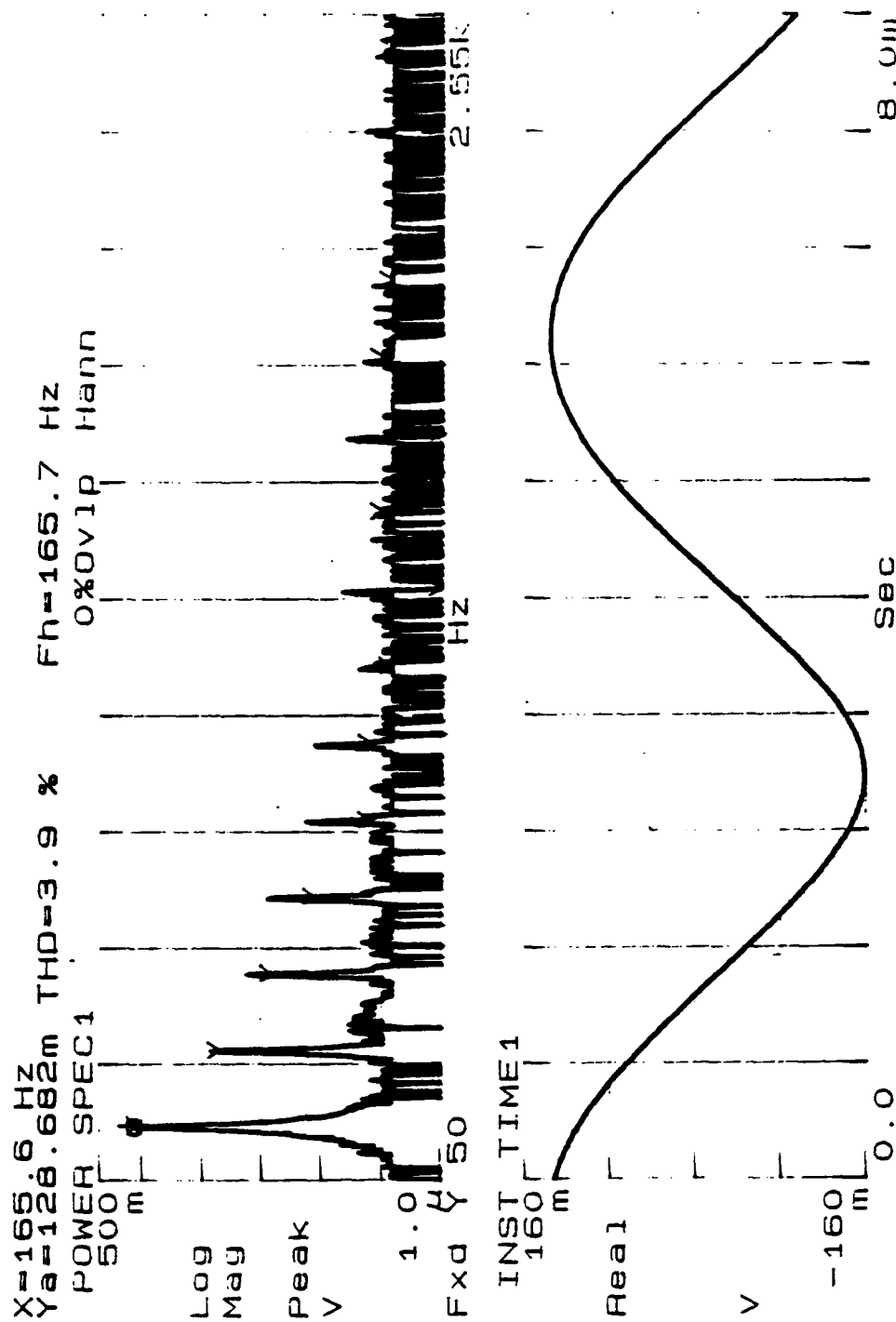
AT 8.128 cm PLUNGER POSITION



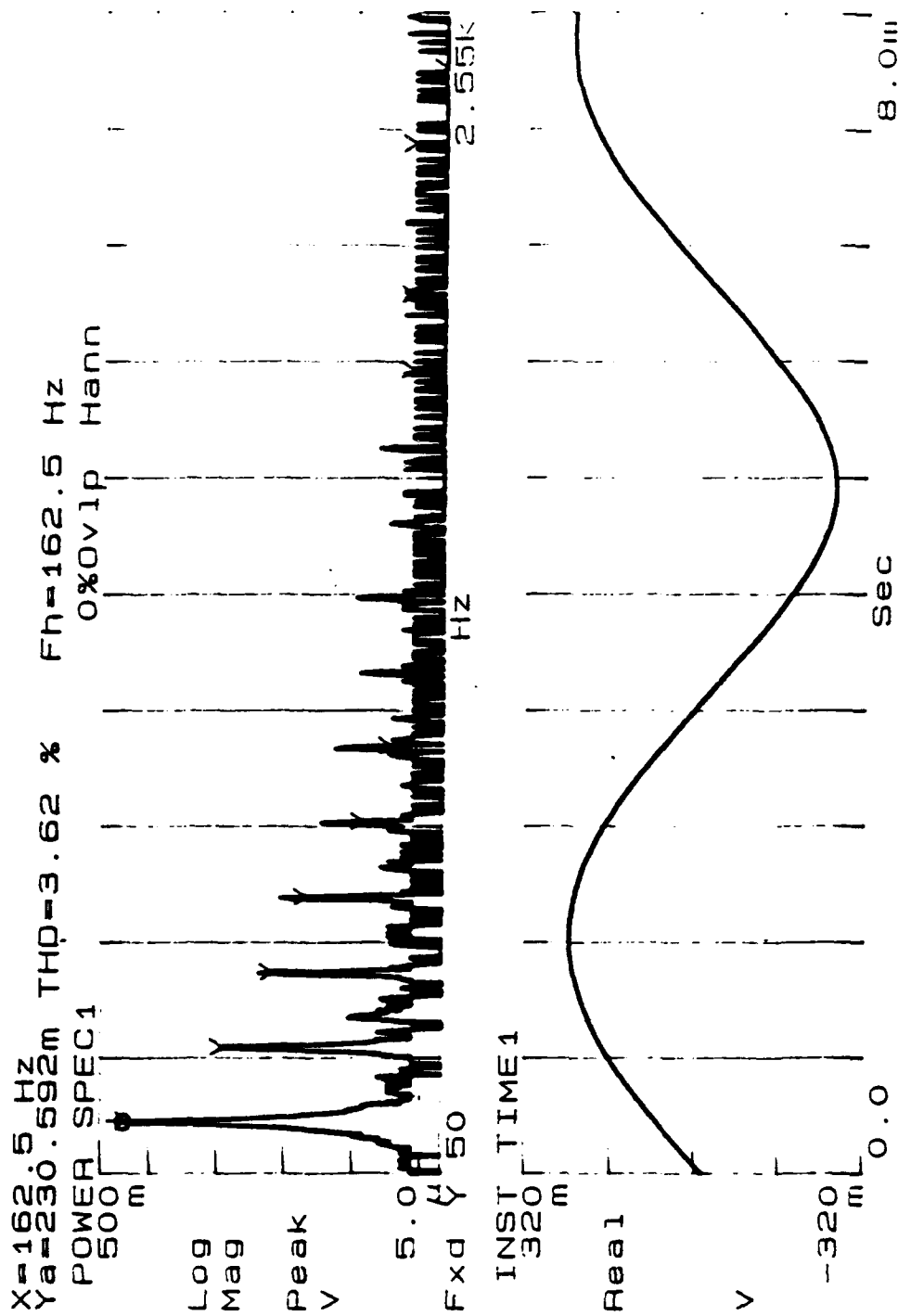
B.1- Spectrum and waveform of the sound generated by the prime mover using a heat exchanger length of 0.257 cm at a mean gas pressure of 8.794 kPa.



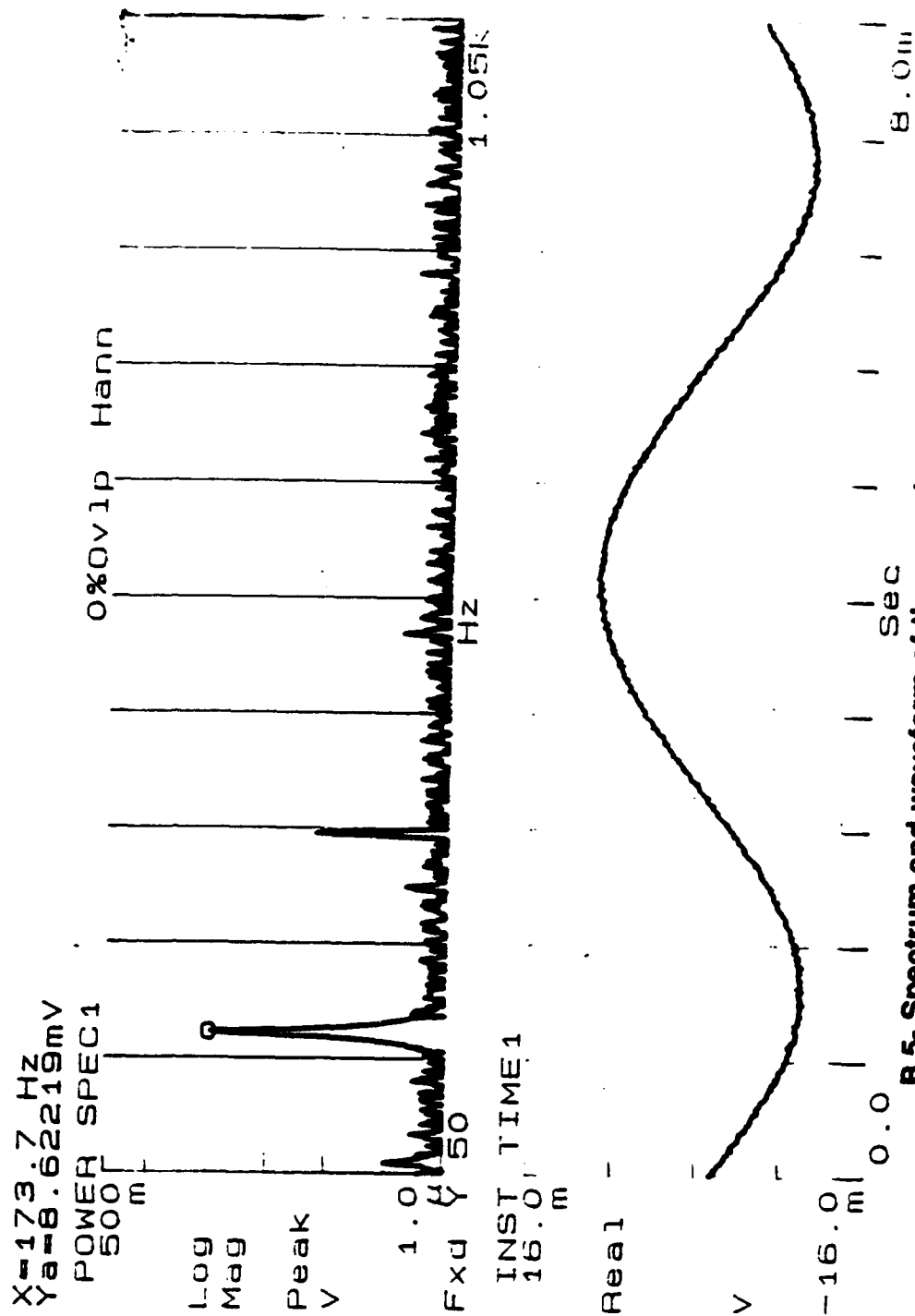
B.2- Spectrum and waveform of the sound generated by the prime
 mover using a heat exchanger length of 0.257 cm at
 a mean gas pressure of 10.92 kPa.



B.3- Spectrum and waveform of the sound generated by the prime
 mover using a heat exchanger length of 0.257 cm at
 a mean gas pressure of 27.62 kPa.



B.4- Spectrum and waveform of the sound generated by the prime
 mover using a heat exchanger length of 0.257 cm at
 a mean gas pressure of 50.12 kPa.

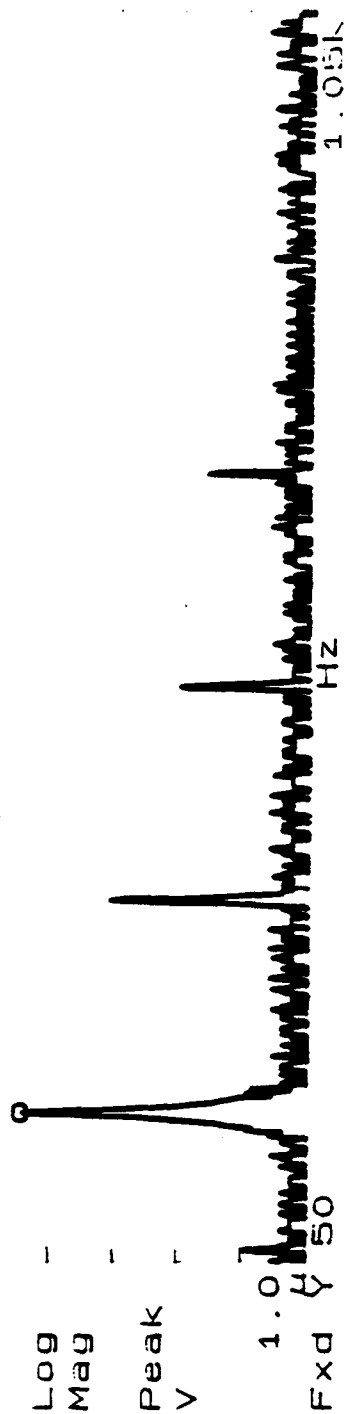


B.5- Spectrum and waveform of the sound generated by the prime mover using a heat exchanger length of 0.569 cm at a mean gas pressure of 8.82 kPa.

X=171.2 Hz
Ya=25.4161mV

POWER SPEC1
500 F
m

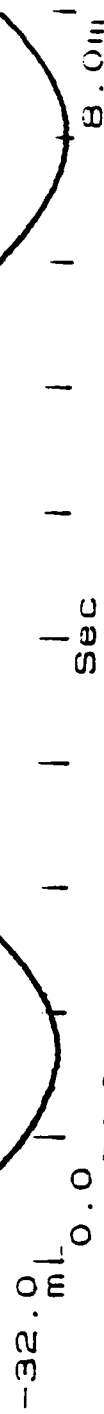
0%Ovlp Hann



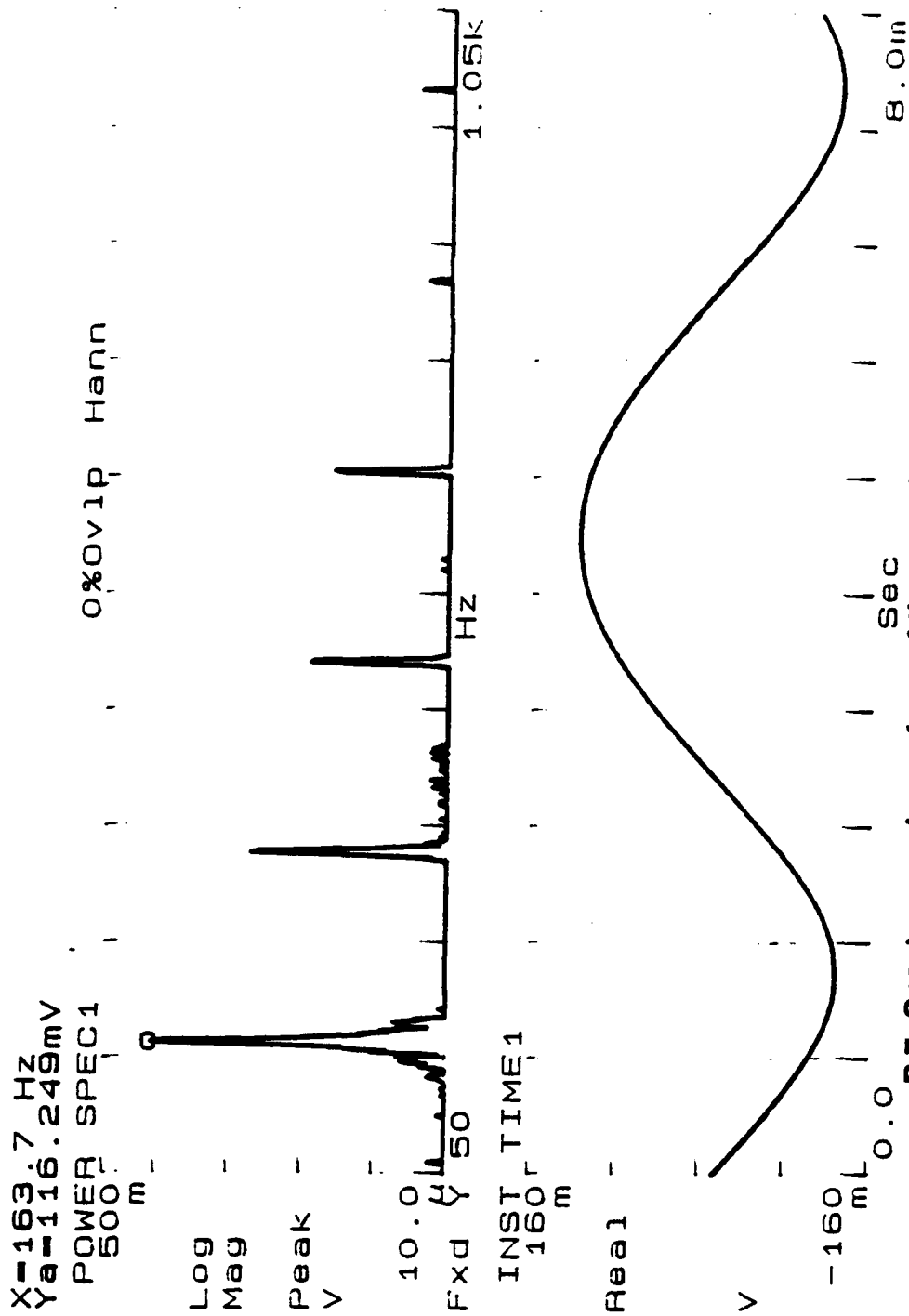
INST TIME1
32.0 m

Real

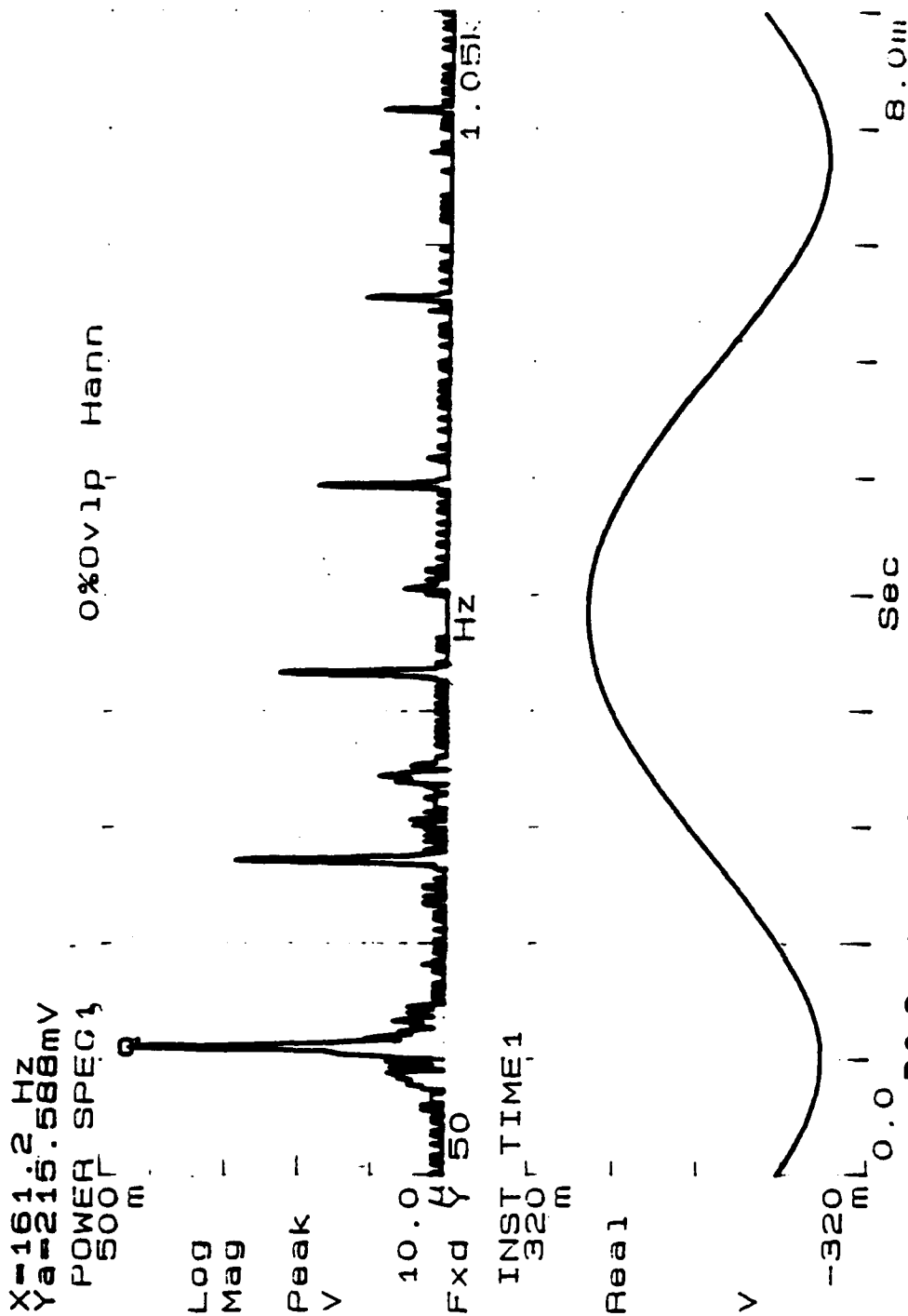
V



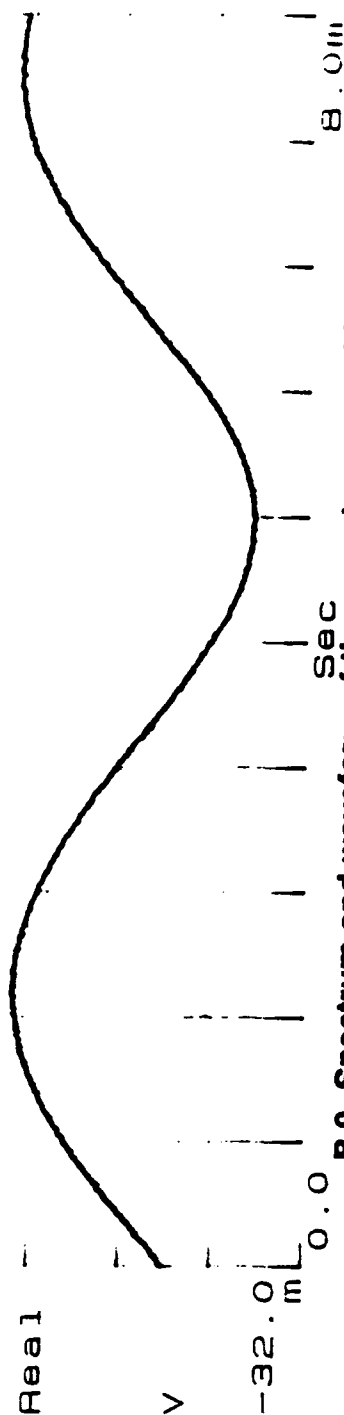
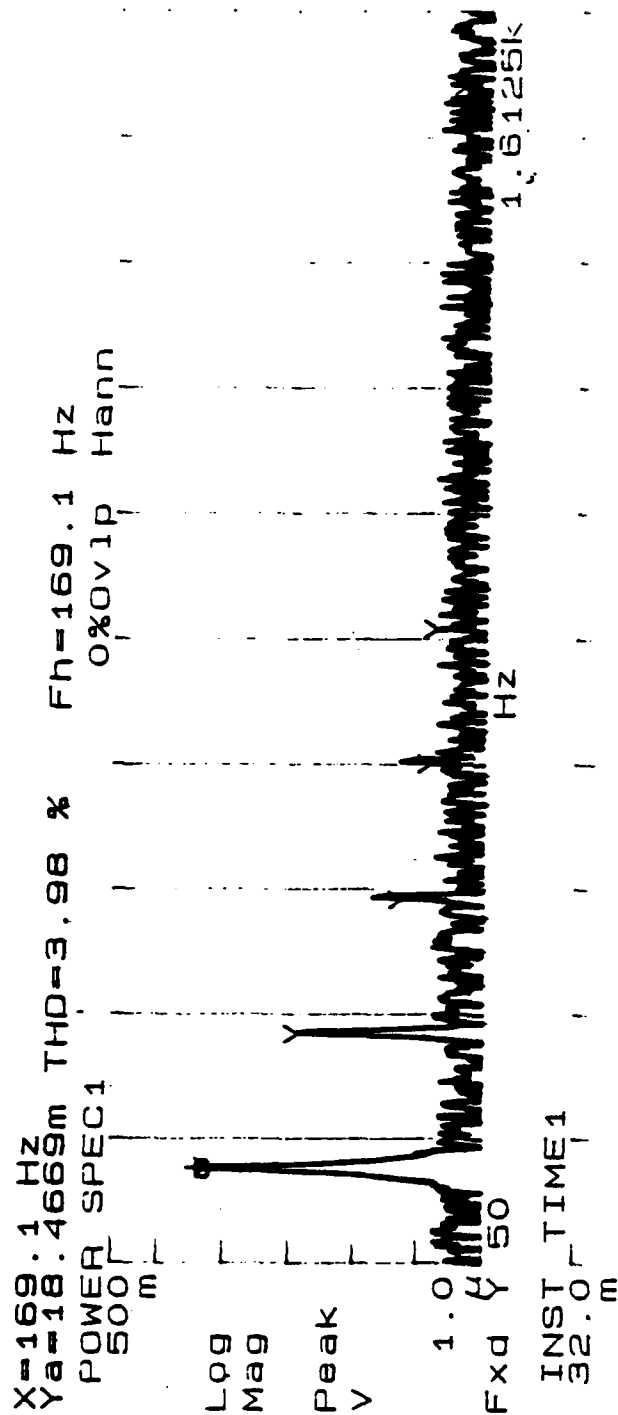
B.6- Spectrum and waveform of the sound generated by the prime mover using a heat exchanger length of 0.569 cm at a mean gas pressure of 10.91 kPa.



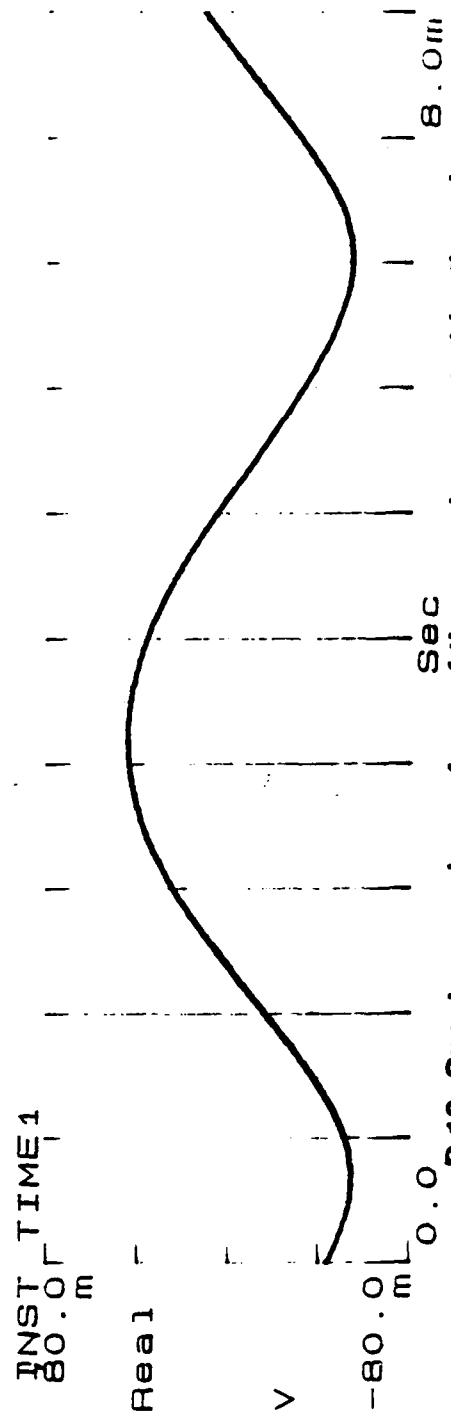
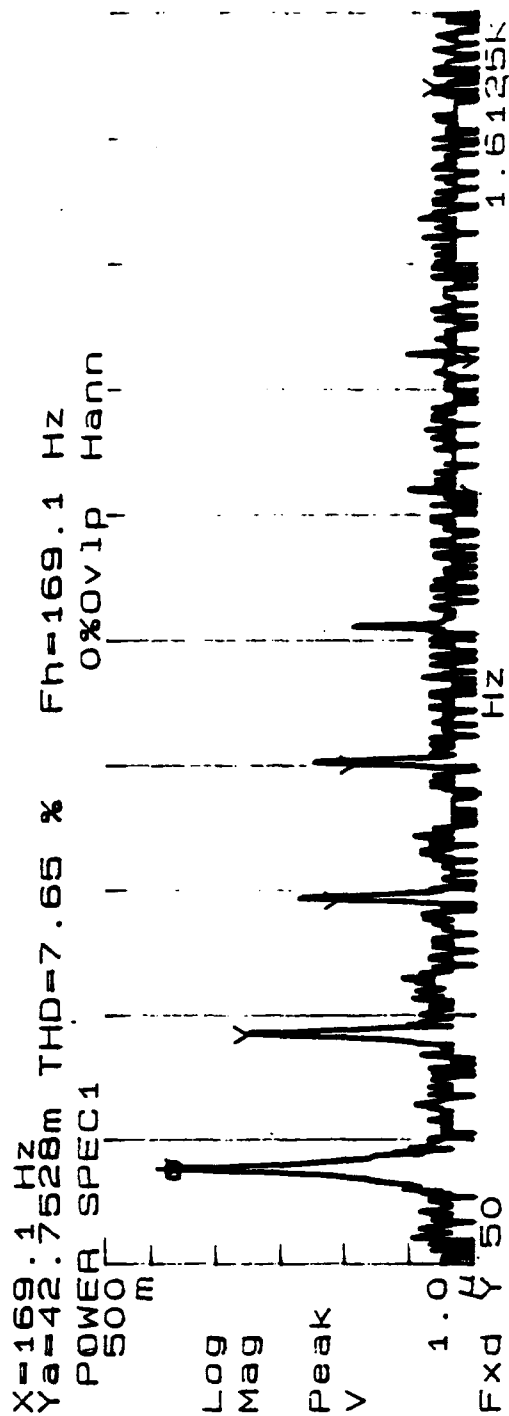
B.7- Spectrum and waveform of the sound generated by the prime
 mover using a heat exchanger length of 0.569 cm at
 a mean gas pressure of 27.81 kPa.



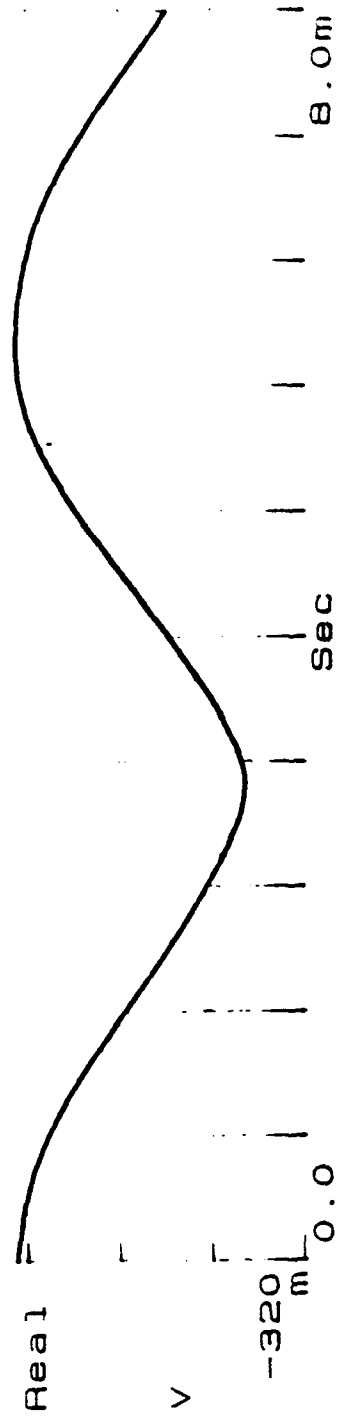
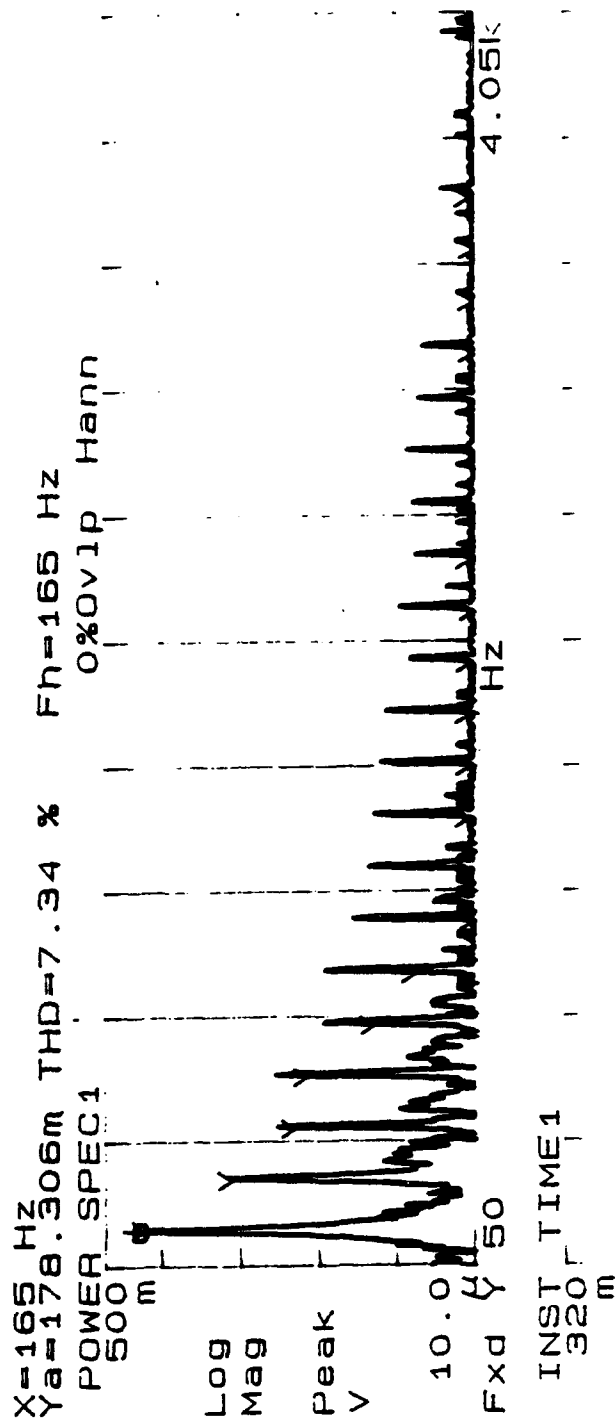
B.8- Spectrum and waveform of the sound generated by the prime
 mover using a heat exchanger length of 0.569 cm at
 a mean gas pressure of 50.16 kPa.



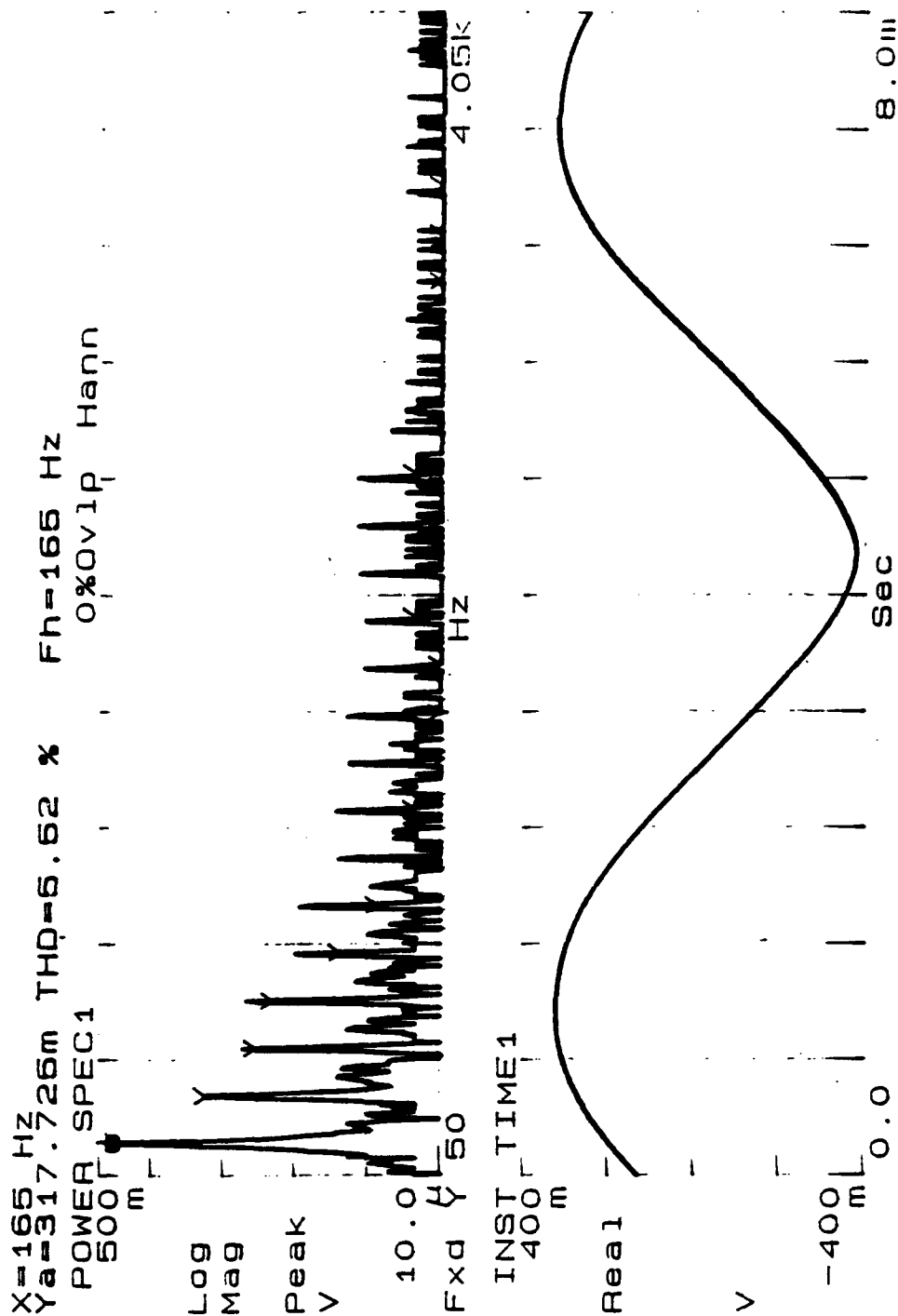
B.9- Spectrum and waveform of the sound generated by the prime mover using a heat exchanger length of 0.82 cm at a mean gas pressure of 8.814 kPa.



B.10- Spectrum and waveform of the sound generated by the prime
 mover using a heat exchanger length of 0.82 cm at
 a mean gas pressure of 10.898 kPa.



B.11- Spectrum and waveform of the sound generated by the prime
 mover using a heat exchanger length of 0.82 cm at
 a mean gas pressure of 27.62 kPa.



B.12- Spectrum and waveform of the sound generated by the prime
 mover using a heat exchanger length of 0.82 cm at
 a mean gas pressure of 49.95 kPa.

LIST OF REFERENCES

1. Swift, G. W., "Thermoacoustic engines," *J. Acoust. Soc. Am.*, Vol. 84, 1145-1180, 1988.
2. Wheatley, J., Hofler, T. J., Swift, G. W., and Migliori, A., "Understanding some simple phenomena in thermoacoustics with applications to acoustical heat engines," *Am. J. Phys.*, 53, 147-162, 1985.
3. Wheatley, J., Hofler, T. J., Swift, G. W., and Migliori, A., "An intrinsically irreversible thermoacoustic heat engine," *J. Acoust. Soc. Am.*, Vol 74, 3153-3170, 1983.
4. Wheatley, J., Swift, G. W., and Migliori, A., "The Natural Heat Engine," *Los Alamos Science*, Fall 1986.
5. Hofler, T. J., "Effective heat transfer between a thermoacoustic heat exchanger and stack," *J. Acoust. Soc. Am.*, Vol 94(3) Pt.2, 1993.
6. Carslaw, H. S., and Jaeger, J. C., "Conduction of heat in solids," Eq.4, chap. 3, 2nd edition, Oxford University Press, 1993.
7. Model CIR-1024, Chromalox USA, Pittsburgh, PA
8. Model 740, Keithley Instruments Inc., Cleveland, OH, 44139
9. Model 22250, Hewlett-Packard Company, Palo Alto, CA 94304
10. Model CN9000, Omega Engineering Inc., Stamford, CT 06907
11. Model 5530, Techron Division of Crown International, Inc., Elkhart, IN 46517
12. Model 8530C-15, Endevco, San Juan Capistrano, CA 92675
13. Model 3562, Hewlett-Packard Company, Palo Alto, CA 94304
14. Model 7440A, Hewlett-Packard Company, Palo Alto, CA 94304

15. Model 3457A, Hewlett-Packard Company, Palo Alto, CA 94304
16. Gaitan, D. F., and Atchley, A. A., "Finite amplitude standing waves in harmonic and anharmonic tubes," *J. Acoust. Soc. Am.*, Vol 93, 2489-2495, 1993
17. Type 29, GC Electronics, Rockford, IL 61101

INITIAL DISTRIBUTION LIST

- | | | |
|----|--|---|
| 1. | Defense Technical Information Center | 2 |
| | Cameron Station | |
| | Alexandria, Virginia 22304-6145 | |
| 2. | Library, Code 52 | 2 |
| | Naval Postgraduate School | |
| | Monterey, California 93943-5002 | |
| 3. | Professor Anthony A. Atchley, Code PH/Ay | 3 |
| | Department of Physics | |
| | Naval Postgraduate School | |
| | Monterey, California 93943-5000 | |
| 4. | Professor Thomas J. Hofler, Code PH/Hf | 3 |
| | Department of Physics | |
| | Naval Postgraduate School | |
| | Monterey, California 93943-5000 | |
| 5. | Professor William B. Colson, Code PH/Cw | 1 |
| | Chairman, Department of Physics | |
| | Naval Postgraduate School | |
| | Monterey, California 93943-5000 | |
| 6. | Commander Naval Surface Force | 1 |
| | N00 | |
| | U. S. Atlantic Fleet | |
| | Norfolk, Virginia 23511-6292 | |

- | | | |
|----|---|---|
| 7. | LT. Nelson Castro | 2 |
| | Class 132 | |
| | SWOSCOLCOM | |
| | 446 Cushing Rd. | |
| | Newport, Rhode Island 02841-1209 | |
| 8. | Mr. Martin Castro | 1 |
| | 2342 Florida Dr. | |
| | Deltona, Florida 32738-3154 | |
| 9. | Mrs. Teresa Koontz | 1 |
| | 829 Old North George Washington Highway | |
| | Chesapeake, Virginia 23323-2208 | |